NASA Technical Memorandum 87616

NASA-TM-87616 19860005115

LASANT MATERIALS FOR BLACKBODY-PUMPED LASERS

Edited by
R. J. De Young and K. Y. Chen

September 1985

NASA
National Aeronautics and
Space Administration

Langley Research Center
Hampton, Virginia 23665

PREFACE

"The laser is one of those very few devices which can radically alter the notion of what we might do in space and how we might do it." So wrote Jerry Mullin, until 1984, Head of Space Power and Electric Propulsion in OAST. The blackbody laser is a special type of laser uniquely suited for space because it is capable of using the total solar spectrum and can operate in both sunlight and in the Earth's shadow with the aid of thermal storage. This report summarizes a workshop entitled "Lasant Materials for Blackbody Pumped Lasers," held at Langley Research Center on August 1-2, 1985.

The purpose of this workshop was to stimulate fundamental new ideas in the area of blackbody lasers. The emphasis was placed on new lasants and transfer gases and not on laser systems. All the lasants for blackbody lasers were originally suggested in the 1970's and work over the past 3 years has enabled us to define how they operate, their pootential, and their limitations. The purpose of this workshop was to stimulate a wide range of new ideas and intellectual activity. Thus, the underlying concept of this workshop was that intellectual activity can be translated into technical progress.

Several elements in this report are different from the way they were actually presented at the workshop. Two papers by Leon Arriola and John Wilson were not presented at the workshop since they did not fit in the time available. In addition, several molecules to be considered as lasants or transfer gases were suggested after the workshop. Also a list of

vibrational energies for various covalent molecular bonds have been included in the text by Kwan-Yu Chen. Finally, the summaries by the two workshop discussion leaders have been reformulated to provide more evaluation of the concepts than was possible at the workshop. With the exception of these changes, the content of this report was meant to be identical to the workshop itself.

Edmund J. Conway
Head, Space Technology Branch
Space Systems Division

CONTENTS

PREFACE i

1. Introduction to the Workshop on Lasant Materials for Blackbody Pumped Lasers 1
E. J. Conway

2. Cavity Blackbody-Pumped Lasers: Present Research Status 10
W. Christiansen

3. Analytical Investigation of Cavity Blackbody Lasers 28
W. L. Harries

4. A Review of Laser-Pumped Infrared Lasers 48
K. Y. Chen

5. Lasants for Transfer Blackbody-Pumped Lasers 80
R. J. De Young

6. Energy Transfer Mechanisms Between Molecules 112
W. E. Meador

7. Vibrational Excitation of CO by Blackbody Radiation 124
L. Arriola and J. W. Wilson

8. A Method for Analysis of Blackbody Diatomic-Triatomic Lasers . . 137
J. W. Wilson, K. Y. Chen, L. Arriola, J. H. Heinbockel

9. Report from the Cavity-Laser Working Group 157
E. J. Conway

10. Report from the Transfer-Laser Working Group 169
W. E. Meador

11. Workshop Participants 172

LASANT MATERIALS FOR BLACKBODY-PUMPED LASERS

Edited by
R. J. De Young and K. Y. Chen

ABSTRACT

Blackbody-pumped solar lasers have been proposed to convert sunlight into laser power to provide future space power and propulsion needs. There are two classes of blackbody-pumped lasers. The direct cavity-pumped system in which the lasant molecule is vibrationally excited by the absorption of blackbody radiation and laser, all within the blackbody cavity. The other system is the transfer blackbody-pumped laser in which an absorbing molecule is first excited within the blackbody cavity, then transferred into a laser cavity when an appropriate lasant molecule is mixed. Collisional transfer of vibrational excitation from the absorbing to the lasing molecule results in laser emission. A workshop was held at NASA Langley Research Center on August 1 and 2, 1985, to investigate new lasant materials for both of these blackbody systems. Emphasis was placed on the physics of molecular systems which would be appropriate for blackbody-pumped lasers.

Introduction to the Workshop on Lasant Materials for Blackbody Pumped Lasers

by E. J. Conway
Space Technology Branch

The purpose of this workshop was to define new lasants and transfer gases for blackbody pumped lasers. Our goal was to find gases with the correct energies and lifetimes for use as lasants and/or transfer gases. The more immediate goal of the participants was to suggest molecules, currently available, (or to be synthesized) which either satisfy criteria which we develop in this workshop or which deserve further study because from limited information they seem to satisfy the criteria. Thus, the workshop was interested in the identification of molecules and the rational for suggesting them.

The workshop was structured in a very simple way. There were two basic kinds of blackbody lasers to be discussed, the cavity laser and the transfer laser. We focused on the cavity laser first because it was the simplest in the sense of molecular-level concepts. We addressed the physics of optical absorption and laser emission. Then, later in the day, after a demonstration of a transfer laser, we discussed the physics of the transfer laser. Here, we added molecular energy transfer from one molecule to another to the concepts already involved in the cavity laser. We talked about the physics of the transfer gas and the transfer-lasant gas combinations. Next there were two parallel workshop sessions, one on cavity lasants and the other on transfer-lasant gas combinations. Finally, there were reports on the workshops by the two session discussion leaders.

"The Program" or "Solar-Pumped Lasers for Space Power Transmission," which is really a better name, includes lasers of two different types, direct solar-pumped lasers and indirect solar-pumped lasers, also known as blackbody lasers (fig. 1.1). Let me discuss first the direct solar-pumped lasers. Much of the program has focused on photodissociation lasers. Three lasants, which have been shown to lase photodissociatively, are listed in figure 1.1, C_3F_7I, C_4F_9I, and IBr. A second general type of direct solar-pumped laser works on the photoexcitation principle without photodissociation. Examples of these include solar-pumped lasing using neodymium ions either in a liquid or solid host, dye lasers, and molecular vapor lasers. We are currently interested in several general types of molecular vapor lasers including those based on metals, on nonmetallic elements, and on compounds.

Indirect solar-pumped lasers are often called blackbody lasers. The concept is that the total sun solar spectrum will be captured and changed into heat. A high temperature cavity will be created and thermal radiation from the blackbody cavity will be used as the pumping radiation for the lasers. The first laser to be considered here is the cavity laser. In a cavity laser, the laser cavity passes through the blackbody cavity. Thus the lasant is within a blackbody cavity and subject directly to the thermal radiation pumping. Figure 1.1 shows two examples of lasants which have lased in a cavity with blackbody pumping, CO_2 and N_2O.

Another type of blackbody laser is the transfer laser. In this case, two gases are involved. The first of these, the transfer gas, flows through the blackbody cavity and becomes vibrationally excited by the

blackbody radiation. Then the transfer gas is mixed with the lasant. Energy transfer occurs and the lasant emits radiation in the laser cavity. Two transfer-gas/lasant couples which have lased so far include N_2/CO_2 and CO/CO_2.

Lets consider the systems-level advantages of blackbody lasers. In space, with appropriate thermal energy storage, blackbody lasers could operate in the Earth's shadow. This is an exceptional advantage for them, because, in contrast, direct solar-pumped lasers do not work when not directly being excited by the sun. Thus one blackbody pumped laser can operate throughout an entire orbit in space. The second advantage of a blackbody pumped laser is that it really does not depend on the source or spectrum of the incident light, only on the total quantity of energy which is degraded into thermal energy. Thus, operation of a blackbody laser is possible not only with solar energy, but also from chemical energy, electrial energy, or nuclear thermal energy. Thus, blackbody lasers are insensitive to the primary energy source. Third, because in space a blackbody laser could use the entire solar spectrum, it offers some potential for minimizing the concentrator size associated with large solar-pumped lasers. Fourth, since a blackbody laser is not strongly sensitive to the spectrum of the incident energy this type of laser can operate on the ground or in space. Thus, blackbody-pumped lasers have several broad system advantages over some of their more dramatic cousins, the photodissociation and photoexcitation lasers.

It is appropriate to briefly review the history of blackbody lasers. The anticedent of the current cavity laser can well be said to have been an

experiment in which the radiant energy from an external flame was used to pump CO_2 laser in a nearby tube. This occured about 1970. In the latter 1970's, a blackbody laser trade study was performed by Mathematical Science Northwest which described the cavity laser and considered some of its advantages and disadvantages. In 1981, the first physics model of a blackbody laser was developed at North Carolina State University as an element of Langley's program. In 1982, the first in-cavity blackbody CO_2 laser was achieved by Prof. Walter Christiansen at the University of Washington. In 1984, he achieved blackbody lasing with N_2O as the lasant. Also in 1984, an advanced model for comparison with the experiment was developed at the University of Washington to explain the results of some of the recent experimental work. More recently, Prof. Wynn Harries of Old Dominion University also developed an advanced model.

The transfer laser developed from quite a different direction. In 1966, the first gas dynamic lasers were developed by Hertzberg and Kantrowitz. In 1972, a group at the University of Illinois developed the first thermal radiation-pumped transfer laser. In 1978, the trade study by Mathematical Science Northwest on blackbody lasers also considered transfer lasers and discussed both their advantages and their limitations. In 1982, Langley developed its own transfer laser program starting with N_2 into CO_2. In 1985, the emphasis was shifted to other transfer-gas/lasant combinations particularly CO/CO_2 and CO/N_2O. Also in 1985, a mathematical model of the CO/CO_2 transfer laser was initiated at Langley with the help of researchers at Old Dominion University.

To define new lasants and transfer gases for the two blackbody laser types, we need to clarify the laser types and their limitations.

Figure 1.2 identifies some of these limitations. The CO_2 cavity laser is a concept inwhich CO_2 absorbs blackbody radiation near 4 micrometers to excite the upper laser level leading to lasing at 10.6 micrometers. The lasant gas in this cavity laser is a mixture of CO_2, helium, and argon. The limitaion of this laser occurs because CO_2 has a very strong absorption line that is also very narrow. This means that CO_2 has a very small absorption depth over a very small region of the spectrum. The small absorption depth limits both the useful upper density of the gas and the useful upper tube diameter. The low density gas and the small tube diameter limit the high power operating potential of this laser type.

The CO/CO_2 laser concept involves CO vibrations excited by absorption of 4 micrometer blackbody radiation and subsequently mixed with CO_2 gas. The CO vibrational energy is transferred to CO_2 leading to lasing action. For this concept, the lasing gas constituents are CO and CO_2. The limitations occur because CO and CO_2 have a vibrational energy mismatch. This mismatch favors the transfer of energy from CO_2 to CO, the reverse of what is required. Kinetics limit the density of excited CO_2, and most important, the high power potential of this laser.

Figure 1.3 shows the spectral emissive power of a blackbody cavity. Plotted on this figure are hemispherical emissive power in watt/micrometer against the wavelength in micrometers. Look at the CO_2 and CO absorption regions (between 4 and 5 micrometers) for the three curves, 1500°K, 2000°K, and 2500°K. It is clear that as temperature increases, there is a small advantage to higher temperatures in this spectral band. However, if we

could find molecules which absorbed between 1.5 and 2 micrometers, one can see that an orders of magnitude increase can be gained. Thus, there are several advantages in looking for a shorter wavelength and broader absorption band lasant and transfer gases for blackbody lasers. That is the technical purpose of this workshop.

THE PROGRAM

SOLAR-PUMPED LASERS FOR SPACE POWER TRANSMISSION

DIRECT SOLAR-PUMPED LASERS

PHOTODISSOCIATION

- o C_3F_7I
- o C_4F_9I
- o IBr

PHOTOEXCITATION

- o Nd: LIQUID AND SOLID
- o DYE LASERS
- o MOLECULAR VAPOR LASERS
  - o METALS
  - o NON-METALIC ELEMENTS
  - o COMPOUNDS

INDIRECT SOLAR-PUMPED BLACKBODY LASERS

CAVITY

CO_2

N_2O

TRANSFER

N_2-CO_2

CO-CO_2

Fig. 1.1

BLACKBODY LASER SYSTEMS

CO_2 CAVITY LASER

- o CONCEPT
  - CO_2 ABSORBS BLACKBODY RADIATION TO EXCITE VIBRATIONS
- o LASANT GAS CONSTITUENTS
  - CO_2
  - He
  - Ar
- o LIMITATION
  - LARGE ABSORPTION CROSS SECTION → SMALL ABSORPTION DEPTH
  - SMALL ABSORPTION DEPTH LIMITS GAS DENSITY AND TUBE DIAMETER
  - LOW DENSITY AND SMALL DIAMETER LIMIT HIGH POWER OPERATING POTENTIAL

CO-CO_2 TRANSFER LASER

- o CONCEPT
  - CO VIBRATIONALLY EXCITED BY ABSORPTION OF BB RADIATION
  - CO SUBSEQUENTLY MIXED WITH CO_2
  - CO VIBRATIONAL ENERGY TRANSFERRED TO CO_2
- o LASANT GAS CONSTITUENTS
  - CO_2
  - CO
- o LIMITATION
  - CO-CO_2 HAVE VIBRATIONAL ENERGY MISMATCH
  - MISMATCH FAVORS TRANSFER FROM CO_2 TO CO
  - KINETICS LIMIT DENSITY OF EXCITED CO_2 AND HIGH POWER POTENTIAL

Fig. 1.2

Fig. 1.3
BLACKBODY SPECTRAL EMISSIVE POWER

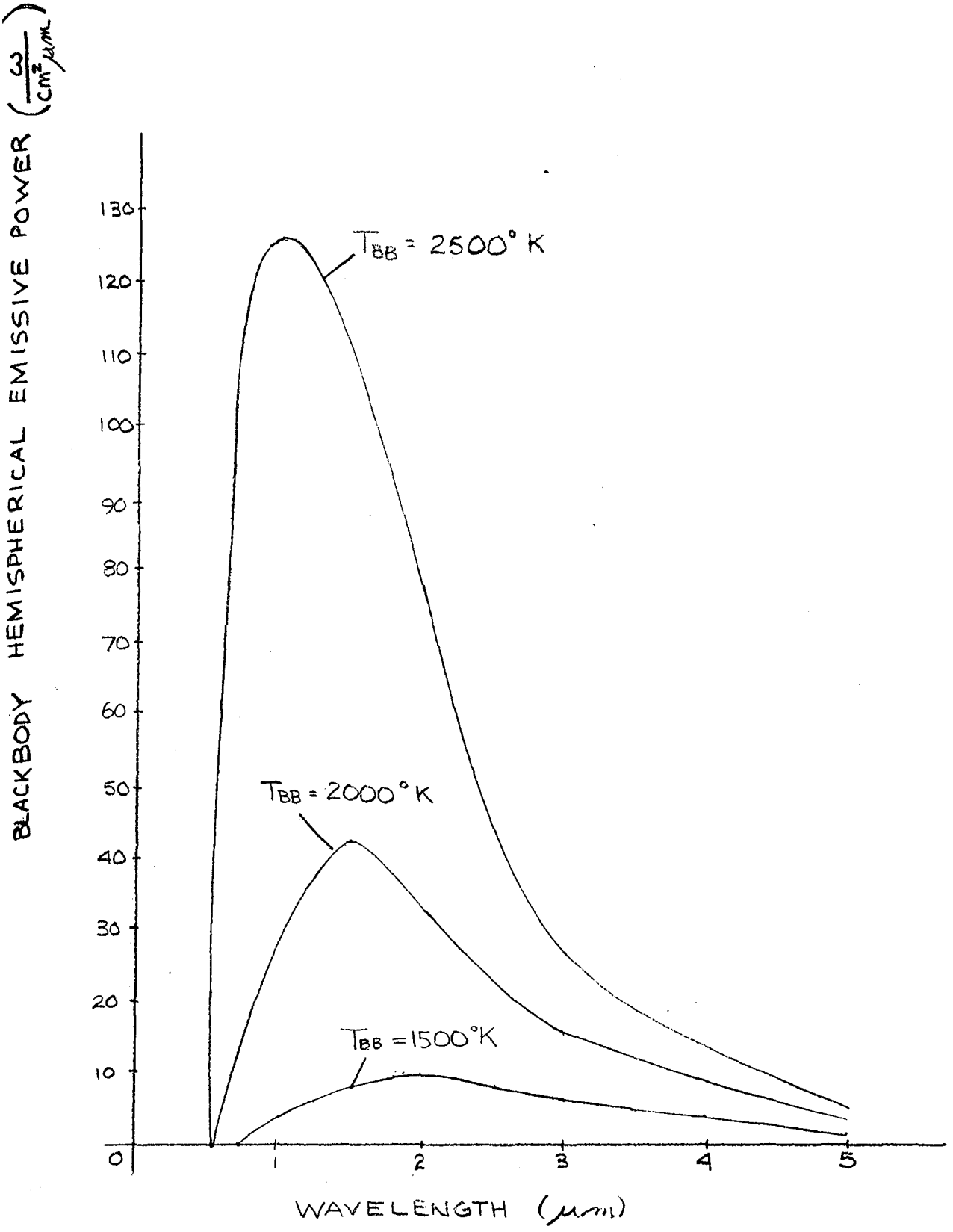

CAVITY BLACKBODY-PUMPED LASERS: PRESENT RESEARCH STATUS

Walter Christiansen
University of Washington
Seattle, Washington

Cavity pumped blackbody lasers have made substantial research progress at the University of Washington where they were first demonstrated in 1982. Presently two systems are in operation, the CO_2 and the N_2O system, both lase near 10 microns with pumping from a blackbody cavity. The basic concept for a blackbody cavity laser is shown in figure 2.1. Here a laser is surrounded by a thermally insulated cavity in which solar radiation is captured thereby heating the blackbody cavity wall but not the laser tube or lasant. The equilibrium radiation field produced by the cavity wall is approximately 1500-2500°K. This is used to optically pump the laser as an indirect pump; the cycle is closed with additional pump heat exchangers which circulate the lasant keeping it near room temperature.

A comparison between the direct solar-pumped laser efficiency and one which is indirectly pumped by a blackbody cavity, figure 2.2, shows that they are similar to a Carnot cycle. The blackbody system is still quite efficient (85 percent) even taking into account the enthalpy production of the indirect method. For a more practical engine cycle the comparison at maximum work throughput is η_{pract}. Even here the potential for good efficiency is evident in the indirect method.

Figure 2.3 shows the blackbody spectrum used to optically pump the lasant material. The specific equilibrium radiation spectrum is plotted

versus frequency and oven temperature. The 6000°K spectrum would roughly correspond to the Sun temperature, whereas the blackbody cavity would probably operate at 1500-2500°K.

Figure 2.4 shows the physical principle behind the blackbody laser idea. An incident spectrum is shown at 1 where it is practically absorbed by the medium and shown as a notch in the spectrum at 2. On reflection from the blackbody wall, the spectrum is completely thermalized and remitted again at 3. Once again it is absorbed, 4, as was previously done. In this way the radiation energy in the blackbody cavity is converted into the pumping frequency of the laser.

In figure 2.5 is shown the blackbody efficiency curve for the CO_2 system. It can be shown that the system efficiency, η, is given by

$$\eta = \frac{\eta_L \eta_C}{1 + P_T/P_m} \tag{2.1}$$

here η_L and η_C are the laser efficiency and cavity capture efficiency respectively; P_T/P_m is the ratio of broadband absorption in the laser tube wall to that of the lasant medium. If this ratio can be made small, or at least near the order of 1, the blackbody efficiency η is many orders of magnitude better than a directly pumped CO_2 system, that is CO_2 pumped directly by the solar spectrum. Thus, great effort is made in trying to keep the amount of blackbody absorption in the laser tube to a minimum. Materials are known which are broadband blackbody transmitters and are shown in figure 2.6.

Figure 2.7 is an example of an infrared laser media. The upper figure depicts CO_2 gas in which the 4.3 micron radiation pumps the (001)

upper laser level. Collisional effects are shown as straight lines while optical processes are shown as wavy lines. The lower figure shows a CO/CO_2 transfer laser in which optical energy absorbed by CO is used to pump CO_2 through collisional transfer resulting in CO_2 lasing at 10.6 μm. CO can also be made to lase independent of CO_2 provided the CO is cooled on the order of 100°K. In this case the lasing wavelength is approximately 5 μm.

Figure 2.8 shows the experimental setup at the University of Washington. This device has an electrically heated blackbody cavity which can be moved over the laser and cooling tubes, initiating lasing in the optical cavity. The device has a 50 cm long gain length and 8 mm diameter laser tube and has produced CW laser outputs of approximately 200 milliwatts. Figure 2.9 shows an example of the laser output with two CO_2 isotopes in the lasing mixture. In this case only the heavy CO_2 isotope lases, experimental points are shown as circles. Note that by mixing isotopes an increase in laser power was found. Figure 2.10 shows an example of laser output using a mixture of two molecular species. In this case only N_2O lased and the result showed definite evidence of V-V pumping between the species (experimental points are circles). These results are encouraging since they allow a broader absorption bandwidth to pump the laser.

A system study was conducted to scale these cavity blackbody-pumped lasers to high output powers. In figure 2.11 the power is increased by combining the outputs of a number of laser tubes. Each laser tube power is proportional to length, as the diameter is limited by the absorption depth and heat transfer to the walls. Note that the laser tubes are cooled. Such a system demands very long laser gain lengths, and an alternative

concept is shown in figure 2.12 which shows a CO mixing laser. In this sketch CO is mixed with CO_2 to produce a CO_2 laser; but if the gas were cooled to approximately 100°K, CO would lase on a partial inversion at 5 microns without the need for CO_2.

Figure 2.13 shows a schematic of a three-level laser. Wavy lines are radiation transitions and the solid lines are collisional transitions. A comparison of some infrared lasant gases is shown in figure 2.14. The first column is a list of potential lasants, the second column represents the steady state gain calculation where numbers less than 1 permit CW lasing. It appears that OCS can only lase in a pulsed mode. The last column is the relative measure of the important collisional loss mechanisms to the radiative pump; the larger the number, the better the potential blackbody lasant. The factors which are the most important for any optically-pumped blackbody cavity laser are, first, the bandwidth of the absorber given by

$$F = \frac{\pi \int B_\nu \, d\nu}{\sigma T^4} \tag{2.2}$$

second, the optical depth which determines the diameter of the laser tube; third, the collisional to radiative lifetime of the upper laser level; fourth, the threshold for lasing which should be a minimum; and lastly, the molecule should be chemically stable. Other potential lasant molecules should be compared to these criterion to deteremine their likelihood as blackbody lasants.

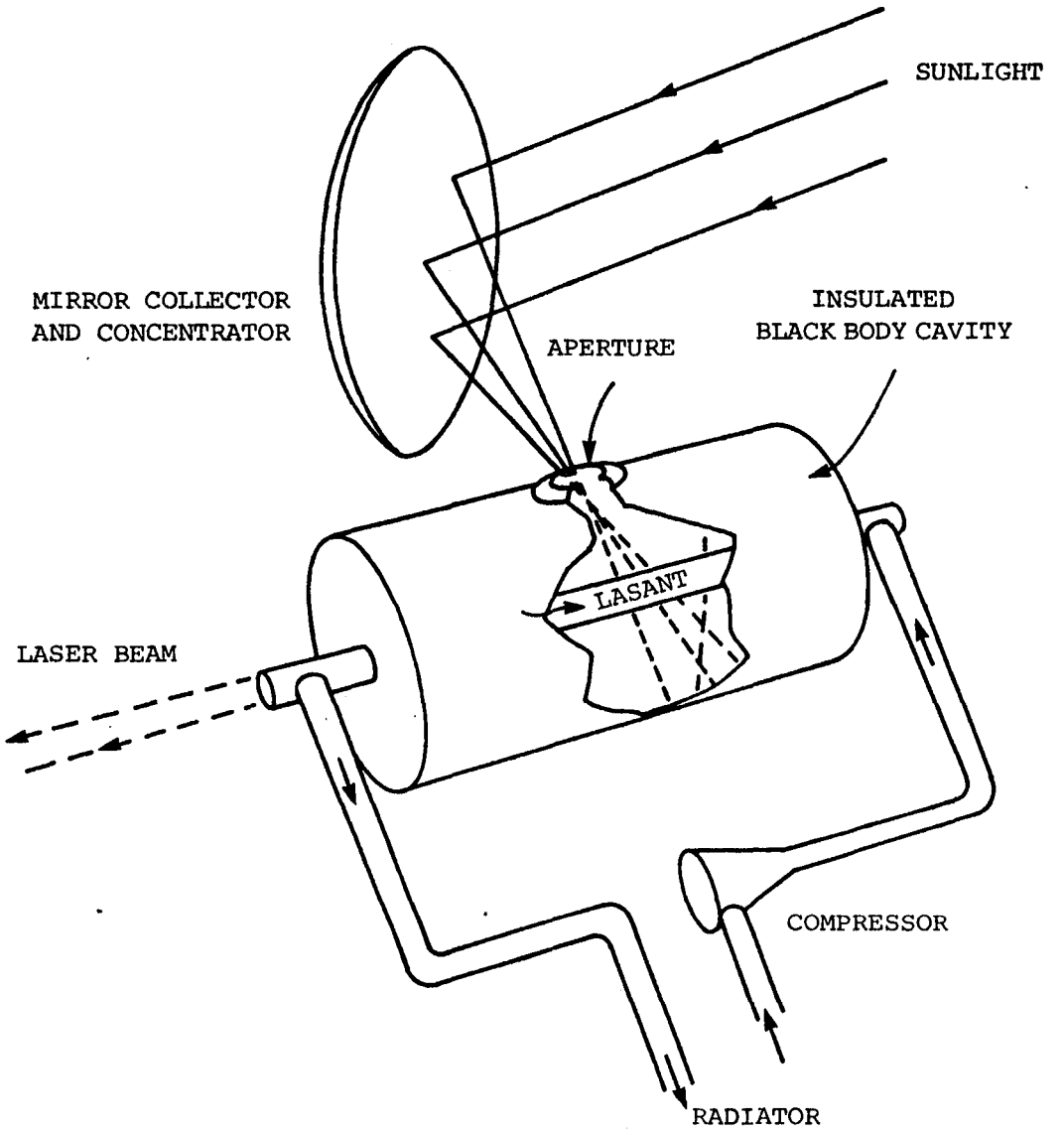
SUNLIGHT
MIRROR COLLECTOR
AND CONCENTRATOR
APERTURE
INSULATED
BLACK BODY CAVITY
LASANT
LASER BEAM
COMPRESSOR
RADIATOR

Fig. 2.1

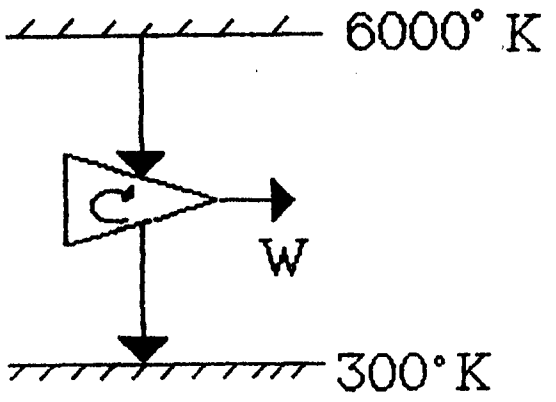

$$\eta_c = 1 - \frac{300}{6000} = 0.95$$

$$\eta_{pract} = 1 - \sqrt{\frac{300}{6000}} = 0.78$$

IDEAL DIRECT METHOD

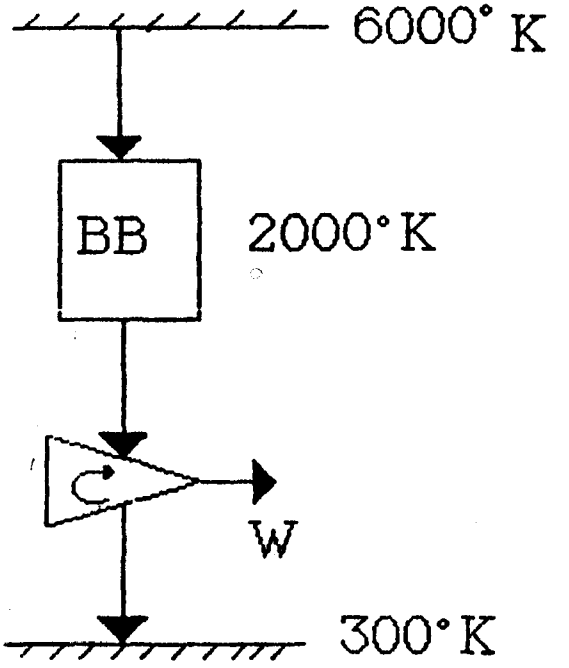

$$\eta_c = 1 - \frac{300}{2000} = 0.85$$

$$\eta_{pract} = 1 - \sqrt{\frac{300}{2000}} = 0.6$$

IDEAL INDIRECT METHOD

Fig. 2.2

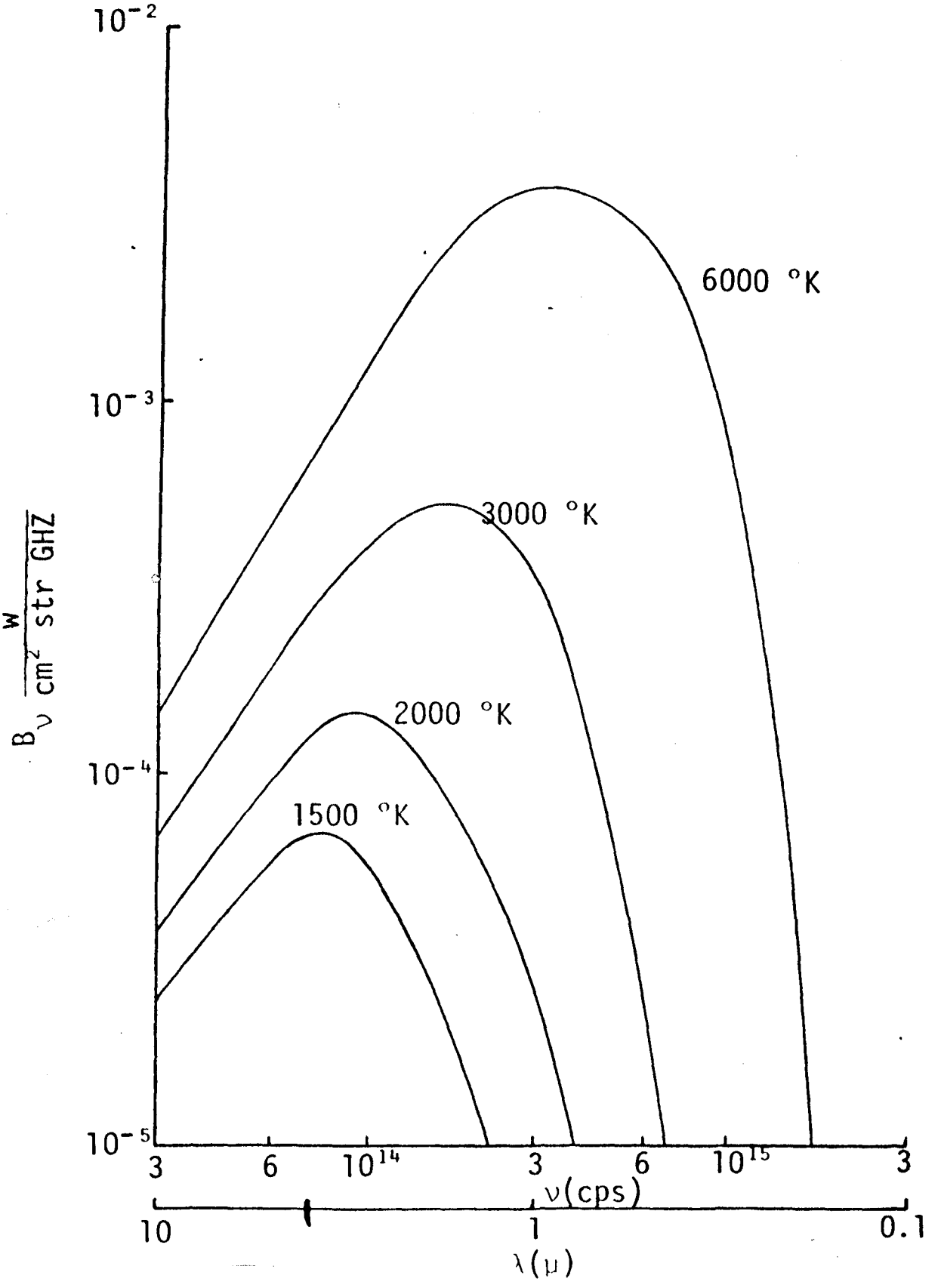
10^{-2}
10^{-3}
10^{-4}
10^{-5}
$B_\nu \frac{W}{cm^2\ str\ GHZ}$
6000 °K
3000 °K
2000 °K
1500 °K
3
6
10^{14}
3
6
10^{15}
3
ν(cps)
10
1
0.1
λ(μ)

Fig. 2.3

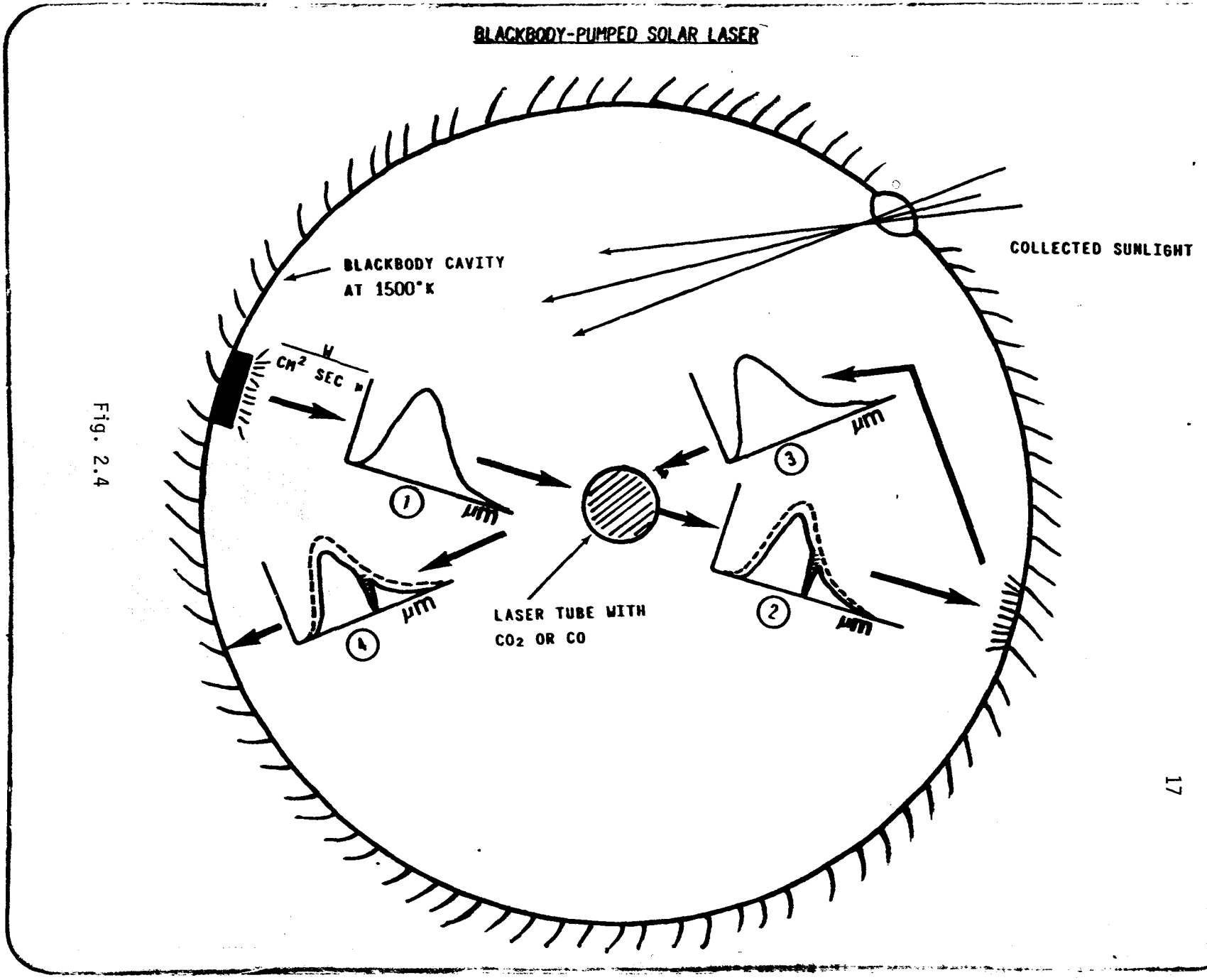
BLACKBODY-PUMPED SOLAR LASER
BLACKBODY CAVITY
AT 1500°K
COLLECTED SUNLIGHT
W
CM² SEC μm
1
3
2
4
μm
LASER TUBE WITH
CO₂ OR CO

Fig. 2.4

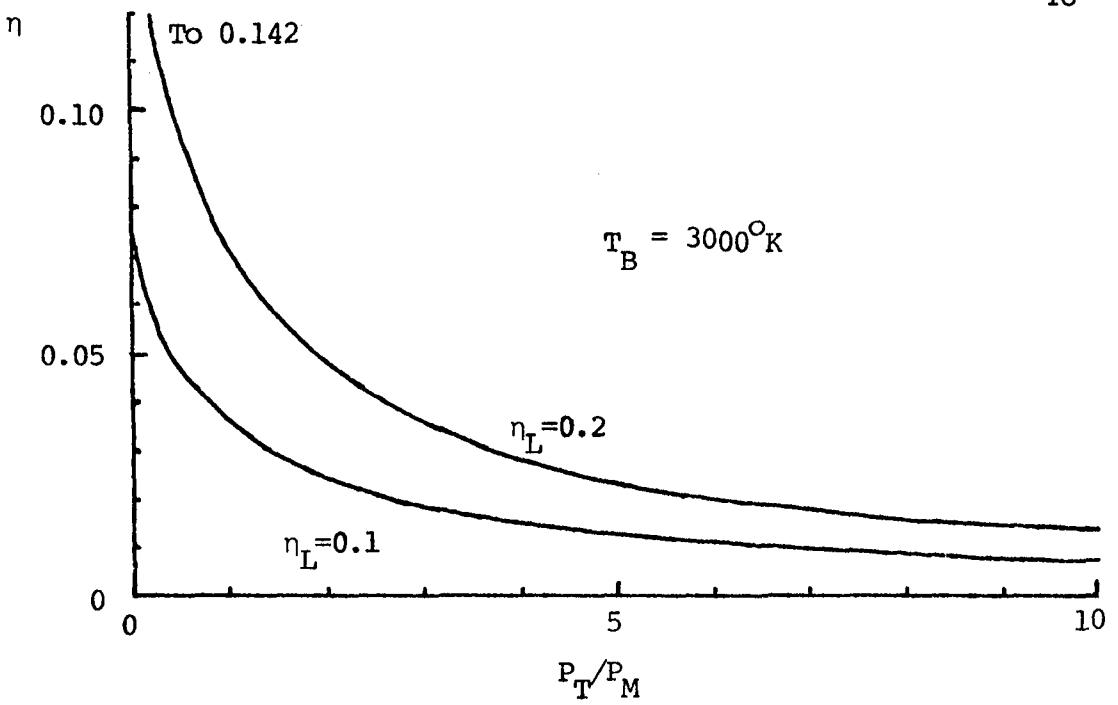
η
To 0.142
0.10
0.05
0
$T_B = 3000^{O}K$
η_L=0.2
η_L=0.1
0
5
10
P_T/P_M

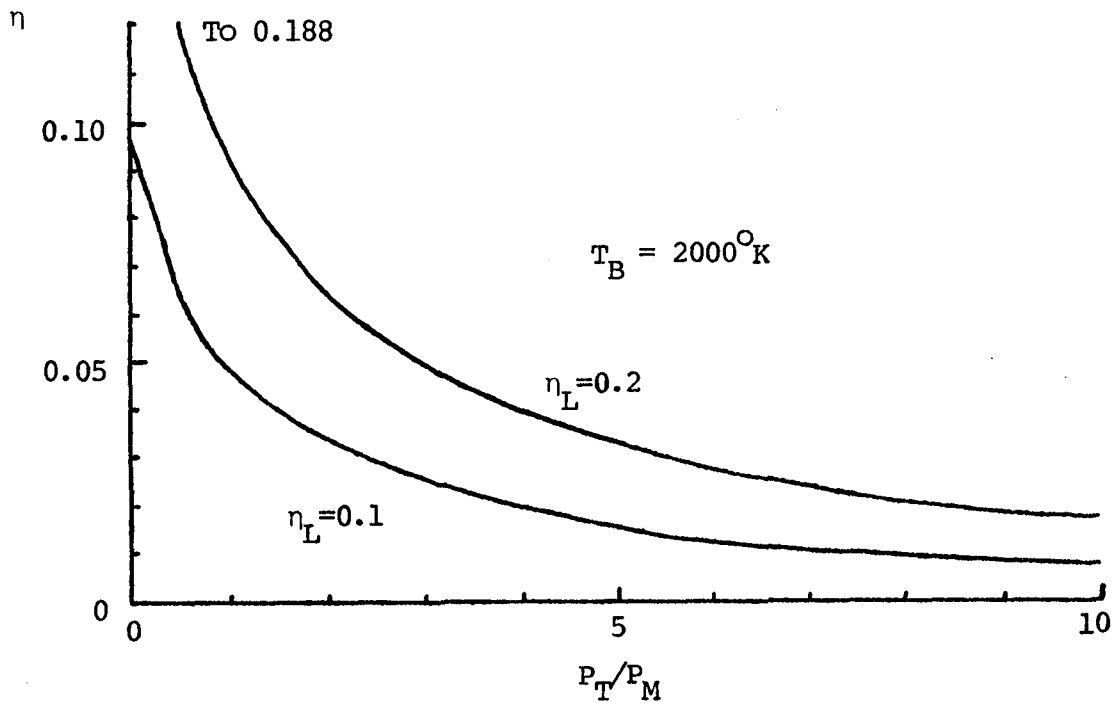
η
To 0.188
0.10
0.05
0
$T_B = 2000^{O}K$
η_L=0.2
η_L=0.1
0
5
10
P_T/P_M

Fig 2.5

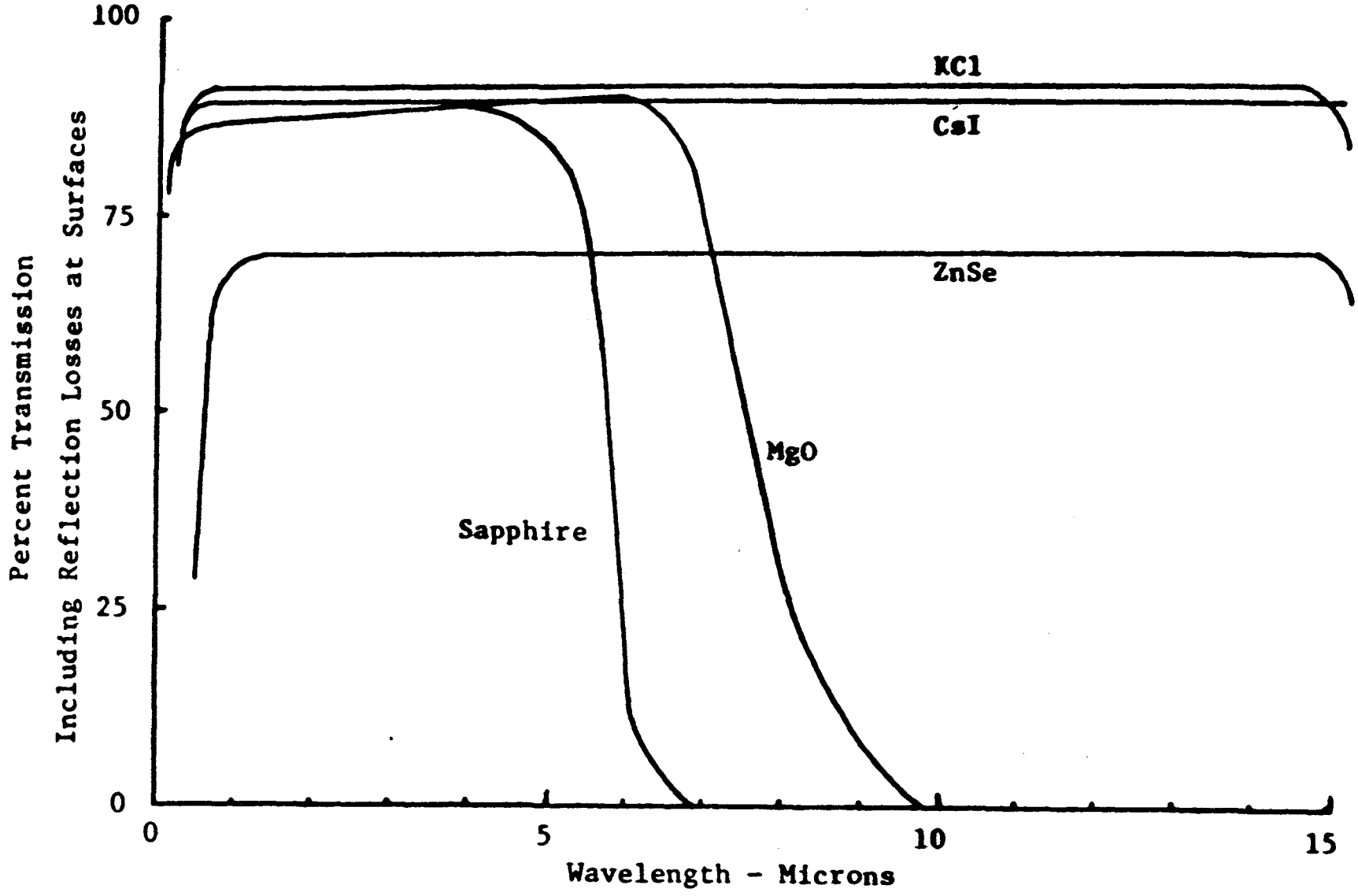
100
75
50
25
0
Percent Transmission
Including Reflection Losses at Surfaces
KCl
CsI
ZnSe
MgO
Sapphire
0
5
10
15
Wavelength - Microns

Fig. 2.6

BLACKBODY SOLAR-PUMPED LASERS

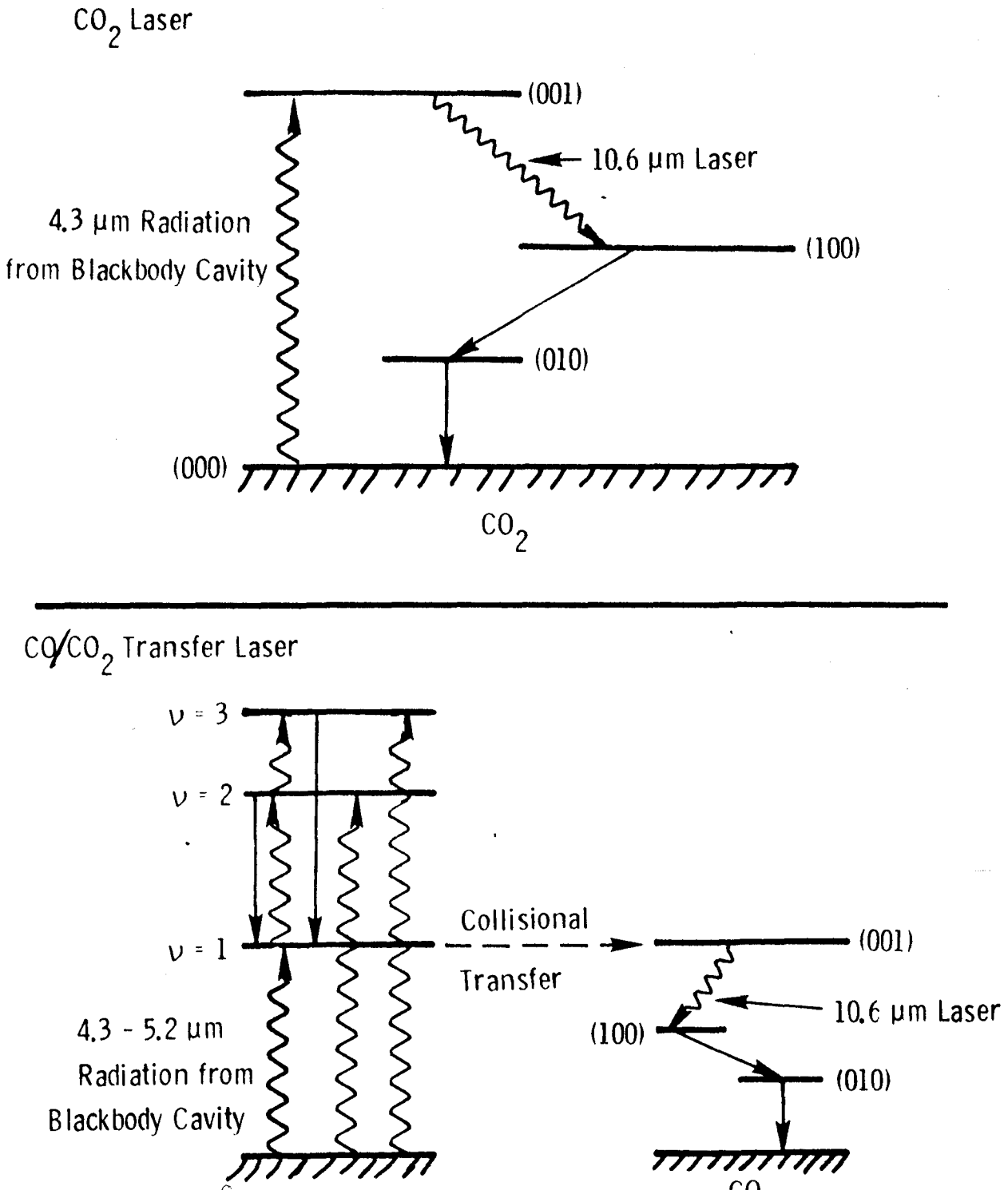

Fig. 2.7

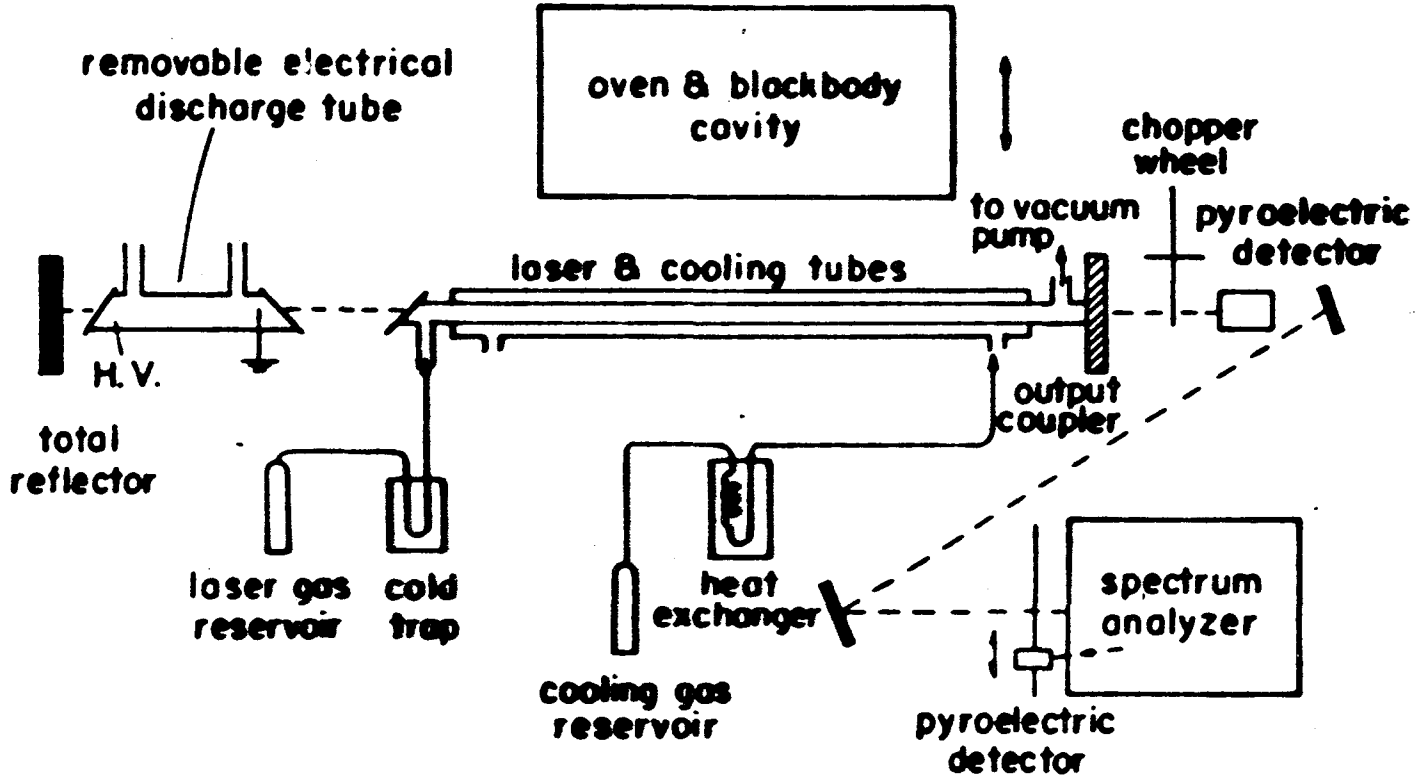
removable electrical discharge tube
oven & blackbody cavity
chopper wheel
to vacuum pump
pyroelectric detector
laser & cooling tubes
H.V.
output coupler
total reflector
laser gas reservoir
cold trap
heat exchanger
spectrum analyzer
cooling gas reservoir
pyroelectric detector

Fig. 2.8

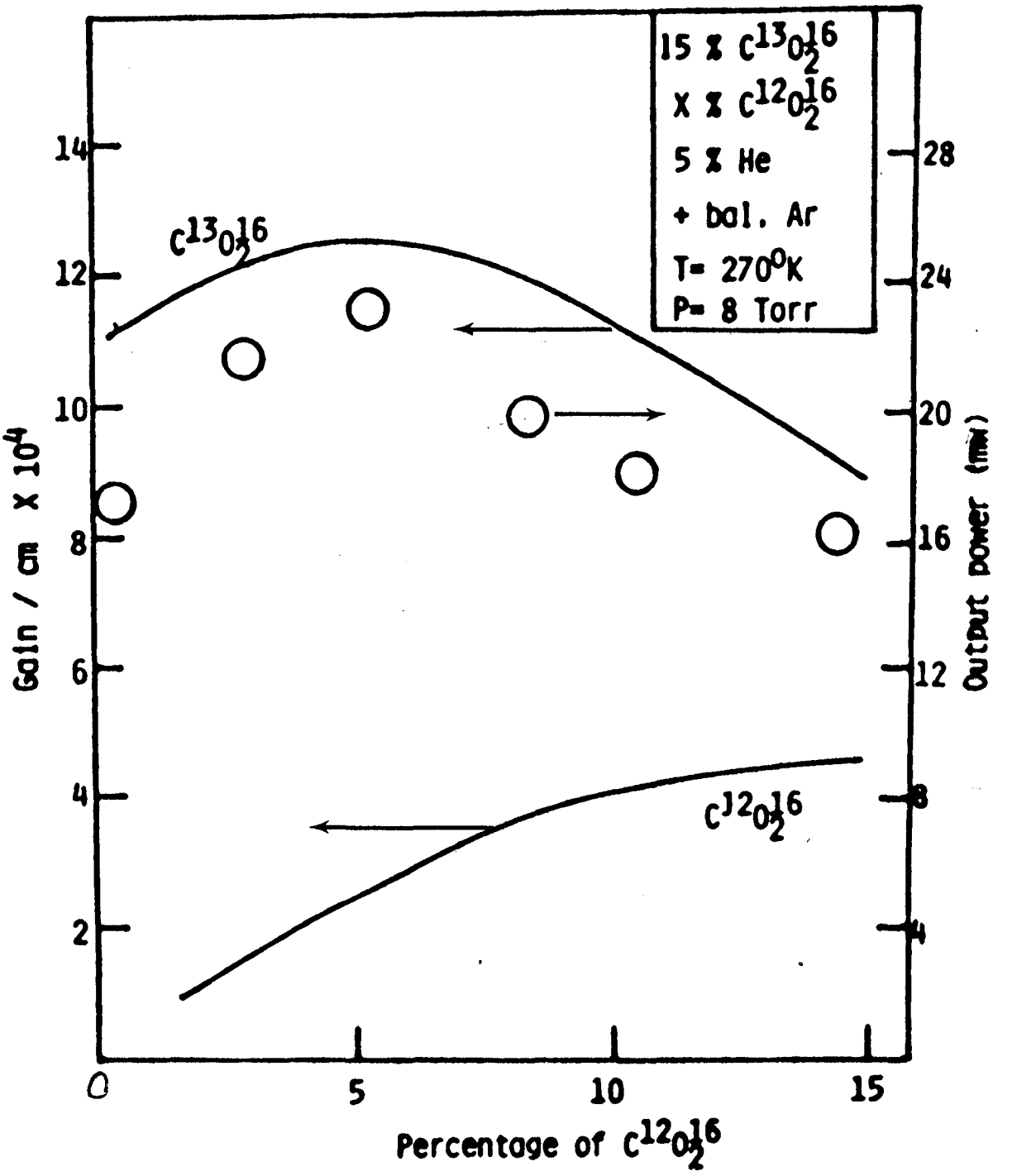
15 % $C^{13}O_2^{16}$
X % $C^{12}O_2^{16}$
5 % He
+ bal. Ar
T= 270°K
P= 8 Torr
$C^{13}O_2^{16}$
$C^{12}O_2^{16}$
Gain / cm X 10^4
Output power (mW)
Percentage of $C^{12}O_2^{16}$
0
5
10
15
2
4
6
8
10
12
14
4
8
12
16
20
24
28

Fig. 2.9

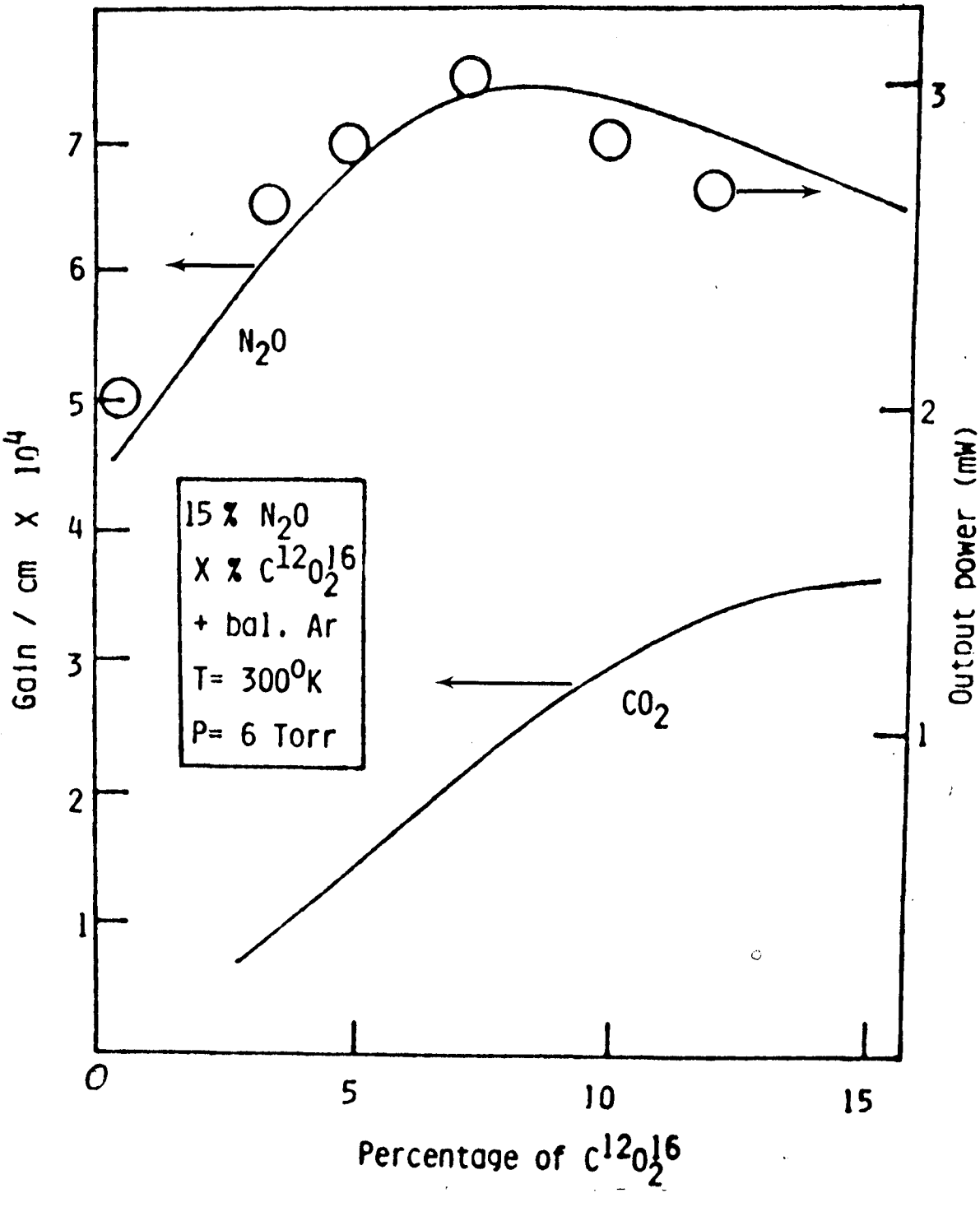
Gain / cm X 10^{-4}
Output Power (mW)
Percentage of $C^{12}O_2^{16}$
N_2O
CO_2
15 % N_2O
X % $C^{12}O_2^{16}$
+ bal. Ar
T= 300°K
P= 6 Torr
0
5
10
15
1
2
3
4
5
6
7

Fig. 2.10

STATIC INDIRECT OPTICALLY PUMPED GAS LASER

LASANT: 12 ISOTOPES OF CO_2 AND HELIUM (24 TORR, 300 °K)

GAIN: $g_0 \stackrel{\sim}{=} 0.13\ m^{-1}$

LASER EFFICIENCY: $\eta_L = 36\%$

BLACK BODY TEMP.: $T_B = 2000$ °K

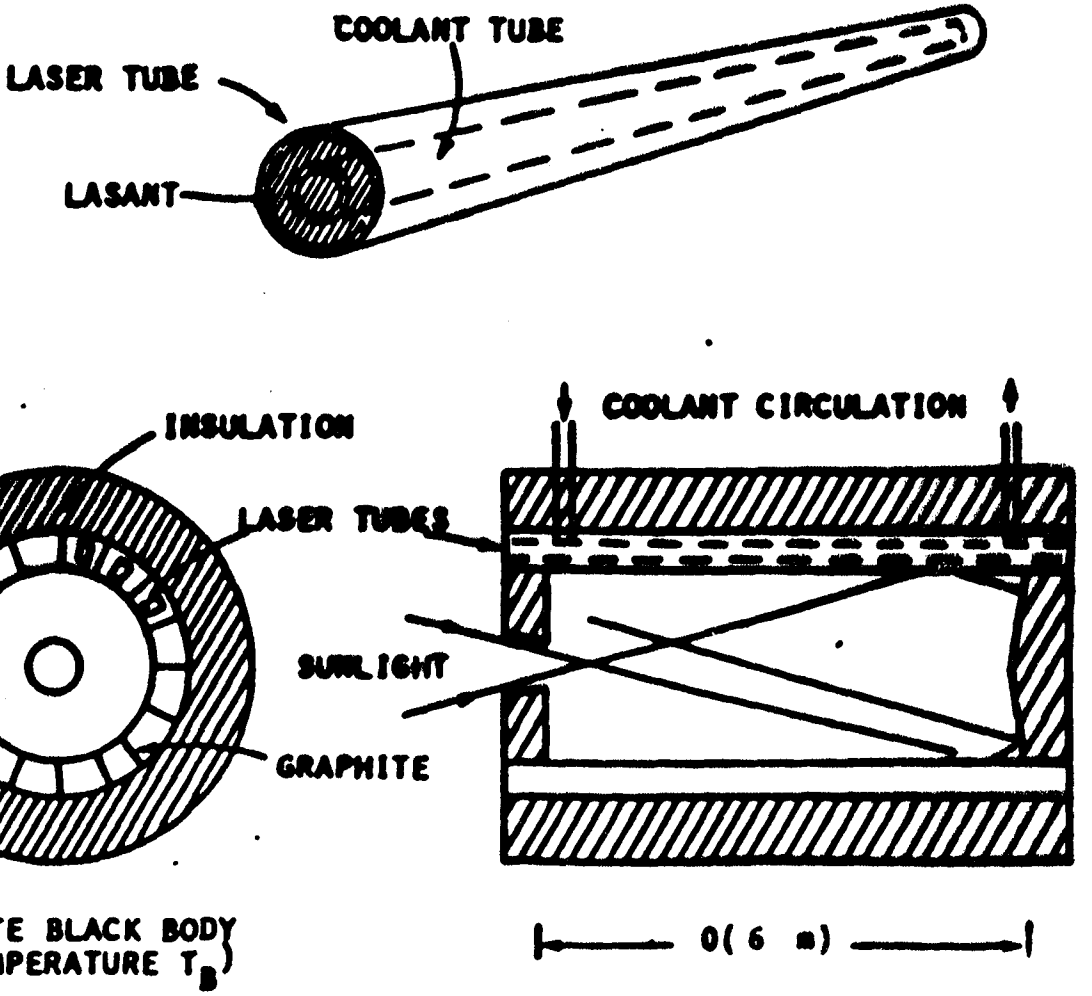

Fig. 2.11

(a) ISOMETRIC VIEW

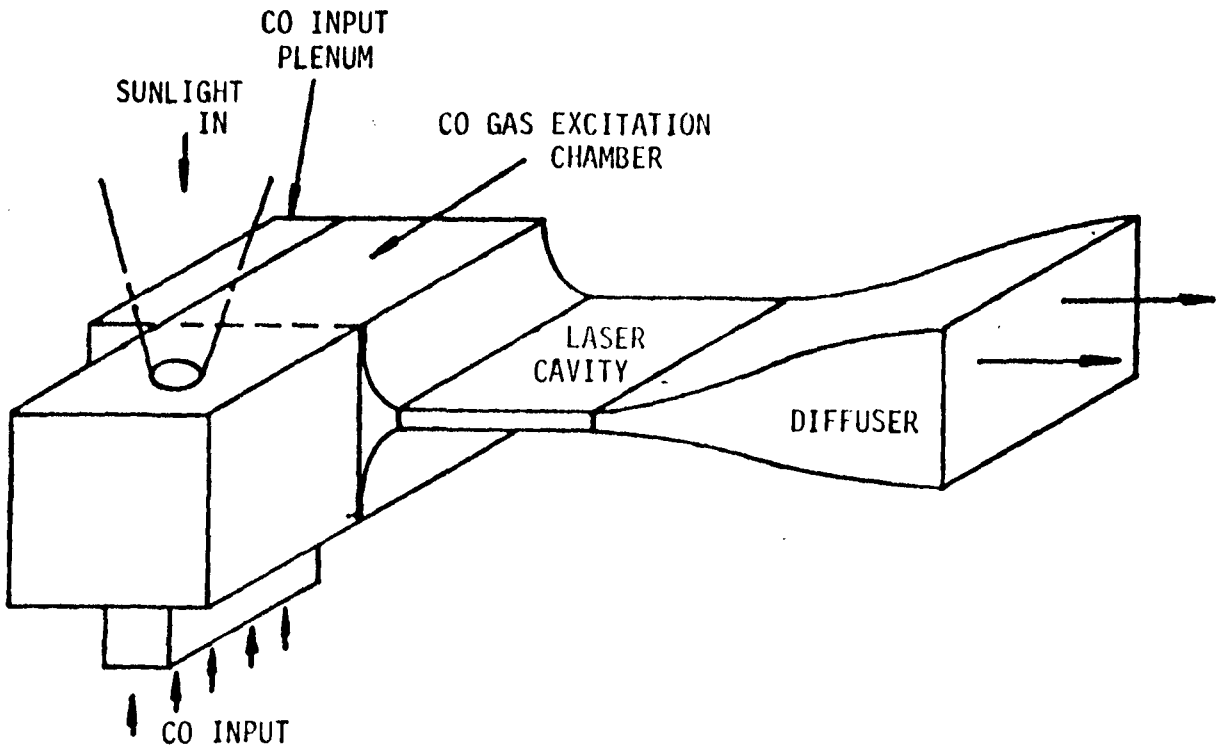

(b) ENLARGED SIDE VIEW OF BLACKBODY AND LASER CAVITIES

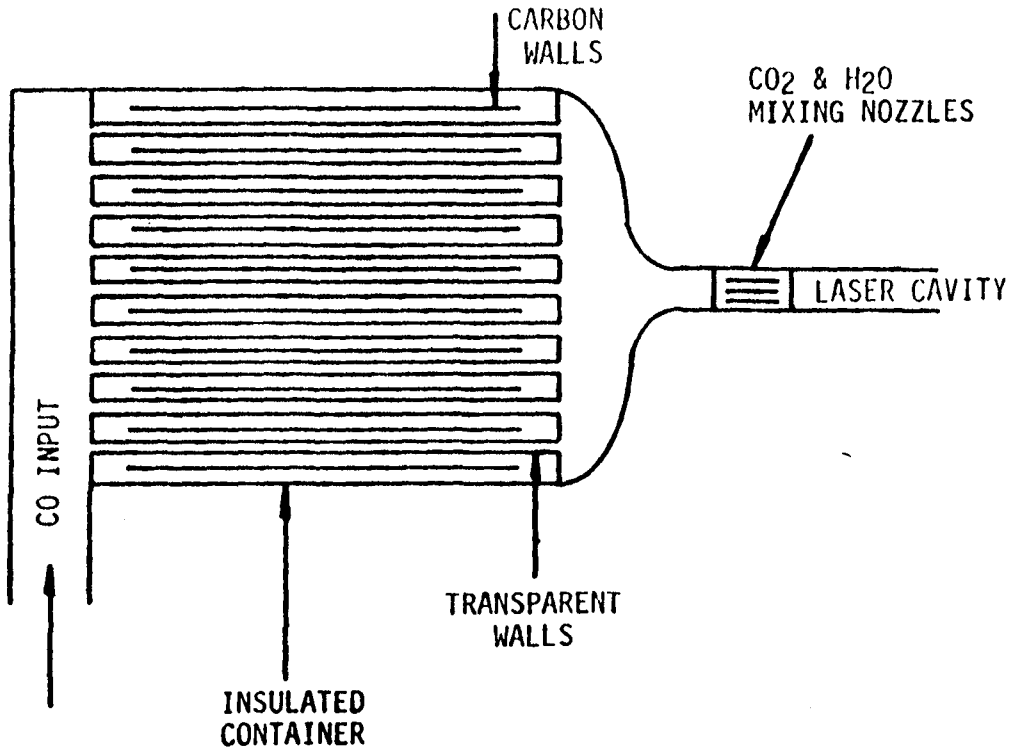

Fig. 2.12

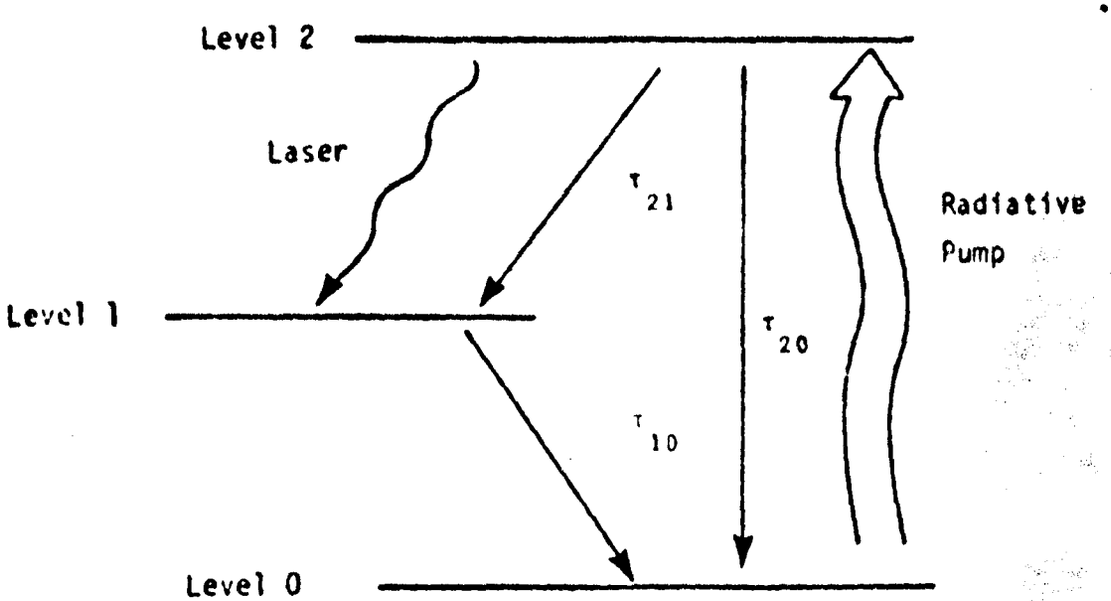

The Three Level Laser

Fig. 2.13

Potential Infrared Pumped - Infrared Lasants

Laser Molecule	$\frac{g_2\tau_{10}}{g_1\tau_{21}}$	$0\left(\frac{pt_2}{\tau_R}\right)$ torr
CO	<1	1000
CO_2	<1	1
N_2O	<1	0.5
CS_2	<1	0.2
OCS	>1	10^{-2}
HF	<1	$3(10^{-4})$
DF	<1	$3(10^{-4})$
C_2H_2	<1	$2(10^{-5})$

Fig. 2.14

ANALYTICAL INVESTIGATION OF CAVITY BLACKBODY LASERS

W. L. Harries
Department of Physics
Old Dominion University, Norfolk, VA 23508

Introduction

The purpose of this talk is to review briefly the physical processes which occur in a blackbody cavity laser, and show how the characteristics of the lasing medium affect the efficiency when used as a solar energy converter. The characteristics of an "ideal" lasant will then be described. The blackbody concept[1] has been outlined by Dr. Walter Christiansen in the previous talk.

Overall Considerations of Lasing Media

In general, high laser efficiency requires a lasing medium of the molecular rather than atomic variety. The reason is that the laser efficiency depends on the "quantum efficiency" η_Q:

$$\eta_Q = (E_u - E_l)/Eu$$

where E_u and E_l are the energies of the upper and lower laser levels, respectively. Each absorbed photon gives up energy E_u, while the emitted photon possesses energy $E_u - E_l$, and to recover the absorbed energy, η_Q should be high. Figure 3.1 compares atomic with molecular systems. For the atomic system shown $\eta_Q = 1/6$. Also shown is a range of energies for molecular dissociation leading to an excited atom X* which causes lasing. If 5eV were needed for dissociation then as the energy of X* is usually 0.1 - 1eV then $\eta_Q \leq 0.2$. Molecular levels are a few tenths of an eV above ground, but although both E_u and E_l are now quite

low, η_Q is much higher, typically around 0.5 as shown. For CO_2, which we shall take as an example for the rest of this talk, $\eta_Q = 0.43$.

The Blackbody Cavity

The intensity of radiation in a blackbody cavity is given by Planck's radiation law and the radiation flux, $E(\lambda, T_b)$, per unit wavelength vs λ for different cavity temperatures T_b are given in figure 3.2. Also shown are the location of the absorption line for CO_2 at 4.256 μm, and a possible dissociation wavelength at 0.5 μm (2eV for Br_2). The peak wavelength λ_m and blackbody temperature T_b are connected by Wien's displacement law: $\lambda_m T_b = 0.29$ (cm K). An ideal lasant should absorb at a wavelength λ_a which approaches λ_m so that the increased radiation intensity would give higher laser output and also E_u and η_Q would be higher.

The blackbody cavity would re-radiate out through the orifice where the Sun's radiation entered (Prevost's theory of exchanges), leading to a cavity efficiency η_c:[1]

$$\eta_c = 1-4(T_b/5785)^4$$

where 5785 K is the Sun's temperature. A plot of η_c vs T_b (fig. 3.3) indicates that T_b should not be much greater than 2000 K, a value also predicated from material considerations.

---

[1] W. A. Christiansen, "A New Concept for Solar Pumped Lasers," pp. 346-356 in "Radiation Energy Conversion in Space," vol. 61 of Progress in Astronautics & Aeronautics, 1979, K. H. Billman, editor.

The "Source Term" for the Upper Laser Level

The source term is the rate of pumping the upper laser level. It depends on the energy flux in the cavity, $E(\lambda_a,T_b)d\lambda_a$ $(W\text{-}cm^{-2})$ where λ_a is the absorption wavelength and $d\lambda_a$ the absorption bandwidth. This energy flux enters the laser medium and the fraction F per unit volume absorbed between a depth X_1 and X_2 below the surface is

$$F = \{\exp(-(CO_2)\ \sigma_a\ X_1) - \exp(-(CO_2)\ \sigma_a X_2)\}/(X_2-X_1)$$

where (CO_2) is the density of the absorbing medium, and σ_a its absorption cross section:

$$\sigma_a = \lambda_a^4\ A_{Gu}/4\pi^2 c\ d\lambda_a$$

where A_{Gu} is the Einstein coefficient for the transition ground to upper level, and c is the velocity of light.

The number of CO_2 molecules in the upper laser level (the asymmetric stretching mode, $CO_2(001)$) produced per cc per sec is

$$S = E(\lambda_a,T_b)\ d\lambda_a\ F\ \lambda_a/hc$$

where h is Planck's constant and dividing by hc/λ_a converts the energy flux absorbed into frequency of events producing the upper laser level per cc.

The characteristics of the lasing material determining S are λ_a, $d\lambda_a$ and A_{Gu}, but S also depends on the density of the absorbing medium. The absorbing wavelength λ_a should be chosen to approach λ_m (fig. 3.2). The value of σ_a is not too important, as S depends on

(CO_2) σ_a--and a low σ_a can always be compensated for by increased CO_2 pressure (similarity law). Too high a value of the product (CO_2) σ_a results in all the radiation being absorbed at the outer edges of the lasing medium near the walls, and X_1, X_2 and pressure should be chosen to maximize S. The absorption bandwidth $d\lambda_a$ should be high to increase $E(\lambda_a)d\lambda_a$, although it results in a lower σ_a.

The bandwidth $d\lambda_a$ for CO_2 absorbing at 4.256 μm is actually the sum of the bandwidths of about 30 closely spaced rotational levels near the asymmetric stretching mode vibrational level (fig. 3.4). Each rotational level has a Doppler bandwidth $d\lambda_D$:

$$\frac{d\lambda_D}{\lambda_a} = 7.2 \times 10^{-7} \left(\frac{T_G}{M}\right)^{1/2}$$

where T_G is the CO_2 gas temperature (≈360 K) and M the molecular weight of 44. The Doppler widths could be increased with an ideal lasant of low M operating at high gas temperature. Increasing the bandwidths by pressure broadening might not be feasible if increased collisions depopulated the upper level.

The spread of the rotational lines from 10.1 to 10.8 μm in figure 3.4 increases with gas temperature. The effective $d\lambda_a$ would increase if there were more lines, or the spacing of the rotational levels could be decreased. The spacing in frequency is

$$\Delta\nu = h/4\pi^2 I$$

where h is Planck's constant and I the moment of inertia of the molecule. The ideal lasant should also have a low moment of inertia.

Kinetics of the CO_2 Blackbody Cavity Laser

The lasant must not be at high temperature or the lower level will be filled as will be shown shortly, and as helium has excellent heat conductivity, it is usually introduced. A buffer gas such as argon may also be introduced, which if possible should enhance losses from the lower laser level without affecting the upper level. The ideal lasant may therefore be a mixture of gases, making the choice still more complex. In addition to making the source term S as high as possible, an ideal lasant should have a high density of upper level states N_u, and a low density of lower level states N_l, to give as high an inversion population (N_u - N_l) as possible. (Fig. 3.5) A specific example of the processes determining N_u and N_l in a CO_2-He-Ar mixture is illustrated in figure 3.6.

The ideal lasant should have low cross sections for collisions that deexcite N_u, i.e. low rate coefficients k_1,k_2,k_3, and a low Einstein coefficient A_{Gu}, from the upper level to ground. A low value of A_{Gu} means a metastable upper state. Even more important the filling of the lower level (figs. 3.5, 3.6) from the upper state should be small, as this has a bigger effect on N_u - N_l. (Fig. 3.6 - k_7, k_9, k_{12}, k_{13} should be small.) However, collisions which remove the lower level (k_{10}, k_{11}) are helpful. Losses of all levels to the tube wall occur by gaseous diffusion, which is important at low gas pressures (few torr total pressure).

Temperature Criterion

Experimentally it was found that if the CO_2 lasant became hot, lasing was inhibited.(2) Most of the energy absorbed is deposited as heat in the lasant and must be removed by diffusion to the walls. In gaseous mixtures the coefficient of heat conduction is independent of the total pressure, but depends on the gas ratios, with helium the best heat conductor. Assuming planar geometry the temperature of the lasant in the center of the laser can be calculated, and for CO_2-He-Ar mixtures values around 360-400 K were obtained.

Increasing the gas temperature T_G fills the lower laser level by Boltzmann statistics, as E_l is only 0.165 eV above ground for CO_2. In the steady state the fraction of CO_2 molecules with energies this high is $\exp(-E_l/kT_G) = \exp(-1972/T_G)$ or 0.5 percent at T_G = 360 K. Collisions with molecules whose energy is above E_l can result in the symmetric stretching mode of oscillation--the $CO_2(100)$ lower lasing level. Only one in several thousand collsions accomplishes this, but nevertheless at elevated gas temperatures the density of the lower laser level N_l state can exceed that of the upper laser level N_u, and lasing will cease. The lasant must therefore be cooled and the cooling requirement is yet another reason why an important characteristic of an ideal lasant would be to have E_l as high as possible above ground.

---

[2]R. J. Insuik and W. H. Christiansen, IEEE J. Quantum Electronics QE-20, 622, (1984)

Characteristics of an Ideal Lasant

The lasing medium X is usually mixed with a cooling agent Y, (usually He) and a buffer gas Z which preferably deexcites the lower level. All three components interact in the kinetics of the laser. The ideal lasant should satisfy the following criteria: (1) Number of atoms in the molecule: the lasing medium should have at least three atoms so that there are several energy levels to provide an upper level, and a lower level which cannot be the ground level. (2) Absorption cross section σ_a: it should have an absorption cross section $\sigma_a > 0$ at an appropriate absorption wavelength, λ_a. The cross section need not be large as increasing the pressure can compensate for small σ_a. (3) Absorption bandwidth $d\lambda_a$: this should be as large as possible (although $\sigma_a \propto (d\lambda_a)^{-1}$--see 2 above), as a greater portion of the blackbody spectrum is now utilized. An ideal lasant would have large $d\lambda_a$ if it had a small molecular weight M, and a large moment of inertia I. (4) The laser energy levels E_u, E_l: E_u should be high so λ_a is small, and approaching the peak of the blackbody curves, where the radiation density per unit wavelength is higher and raising $\eta_Q = (E_u - E_l)/E_u$. The lower laser level, E_l, should be high so that the level is not filled by temperature effects. However both E_u and E_l must give a reasonable η_Q. (5) Pumping the upper laser level: absorption in the lasant X at a density (X) cm^{-3}, depends on the correct ((X) σ_a d), where d is the

average depth (between x_1 and x_2) and d should be small, to enable adequate heat conduction to the walls. (6) Losses from the upper laser level: the ideal lasant X should have low losses from its upper level X_u, meaning collisions of the type X_u + X, Y, Z should not deexcite (see fig. 3.6). Spontaneous emission from X_u should also be small, or Einstein coefficient A_{uG} should be small, i.e. a metastable upper level is desirable. (7) Stimulated emission cross section σ_e: should be large for low threshold, high gain, and high power:

$$\sigma_e = \lambda_e^4 A_{uL}/4\pi^2 c d\lambda_e$$

Here λ_e, the lasing wavelength is fixed by E_u-E_l, A_{uL} the Einstein coefficient for spontaneous emission should be large and $d\lambda_e$ the emission bandwidth should be small. (8) Filling the lower laser level: the rate should be small. The two main contributions are collisions from the upper level, requiring rate coefficients such as K_7, K_{12}, k_{13} (fig. 3.6) to be small, and filling by temperature effects should be small meaning E_l should be high, and the gas temperature T_G low. (9) Losses from the lower laser level: should be large so that the density of the lower level states (X_L) is small and (Xu) - (X_L) >> 0. Hence collisions of the type X_L + X, Y, Z should have large deexcitation cross-sections (large rate coefficients K_4,K_5,K_6 in fig. 3.6). It is also helpful to have other vibrational modes at energies in near resonance with E_l, which provide pathways to deplete the lower laser level, e.g. for CO_2, we have (100)→(020)→(010)→(000).

SCALING OF A BLACKBODY CAVITY CO_2 LASER TO 1 MW

In scaling a CO_2 blackbody cavity laser to 1 MW there is a serious limitation due to Planck's Radiation Law, which leads to excessively large surface areas for the laser. If flat "box-type" laser is assumed, the surface areas of the solar collector, and heat radiator are considerably smaller.

Power Density in a Blackbody Cavity

The CO_2 laser absorbs at a wavelength $\lambda_a = 4.256$ μm, with a bandwidth $d\lambda_a = 4 \times 10^{-4}$ μm. Plank's radiation formula then gives the power entering unit area of the laser surface as

$$E(\lambda_a)d\lambda_a = \frac{1.07 \times 10^{-2}}{\exp(3381/T_b) - 1} \quad (W\text{-}cm^{-2})$$

where T_b is the cavity temperature. For T_b = 1500K, and 3000K respectively, $E(\lambda_a)(d\lambda_a)$ = 1.26 and 5.14 mW per square cm, values which are very small. Large power outputs therefore require a large laser surface A_L. There is no concentrating of input flux inside the blackbody cavity, as with parabolic collectors.

We define a device efficiency η as P_{out}/P_{in} where P_{in} is the absorbed power to produce $CO_2(001)$ the upper laser level, and P_{out} is the output power assumed to be 1 MW.

Calculation of the Dimensions of a 1 MW Laser

The model is shown in figure 3.7. A parabolic collector of area A_c collects the sun's radiation of 1.4 KWm^{-2} and the total power P_c is directed into the cavity, which has negligible losses. All of P_c is assumed to be input power P_{in} to the laser of surface area A_L. Although the cavity is at temperature T_b, the temperature of the gas T_G is assumed much lower - 400K. A cooling system removes heat to a radiator of area A_r, at temperature T_r which emits power P_r by Stefan's Law: $P_r = A_r \varepsilon \sigma T_r^4$ where ε the emissivity is assumed unity, σ is Stefan's constant, and $T_r = T_G$. As η is usually much less than 1, $P_r \approx P_{in}$. With these assumptions the areas of the collector A_c and radiator surface A_r can be calculated as shown in Fig. 3.8.

In this simplified treatment A_c, A_L, A_r are proportional to P_{out}/η, only A_L depends on Planck's formula. Assuming cavity temperatures T_b = 1500K and 3000K, and efficiencies of 1% and 10%, the values of the areas are given in figure 3.9. Also given is a representative linear dimension L where L^2 = area, to give a feeling for the size of these components. The radiator may to some extent be folded, while the laser area, A_L, can be shared by the two sides of the laser. However a folded geometry for A_L would be difficult because the surface has to be cooled as shown. Even in the extreme limit with T_b = 3000K and η = 1, A_L is still 20000 m^2 if P_{out} = 1 MW.

Conclusions

The characteristics of an ideal blackbody cavity lasant have been outlined. The choice of an ideal lasant is a complex process depending on a large number of factors, including the choice of a cooling medium and a buffer gas.

Planck's radiation law limits the power input per unit area into a CO_2 blackbody cavity laser making the surface area for high powered lasers excessively large. It is suggested that an alternative application might be small 1 W lasers for communication and surveillance, because it would be easy to maintain the cavity temperatures in synchronous orbits where 72 minutes each day are spent in the earth's shadow.

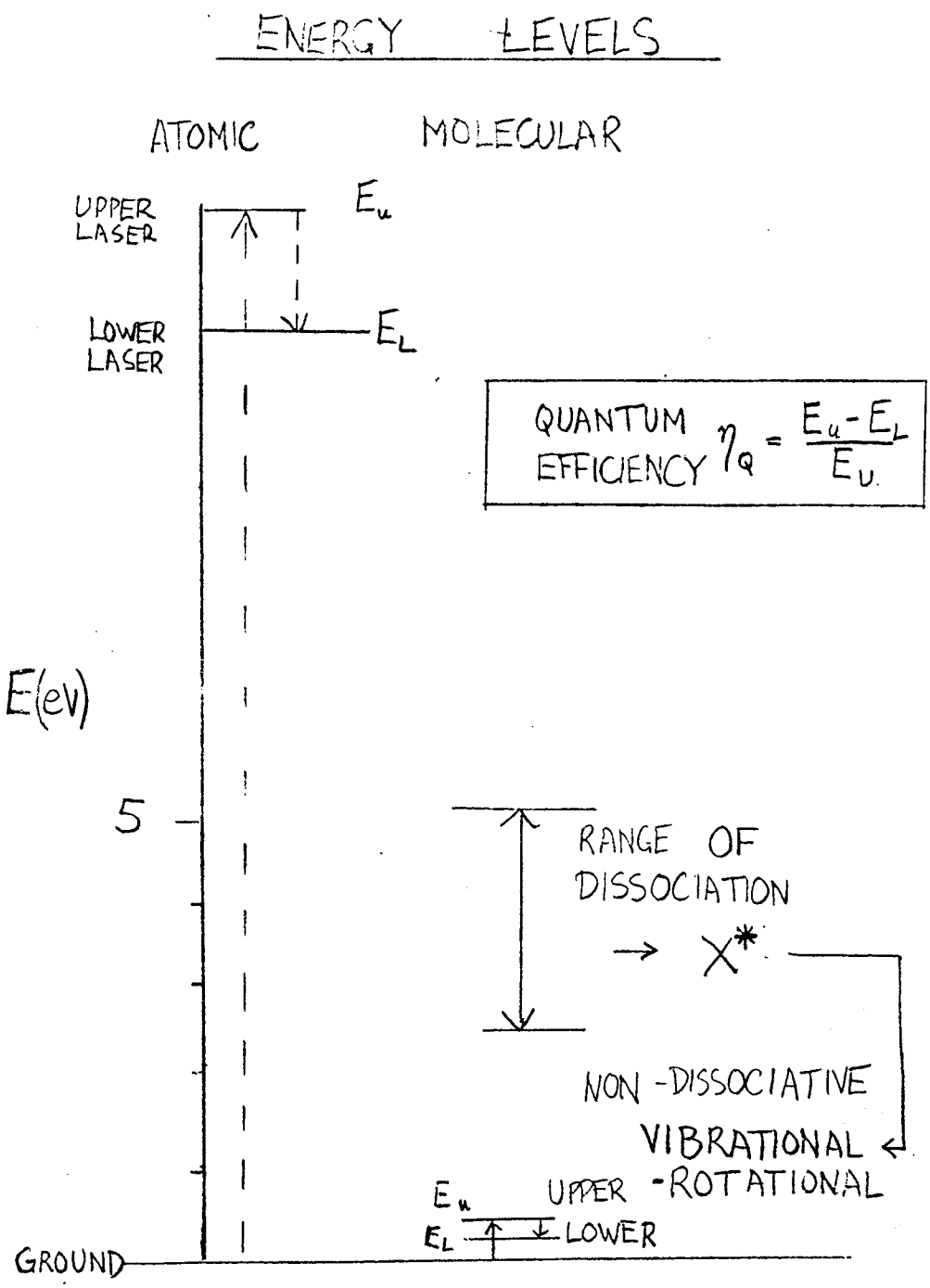
ENERGY LEVELS
ATOMIC
MOLECULAR
UPPER LASER
E_u
LOWER LASER
E_L
QUANTUM EFFICIENCY $\eta_Q = \frac{E_u - E_L}{E_u}$
E(eV)
5
RANGE OF DISSOCIATION
X^*
NON-DISSOCIATIVE
VIBRATIONAL
-ROTATIONAL
E_u UPPER
E_L LOWER
GROUND

Figure 3.1

BLACK-BODY EMISSION CURVES

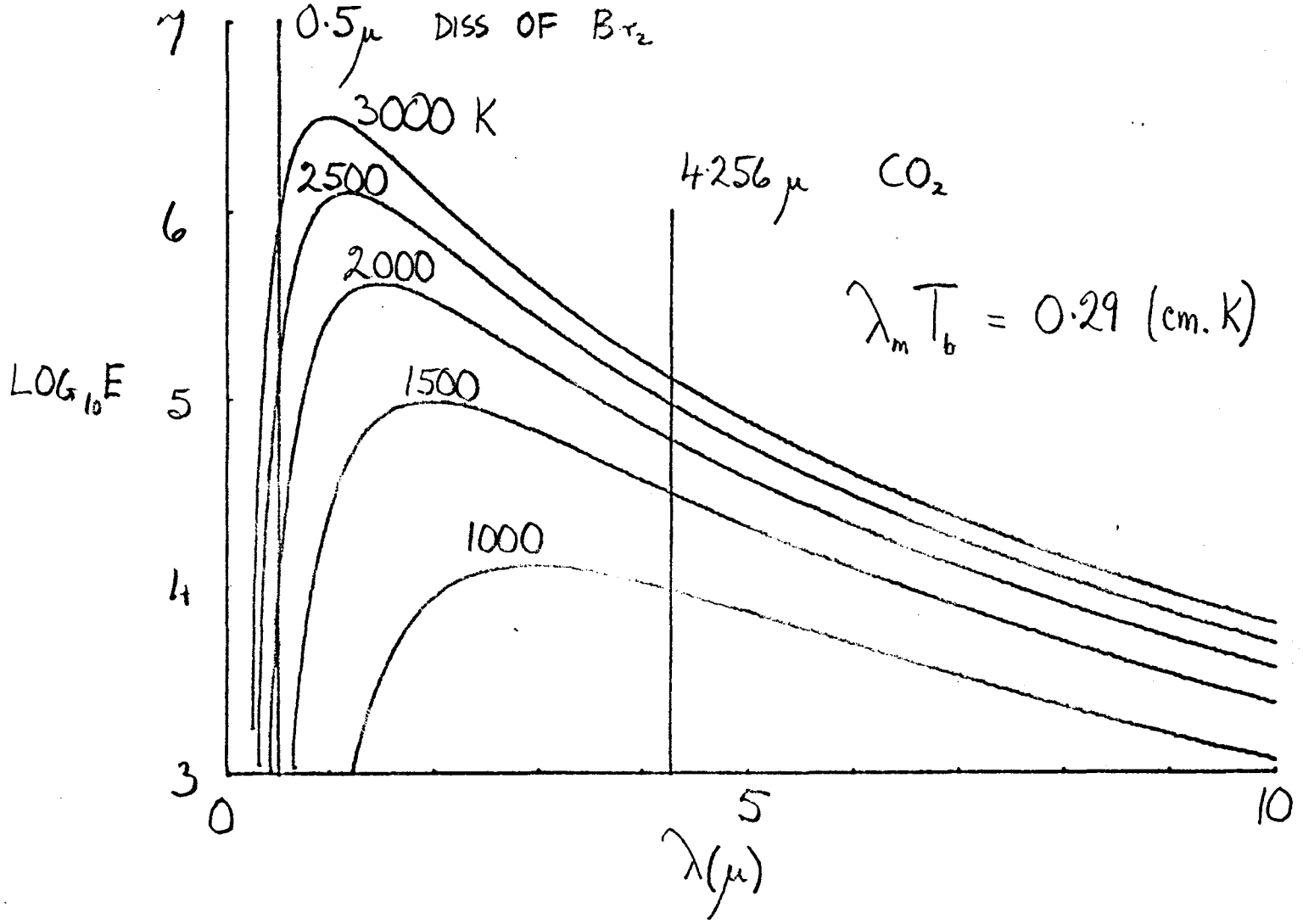

Figure 3.2

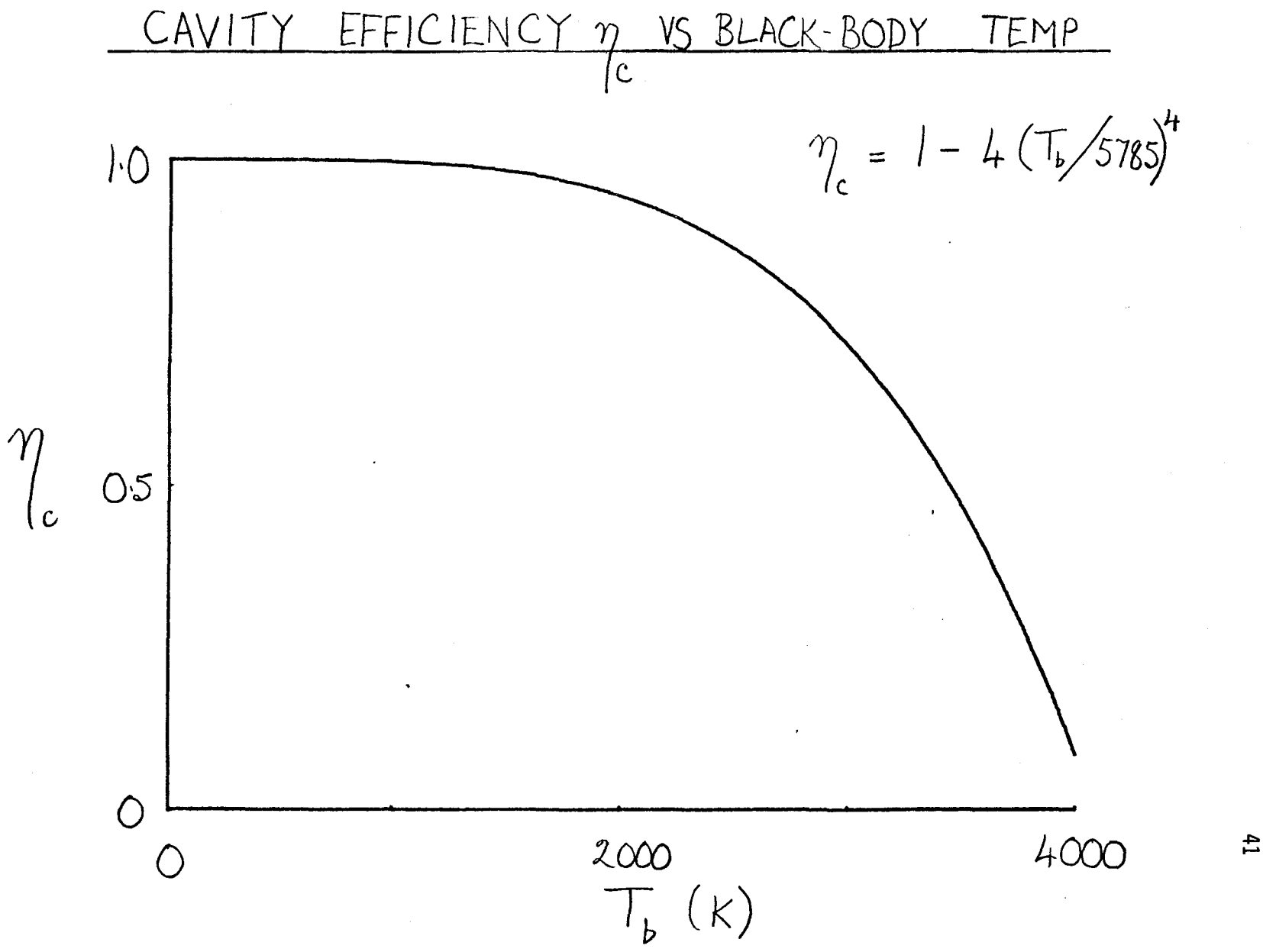
CAVITY EFFICIENCY η_c VS BLACK-BODY TEMP
$\eta_c = 1 - 4(T_b/5785)^4$
1.0
0.5
0
η_c
0
2000
4000
T_b (K)

Figure 3.3

ABSORPTION CROSS-SECTION

$$\sigma_a = \frac{\lambda_a^4 A_{Gu}}{4\pi^2 c \, \Delta\lambda_a}$$

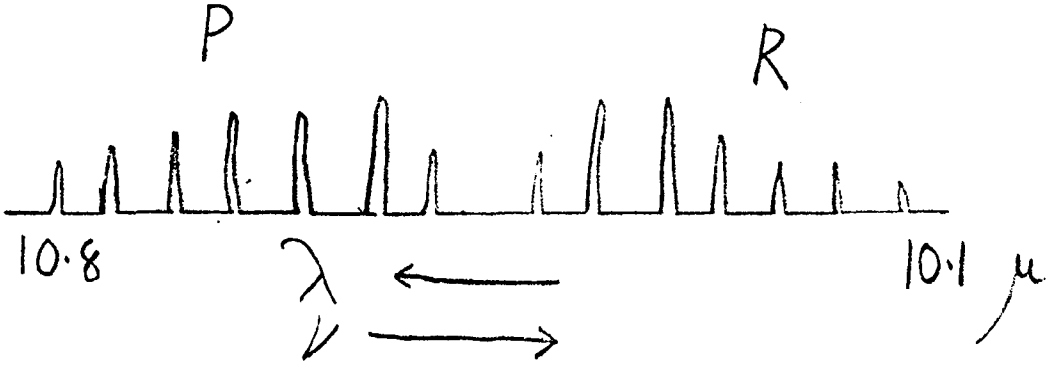

CO_2 HAS ABOUT 40 LINES EACH

WITH A DOPPLER WIDTH.

$$\frac{\Delta\nu}{\nu}_D = \frac{\Delta\lambda}{\lambda}_D = 7.2 \times 10^{-7} \left(\frac{T}{M}\right)^{\frac{1}{2}}$$ ←

SPACING OF ROTATIONAL LEVELS

$$\Delta\nu_R = \frac{\hbar}{2\pi I}$$ ←

I IS MOMENT OF INERTIA

Figure 3.4

PHYSICAL PROCESSES IN BLACK-BODY CAVITY LASER

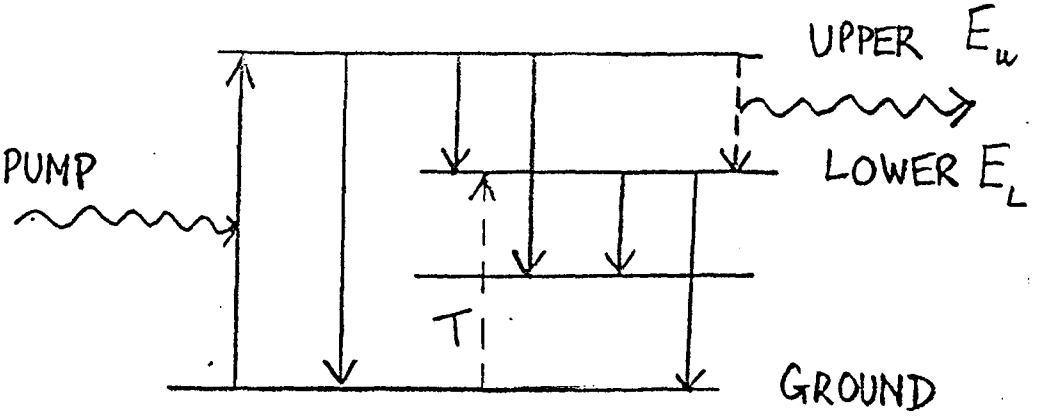

1. ABSORPTION AND PUMPING. ↑
2. LOSS FROM UPPER LEVEL BY COLLISIONS SPONTANEOUS EMISSION & DIFFUSION. ↓
3. FILLING LOWER LEVEL FROM UPPER. ↓
4. FILLING LOWER LEVEL BY TEMPERATURE EFFECTS ↓
5. REMOVE LOWER LEVEL RAPIDLY ↑

∴ NEED NEED LASANT WITH HIGH ABSORPTION, COOLANT (He), AND PROB-ABLY A THIRD MATERIAL TO ENHANCE 5 WITHOUT INCREASING 2 & 3.

Figure 3.5

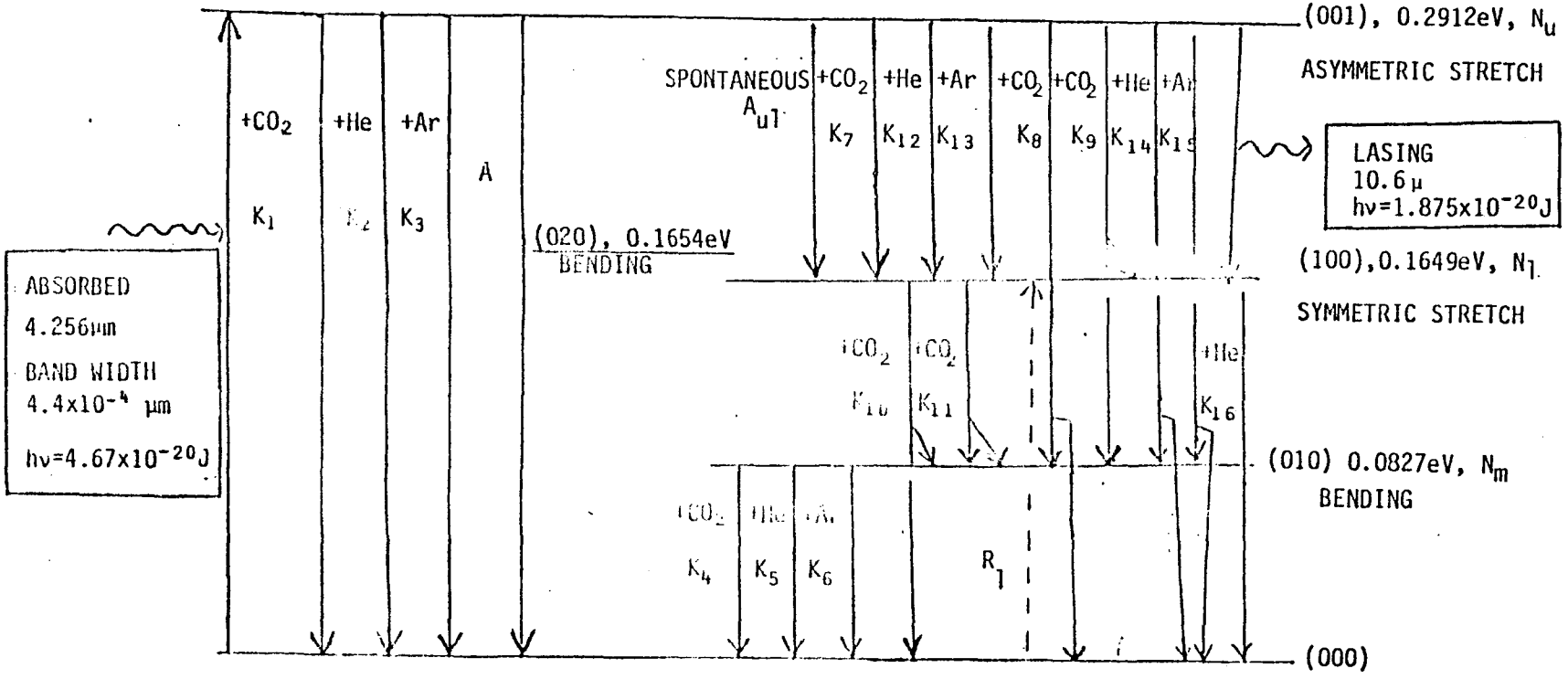

Flow Diagram for CO_2 Black Body Laser

Figure 3.6

SCALING OF 1MW CO_2 BLACK-BODY CAVITY LASER

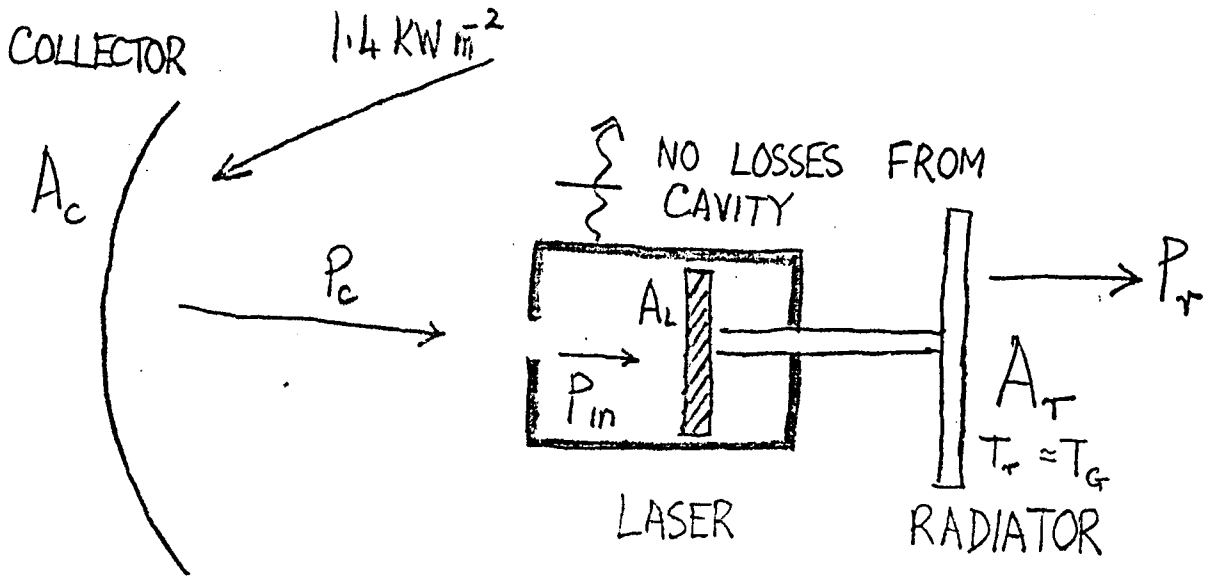

ASSUME: $P_c = A_c \times 1400$ (W)

NO LOSSES FROM OUTSIDE CAVITY

$$P_{in} \simeq P_c$$

$$P_{OUT} = \eta P_{in}$$

$$P_r = (1-\eta) P_{in} \simeq P_{in}; \quad \eta \ll 1.$$

$$P_r = A_r \varepsilon \sigma T_G^4; \quad \varepsilon = 1$$

$$T_G = 400 \text{ K}.$$

Figure 3.7

SURFACE AREA OF COLLECTOR, A_c

ASSUME ALL POWER COLLECTED → $E(\lambda_a)\, d\lambda_a$, — NO LOSSES FROM CAVITY.

$$A_c\,(m^2) \times 1400\,(W\,m^{-2}) \times \eta = P_{out}(W)$$

$$A_c(m^2) = P_{out}(W) \,/\, 1400\,\eta$$

SURFACE AREA OF LASER, A_L

$$P_{in}(W) = E(\lambda_a)\, d\lambda_a (W cm^{-2}) A_L\,(m^2) \times 10^4$$

$$P_{out}(W) = \eta\; P_{in}(W)$$

$$A_L(m^2) = P_{out} \,/\, 10^4 \eta\; E(\lambda_a)\, d\lambda_a$$

SURFACE AREA OF RADIATOR, A_r

ASSUME $P_r \approx P_{in} = P_{out} / \eta$

$$P_r = A_r\, \varepsilon\, \sigma\, T_r^4$$

ε = EMISSIVITY = 1, σ = STEFAN = $5.67 \times 10^{-8}\ W m^{-2} T^{-4}$

$$A_r\,(m^2) = \frac{P_{out}}{\eta\, \varepsilon\, \sigma\, T_r^4}$$

Figure 3.8

1 MW CO_2 BLACK-BODY LASER: AREAS & LENGTH OF SIDE (IF SQUARE) OF COLLECTOR LASER & HEAT RADIATOR

$T_r = 400K$

η	T_b (K)	COLLECTOR		LASER		RADIATOR	
		A_c (m^2)	L_c (m)	A_L (m^2)	L_L (m)	A_r (m^2)	L_r (m)
0.1	3000 1500	7×10^3	84	1.94×10^5 7.94×10^5	441 890	7×10^3	83
0.01	3000 1500	7×10^4	265	1.94×10^6 7.94×10^6	1,390 2,818	7×10^4	263

IF $\eta \to 1$, $T_b = 3000K$

$A_L = 1.94\times10^4\ m$, $L_L = 140\ m$

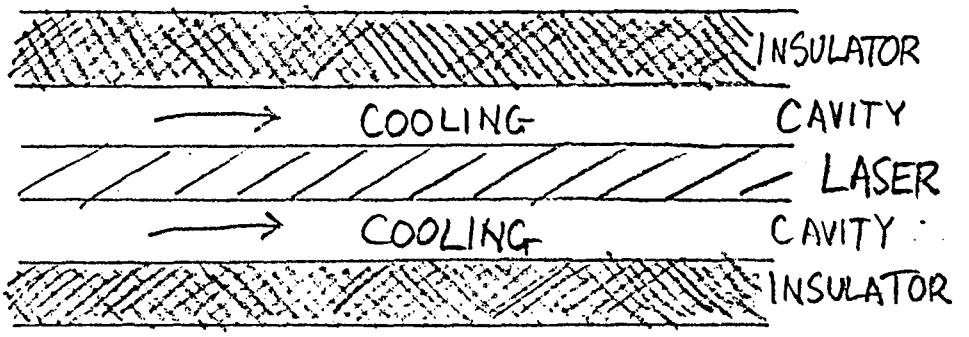

Figure 3.9

A REVIEW OF LASER-PUMPED INFRARED LASERS

Kwan-Yu Chen*
Department of Astronomy
University of Florida
Gainesville, Florida 32611

In this paper, we review the lasing mechanisms of molecules that have demonstrated laser action in the laboratories with laser emissions in the spectral range from 3 to 35 microns. This topic is germane to the workshop because a list of lasants and laser mechanisms will be defined. The pumping sources for these lasers are mainly infrared lasers; however, the case in which excitation of bromine atoms at 2.71 μm by a flashlamp as energy input is also included in the review. A conceptual drawing of lasing mechanisms is shown in figure 4.1. Here three pumping mechanisms are shown, the first being the direct-pumped system in which the lasant molecule absorbs the infrared radiation from pump laser directly, and it is excited into the upper laser level from the ground state. The second system is the indirect-pumped system where the infrared-pump laser first excites an absorbing molecule which stores its vibrational energy. Through collision this energy is transferred to the lasant molecule, populating the upper laser level. In the third system, i.e. in a Br_2-CO_2 mixture, a flashlamp replaces the infrared laser as the pump source for the absorbing molecule.

For more than a decade, surveys of infrared gas-laser systems have been made with the technique of laser pumping. The experimental results

*NASA-ASEE Fellow, 1985 summer
NASA Langley Research Center

provide a broad understanding of basic lasing mechanisms of those molecules. The lasing mechanism of a molecule excited by laser input could be the same for blackbody pumping. Thus one could look for new blackbody lasants by examinations of laser-pumped laser mechanisms. The physical properties (masses, potentials, structures) of these molecules that relate to their vibrational-rotational energies can be examined more closely. From the study of published results and physical properties, general trends might lead to new lasant materials, and/or help to evaluate the physical behaviors of these molecules in the case of blackbody pumping.

Table 4.1 lists various systems that are reviewed. The pumping input was provided by pulsed energy in all systems with the exception of the continuous-wave input for the DF-CO_2 mixture.

Before we consider each individual system, we examine some sample molecular spectra which are important for the understanding of molecular absorption and emission. Figure 4.2 shows the low-dispersion and the high-dispersion absorption band of HCℓ [1,2]. In laser pumping, individual rotational lines can be selectively pumped in the absorbing molecule. However, for blackbody pumping a broad spectral band would contribute to the absorption. The difference between a fundamental absorption band of the bending mode (010) and that of the asymmetric stretching mode (001) of CO_2, is shown in figure 4.3 [2]. Note the many possible vibrational-rotational lines that can absorb. Figure 4.4 shows the difference between the absorption band of CO (diatomic) [3] and that of SF_6 (seven-atomic) [2]. As indicated for SF_6, it is much more difficult to know what particular vibrational-rotational line is really absorbing; in case of blackbody pumping, however, the whole band would be involved in absorption.

Now we examine specific laser pumped systems. Figure 4.5 shows the lasing processes of the direct-pumped CO_2 and N_2O laser [4,5]. Both CO_2 and N_2O are linear molecules; the wavelengths of the pumping and laser energies for the two systems are very similar; and they were both excited from the ground states to the (001) states with laser transitions from (001) to (100). Yet there are basic differences between the two molecules: CO_2 belongs to the point group of $D_{\infty h}$ while N_2O belongs to that of $C_{\infty v}$; the (100) state of CO_2 is infrared inactive while that of N_2O is infrared active. The difference in their laser efficiencies reported later is basically due to the difference in structures of these two molecules, CO_2 being symmetric and N_2O not. Figure 4.6 shows the absorption of CO_2 and emission of N_2O in an indirect-pumped N_2O laser [6]. The physical processes of an indirect-pumped CO_2 laser [7] emitting at 9.6 and 16 μm, and of a direct-pumped $^{12}C^{18}O_2$ laser [8] with six lasing lines are shown in figure 4.7. Figure 4.8 shows transitions of lasing CO_2 (using several oxygen isotopes) in another direct-pumped laser [9], and also its output wavelengths. Essentially, these two figures indicate that a molecule could lase at various wavelengths with selective line pumpings; but the picture would be quite different in broad-band blackbody pumping. Wang et al. [10] reported the first CW indirect-pumped CO_2 laser in a DF-CO_2 system. Kildal and Deutsch [11] reported five indirect-pumped systems each with one of five lasing molecules (4 triatomic and 1 four-atomic), and two direct-pumped systems with two of these triatomic molecules. In 1976, they reported these systems with improved performance, and another indirect-pumped system with five-atomic molecules [12]. Their 1976 work is presented in figure 4.9. The laser transitions of these molecules and the

laser performances are shown; especially interesting are the list of laser efficiencies, the variety of pressures at which the laser actions of different molecules were operated, and the minimum threshold energy needed for laser actions. Under the similar conditions, a non-linear molecule needed a higher threshold than a linear molecule. It is also noted that in the CO-C_2H_2 mixture, vibrational energy was transferred to the infrared-inactive mode (01000) of C_2H_2.

A direct-pumped NH_3 laser was reported by Chang and McGee [13]. The relevant vibrational-rotational states are shown in figure 4.10. Jacobs et al. [14] obtained ten laser wavelengths ranging from 6.27 μm to 35.50 μm. Danielewicz et al. [15] obtained laser lines of NH_3 in the 11-13 μm region. Fry (1976) observed forty-two laser lines in NH_3 ranging from 9.3 to 13.82 μm with direct laser pumping. Figure 4.11 shows the observed laser lines of ammonia and of ethylene by Chang and McGee[16]. The direct-pumped SF_6, an example of a seven-atom molecule, was excited by a laser input. Figure 4.12 shows the two-photon pumping model and a limited range of operating pressures for laser pumped SF_6[18].

Petersen et al. [19] obtained laser actions in CO_2, N_2O, and HCN, each mixed with Br_2. The energy from a flashlamp excited the bromine atom, Br*, which transfers energy to the lasing molecule through electronic-vibrational processes. They [20] also observed laser emission wavelengths of 4.3 μm and 14.1 μm in addition to 10.6 μm from the CO_2; these laser transitions are shown in figure 4.13. Petersen et al. [21]observed lasings of NO and H_2O in the Br*-NO system and the Br*-H_2O system, respectively. They also observed the lasing of N_2O in a Br_2-CO_2-N_2O mixture as well as in a Br_2-HCℓ-N_2O mixture. In these cases indirect-pumping of N_2O was achieved by vibrational-vibrational energy transfer vis CO^2 or HCℓ. Figure 4.14

illustrates both the electronic-vibrational transfers and the electronic-vibrational-plus-vibrational-vibrational transfer of energy.

A plot of observed laser efficiency vs. quantum efficiency for different laser systems is shown in figure 4.15. This could indicate, in part, the system performance limitations for these systems at the present time. Recently, a blackbody direct-pumped CO_2 laser has approached 25 percent efficiency [22]. This is close to the 30-34 percent laser-pumped efficiency.

To pursue the question of vibrational energy of a new complex molecule, let us take a look at the molecular structures of the lasing molecules mentioned above. Figures 4.16, 4.17, and 4.18 show the structures of linear, symmetric-top, asymmetric-top, and spherical-top molecules. The number listed under each molecule are its fundamental vibrational wavenumbers. The line under a number indicates that the particular mode is infrared inactive. Since the vibrational energies of a molecule relate closely to its structure, scientists have for years analyzed the observed infrared spectra of complex molecules to determine the molecular structures. Correlation charts between infrared spectra and structure units (specific grouping) have been published. The charts given in the book entitled "The Infra-red Spectra of Complex Molecules" [23] are presented in figure 4.19a-e for reference. (It should be noted also that the detailed infrared correlation charts are published in "Handbook of Chemistry and Physics" [24]). These charts could guide us in the search for complex molecules as potential lasant materials in the desired spectral regions.

Finally, figure 4.20 shows where in the periodic table of elements the atoms of the lasing molecules are located. Probably one is not surprised to see the limited location since these molecules have low boiling points, i.e. gaseous phase at room temperature.

A summary and some concluding remarks are listed as follows:

1. Laser actions in twelve molecules--1 diatomic, 6 triatomic, 2 four-atomic, 1 five-atomic, 1 six-atomic, and 1 seven-atomic, are reviewed. They are linear, symmetric-top, asymmetric-top, or spherical-top molecules.

2. The wavelengths of these laser outputs are all longer than 3 microns.

3. The thresholds of the input energy for laser action in non-linear molecules would be higher than that for linear molecules.

4. The locations of the atoms of the lasing molecules are limited in the periodic table in this study.

5. Vibrational-vibrational transfer of energy is an efficient mechanism for laser action.

6. Electronic-vibrational transfer, as shown in the case of Br* → molecule, is also a mechanism that should be explored.

7. The systems reviewed here all have pulse-pumping inputs except one case of CW-pumping which gives very low laser efficiency. The major issue for blackbody pumping seems to be whether or not a sufficient excited-state density can be obtained.

8. Laser actions in NH_3 have produced many emission lines. The wavelengths of most of these lines are longer than 10 μm; thus they would not be interested in terms of power output. The observed lines of 6.27 and

6.69 μm could be of interest. With blackbody pumping, NH_3, like SF_6, would absorb in broad band. How they would lase in such a case is not yet predictable.

9. For CO_2 laser, we see that laser efficiency with blackbody pumping is close to that with laser pumping.

10. Laser pumped gas lasers can be used as an effective tool to investigate new lasants quickly.

The writer is grateful to Dr. E. Conway, Head of the Space Technology Branch, Space Systems Division, NASA Langley Research Center, and his staff, and to Professor G. Goglia of Old Dominion University, Co-Director of the NASA-ASEE 1985 Summer Faculty Fellowship Program at NASA/LaRC for their support. He would like to thank Dr. R. De Young for invaluable aids to many aspects of the summer project.

REFERENCES

1. Herzberg, G.: Spectra of Diatomic Molecules, p. 53 (D. Van Nostrand Co., Inc.: New York). 1950.

2. Straughan, B. P., and Walker, S., Editors: Spectroscopy, vol. 2, pp. 178, 182-184, (Chapman and Hall: London). 1976.

3. Horak, M., and Vitek, A.: Interpretation and Processing of Vibrational Spectra, p. 23 (John Wiley & Sons: New York). 1978.

4. Chang, T. Y., and Wood, O. R.: "Optically Pumped Atmospheric-Pressure CO_2 Laser," Appl. Phys. Lett. 21(1), 19-21. 1972.

5. Chang, T. Y. and Wood, O. R.: "Optically Pumped N_2O Laser," Appl. Phys. Lett. 22(3), 93-94. 1973.

6. Chang, T. Y. and Wood, O. R.: "Optically Pumped 42-Atm N_2O Laser," Appl. Phys. Lett. 24(4), 182-183. 1974.

7. Osgood, R. M.: "Optically Pumped 16-μm," Appl. Phys. Lett. 28(6), 342-345. 1976.

8. Buchwald, M. I., Jones, C. R., Fetterman, H. R., and Schlossberg, H. R.: "Direct Optically Pumped Multiwavelength CO_2 Laser," Appl. Phys. Lett. 29(5), 300-302. 1976.

9. Drozdowicz, Z., Rudko, R. I., Linhares, S. J., and Lax, B.: "High Gain 4.3-4.5 μm Optically Pumped CO_2 Laser," IEEE Journ. Quantum Electron. QE-17(8), 1574-1580. 1981.

10. Wang, J. H. S., Finzi, J., and Mastrup, F. N.: "CW Optically Resonance Pumped Transfer Laser in DF-CO_2 System," Appl. Phys. Lett. 31(1), 35-37. 1977.

11. Kildal, H., and Deutsch, T. F.: "Optically Pumped Infrared V-V Transfer Lasers," Appl. Phys. Lett. 27(9), 500-502. 1975.

12. Kildal, H., and Deutsch, T. F.: "Optically Pumped Gas Lasers," in Tunable Lasers and Applications, eds. A. Mooradian, T. Jaeger, and P. Stokseth, pp. 367-377 (Springer-Verlag: New York). 1976.

13. Chang, T. Y., and McGee, J. D.: "Laser Action in 12.812 μm in Optically Pumped NH_3," Appl. Phys. Lett. 28(9), 526-528. 1976.

14. Jacobs, R. R., Prosnitz, D., Bischel, W. K., and Rhodes, C. K.: "Laser Generation from 6 to 35 μm Following Two-Photon Excitation of Ammonia," Appl. Phys. Lett. 29(11), 710-712. 1976.

15. Danielewicz, E. J., Malk, E. G., and Coleman, P. D.: "High-Power Vibration-Rotation Emission from $^{14}NH_3$ Optically Pumped Off Resonance," Appl. Phys. Lett. 29(9), 557-559. 1976.

16. Chang, T.Y., and McGee, J. D.: "Off-Resonant Infrared Laser Action in NH_3 and C_2H_4 Without Population Inversion," Appl. Phys. lett. 29(11), 725-727. 1976b.

17. Fry, S. M.: "Optically Pumped Multi-Line NH_3 Laser," Optics Comm. 19(3), 320-324. 1976.

18. Barch, W. E., Fetterman, H. R., and Schlossberg, H. R.: "Optically Pumped 15.90 μm SF_6 Laser," Optics Comm., 15(3), 358-360. 1975.

19. Petersen, A. B., Wittig, C., and Leone, S. R.: "Infrared Molecular Lasers Pumped by Electronic-Vibrational Energy Transfer from $Br(4^2P_{1/2})$: CO_2, N_2O, HCN, and C_2H_2," Appl. Phys. Lett. 27(5), 305-307. 1975.

20. Petersen, A. B., Wittig, C., and Leone, S. R.: "Electronic-to-Vibrational Pumped CO_2 Laser Operating at 4.3, 10.6, and 14.1 μm," Journ. Appl. Phys. 47(3), 1051-1054. 1976.

21. Petersen, A. B., Braverman, L. W., and Wittig, C.: "H_2O, NO, and N_2O Infrared Lasers Pumped Directly and Indirectly by Electronic-Vibrational Energy Transfer," Journ. Appl. Phys., 48(1), 230-233. 1977.

22. Christiansen, W.: "Blackbody-pumped Co_2 laser at University of Washington," private comm. 1985.

23. Bellamy, L. J.: The Infra-red Spectra of Complex Molecules. 3rd ed. (Chapman and Hall: London). 1975.

24. Weast, R. C., Editor: Handbook of Chemistry and Physics, 55th ed., pp. F224-F232, (CRC Press: Cleveland). 1974.

I. Direct-pumped by laser

Lasing molecule	Wavelength of laser output, μm
CO_2	10.6, 4.35, 17.46
CS_2	6.6
OCS	19.
NH_3	12.8, 11.46-12.81, 6-35, 12.08, 9.3-13.8
SF_6	15.9
C_2H_4	10.53
N_2O	10.8

II. Indirect-pumped by laser

Intermediate molecule	Lasing molecule	Wavelength of laser output, μm
CO_2	N_2O	10.9
CO	OCS	8.3
CO	CO_2	10.6
CO	N_2O	10.9
CO	C_2H_2	8.
CO	CS_2	11.5
CO	SiH_4	7.95
HBr	CO_2	16
DF	CO_2	10.6

III. Pumped by flash lamp, electronic-vibrational energy transfer from $Br(4^2P_{1/2})$

Lasing molecule (mixed with Br_2)	Wavelength of laser output, μm
CO_2	10.6
HCN	3.85, 8.48
NO	5.5
H_2O	7.09-7.74
N_2O (V-V transfer from CO_2 or HCℓ)	10.9

Table 4.1 List of molecules and lasing wavelengths.

I. Direct-Pumped System

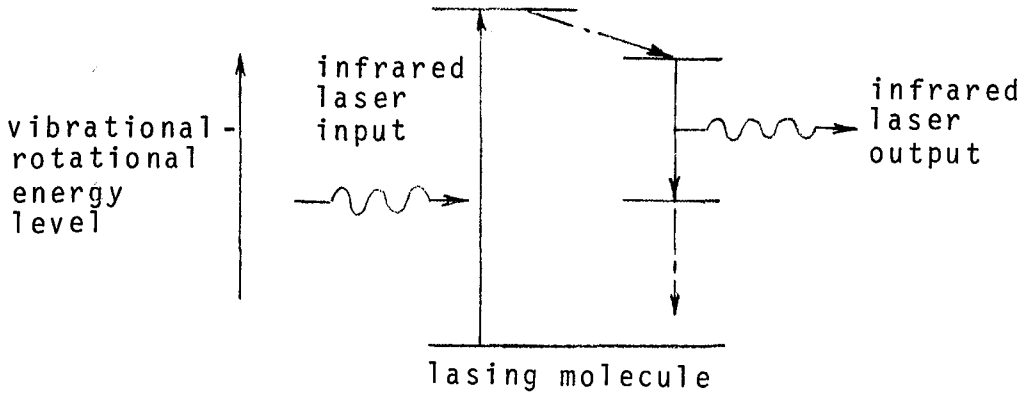

II. Indirect-Pumped System

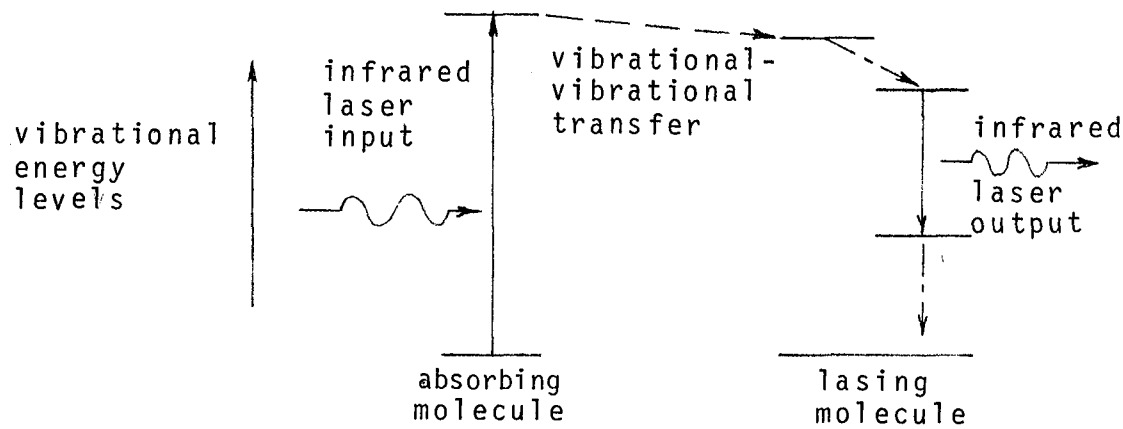

III. Flashlamp-Pumped System

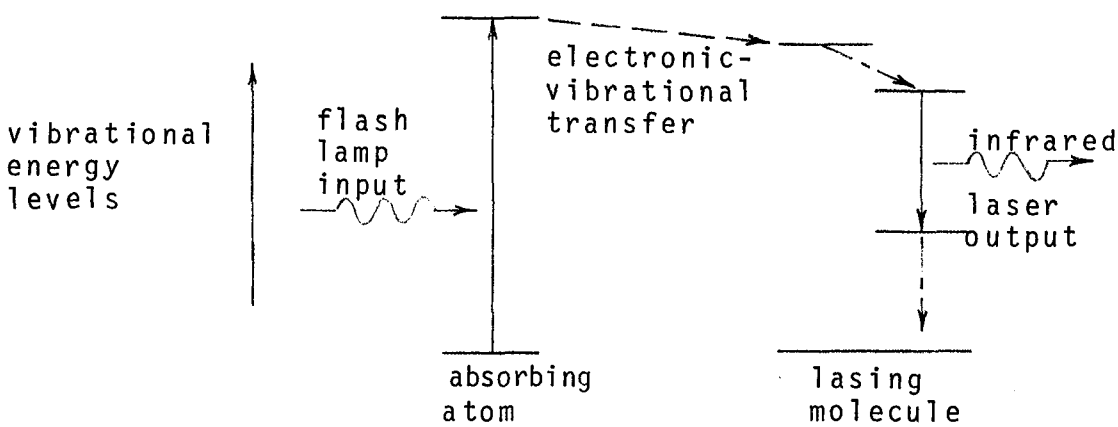

Fig. 4.1 Basic laser concept.

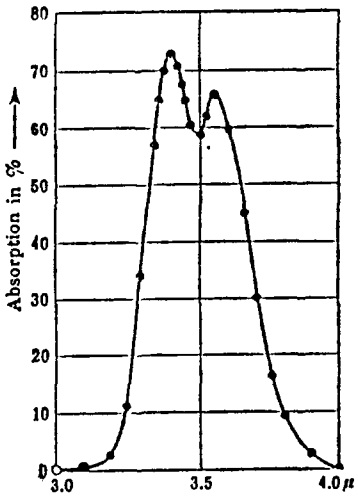

FIG. 30. Fundamental Absorption Band of HCl in the Near Infrared [after Burmeister (148)]. With the dispersion used, the band has two maxima (Bjerrum double band). With larger dispersion, a further resolution is observed (Fig. 32).

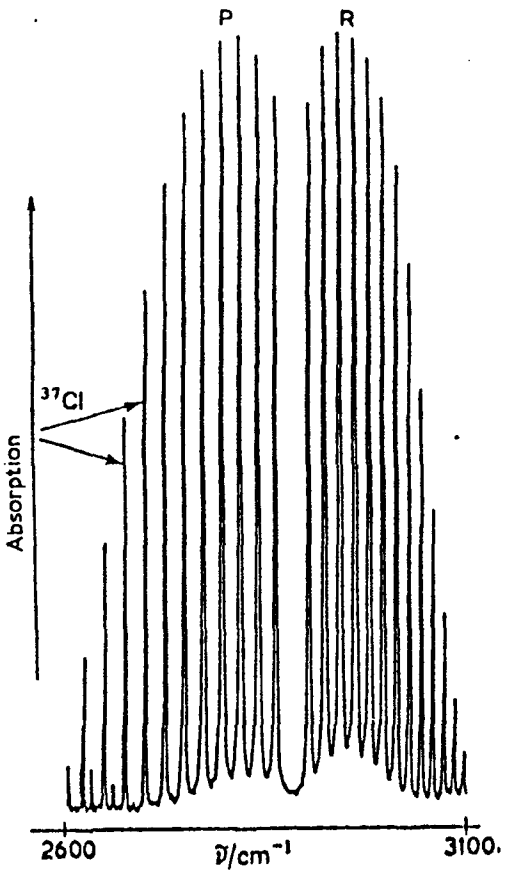

Fig. 4.19 The 1←0 transition of HCl (gas pressure 26 cm Hg in a 10-cm cell), showing the P- and R-branches. The shoulder on the low wavenumber side of each rotational line is due to the ^{37}Cl isotope.

Fig. 4.2 Fundamental absorption band of HCl. (After Herzberg [1], and Straughan and Walker [2])

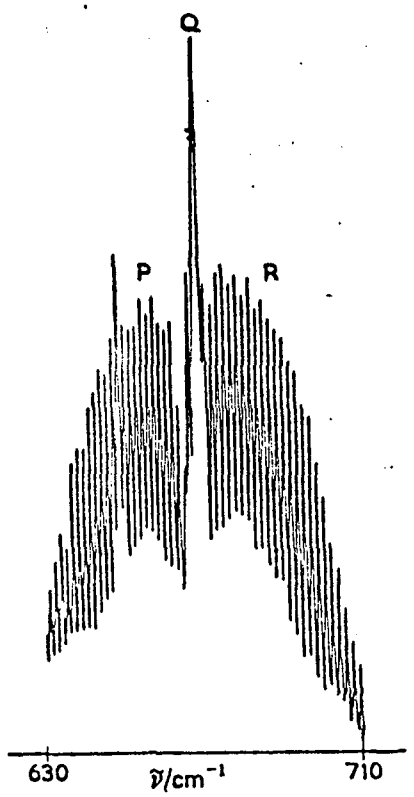

Fig. 4.22 Infrared spectrum of the CO_2 bending mode, showing the PQR structure.

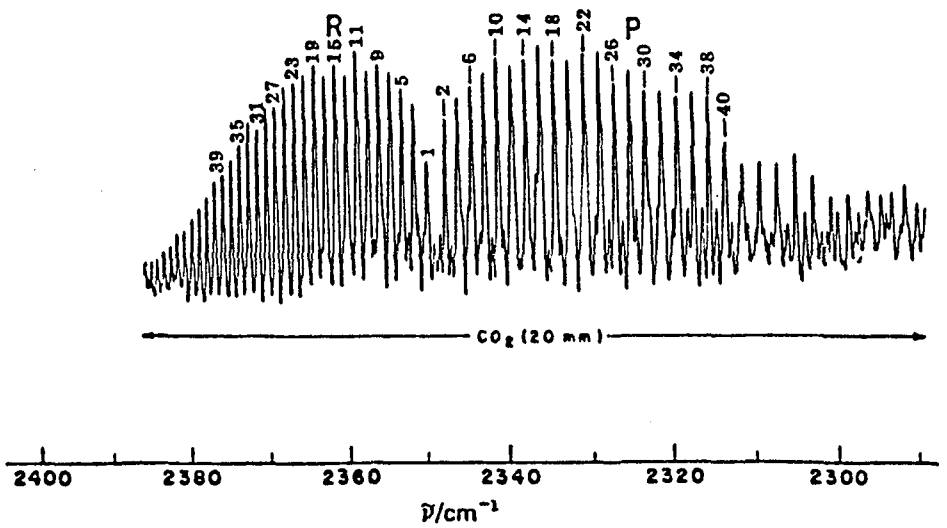

Fig. 4.23 Fine structure in the fundamental absorption band $\tilde{\nu}_3$ of CO_2. (From ref. 4.2.)

Fig. 4.3 INfrared spectra of two absorption bands of CO_2. (After Straughan and Walker [2])

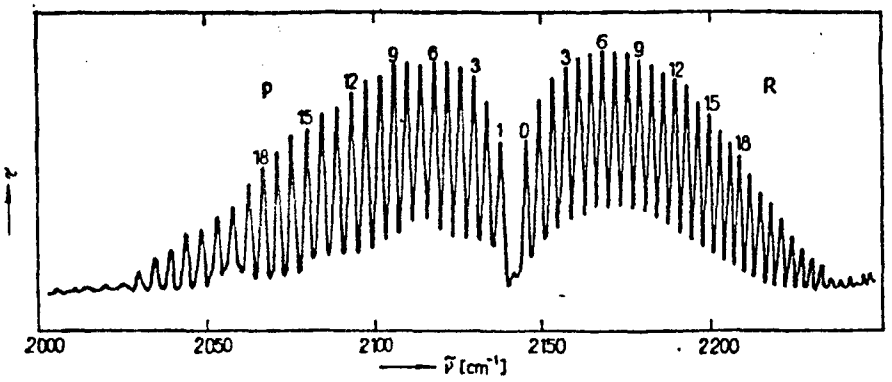

Fig. 4. Rotational-vibrational $v_{1\leftarrow 0}$ band for carbon monoxide CO from the experimental infrared spectrum. The bands in the R- and P-branches are numbered by the rotational quantum numbers of the initial rotational states. The Q-branch does not appear in this band in consequence of the selection rules.

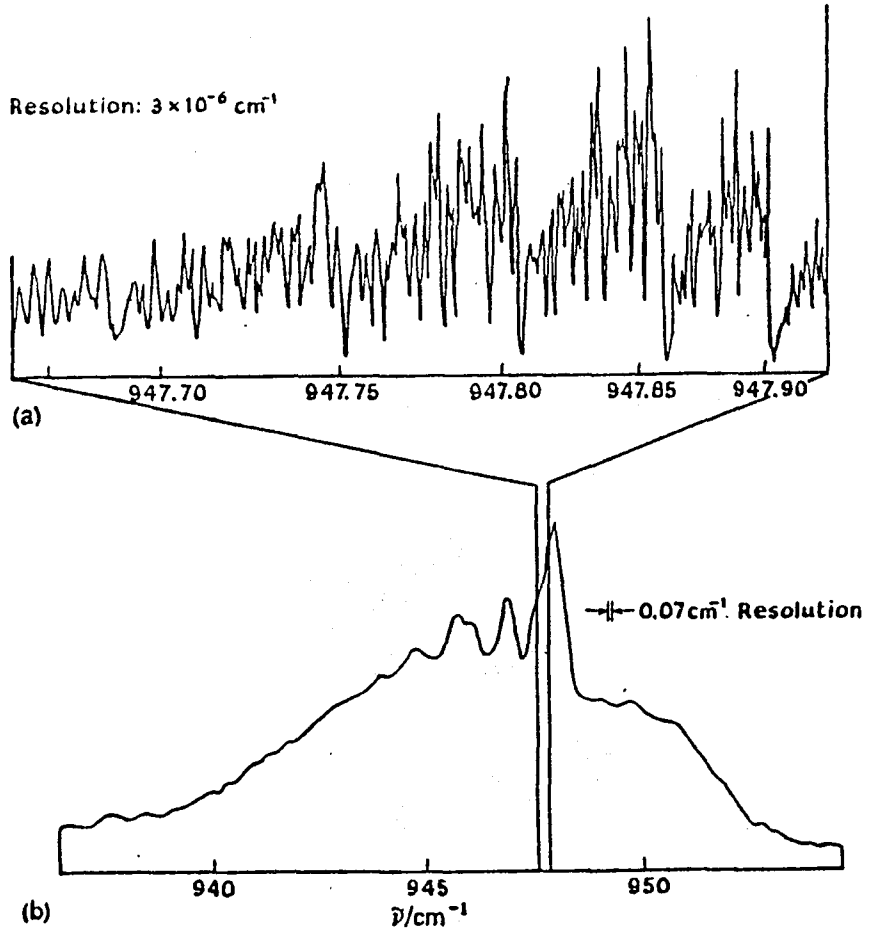

Fig. 4.21 Fine structure of the antisymmetric stretching mode of SF_6 resolved using (a) a diode laser, and (b) a grating spectrometer. (From ref. 4.8.)

Fig. 4.4 Absorption spectra of CO and SF_6. (After Horak and Vitek [3] and Straughan and Walker [2])

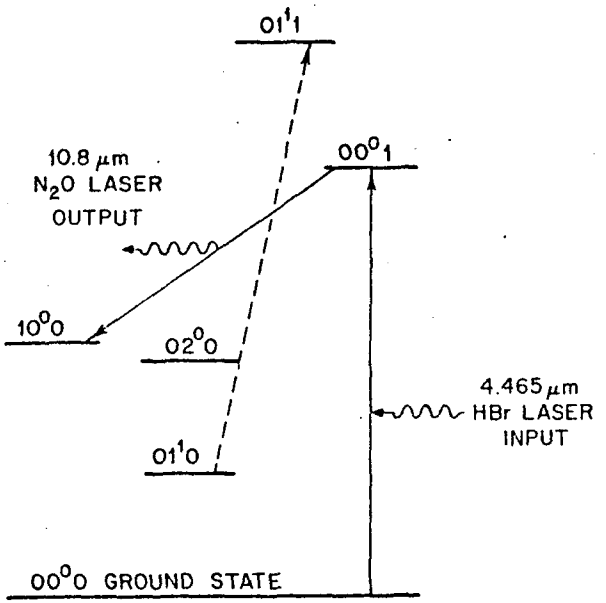

FIG. 1. Vibrational energy level diagram for N_2O (partial).

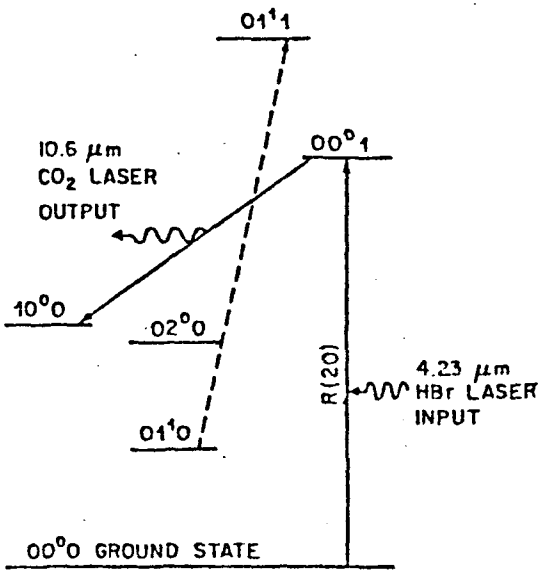

FIG. 1. Vibrational energy level diagram for CO_2 (partial).

Fig. 4.5 Direct-pumped CO_2 and N_2O lasers. (After Chang and Wood [4, 5])

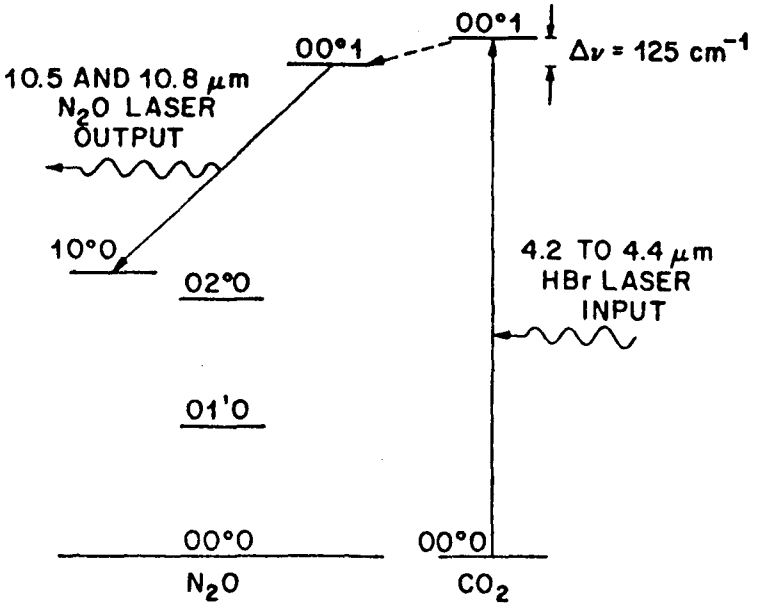

FIG. 1. Vibrational energy level diagram for N_2O and CO_2 (partial), illustrating the optical transfer laser process.

Fig. 4.6 Indirect-pumped N_2O laser. (After Chang and Wood [6])

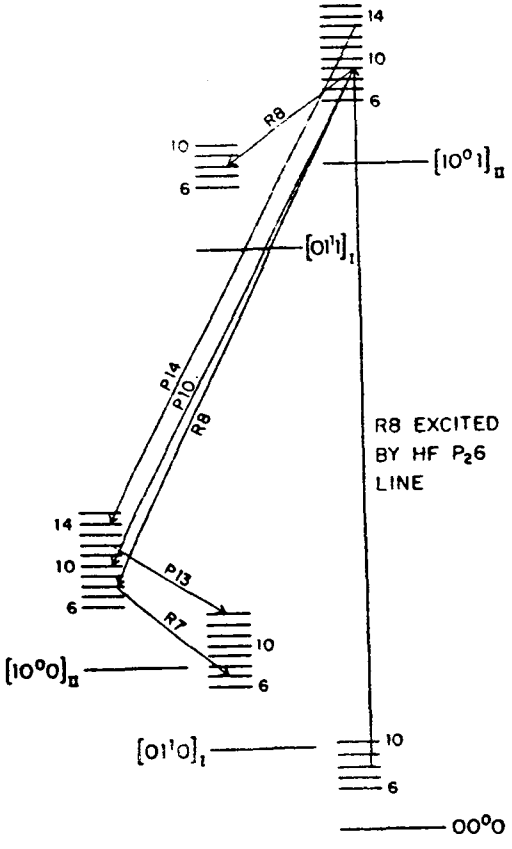

FIG. 1. Representative lasing lines from $^{12}C^{18}O_2$ pumped by P_26 line of HF laser. See text for cell pressure at which these and other lines oscillated.

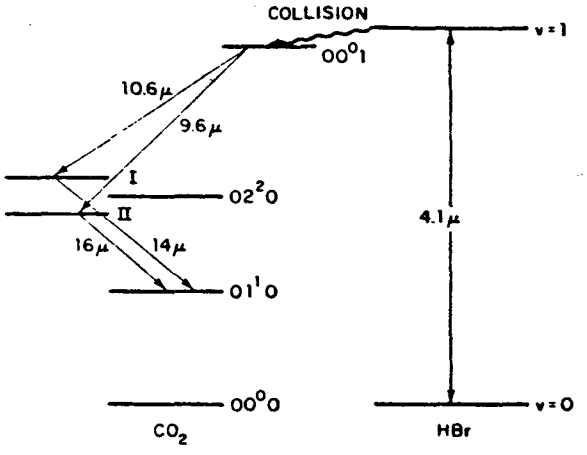

FIG. 1. Simplified vibrational-energy-level diagram of CO_2 and HBr which summarizes physical processes involved in 16- and 14-μm CO_2 laser.

Fig. 4.7 An indirect-pumped CO_2 laser emitting at 16 μm and a direct-pumped CO_2 laser emitting at 4.3 μm. (After Osgood [7], and Buchwald et. al. [8])

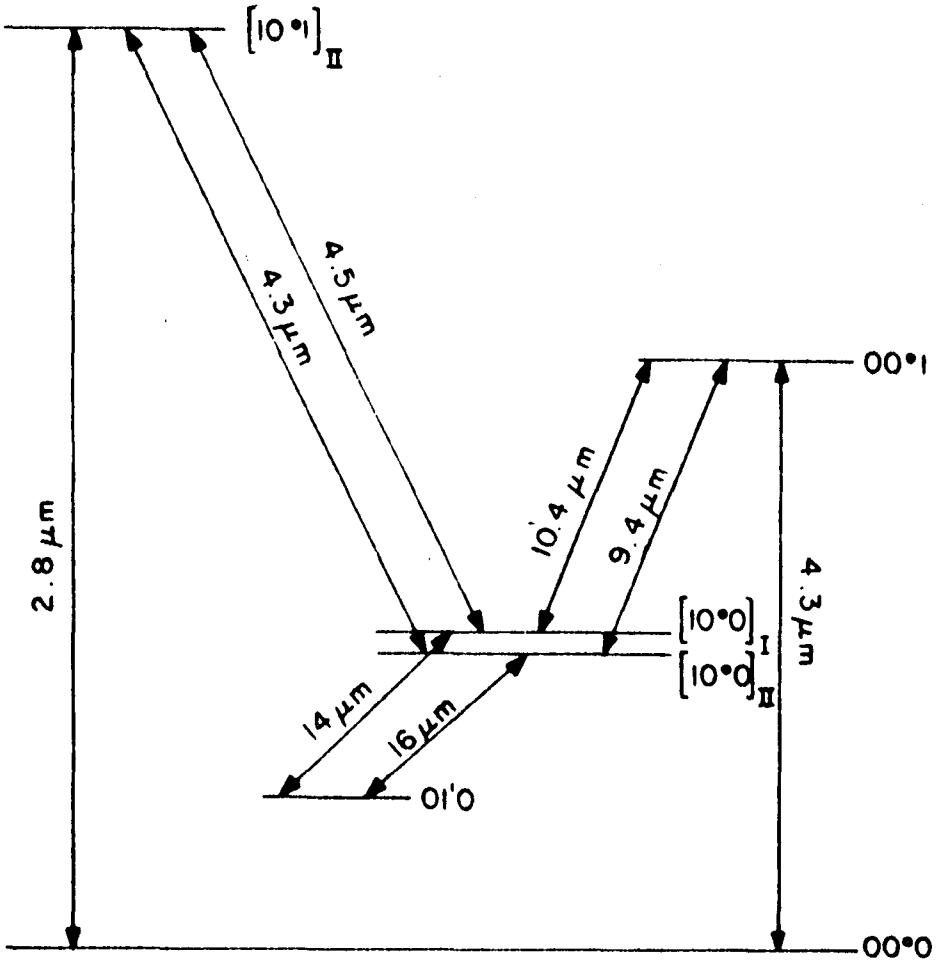

Fig. 1. Energy levels of CO_2.

TABLE I
OPTICALLY PUMPED CO_2 LASER OUTPUT WAVELENGTHS

Molecule	HF Pump Line	Output Wavelength (μm)
$^{12}C^{18}O_2$	$P_2(6)$	4.346
		4.371
$^{12}C^{16}O^{18}O$	$P_2(5)$	4.314
		4.340
$^{13}C^{16}O^{18}O$	$P_2(5)$	4.473
	$P_2(8)$	4.528

Fig. 4.8 A direct-pumped CO_2 laser. (After Drozdowicz et. al. [9])

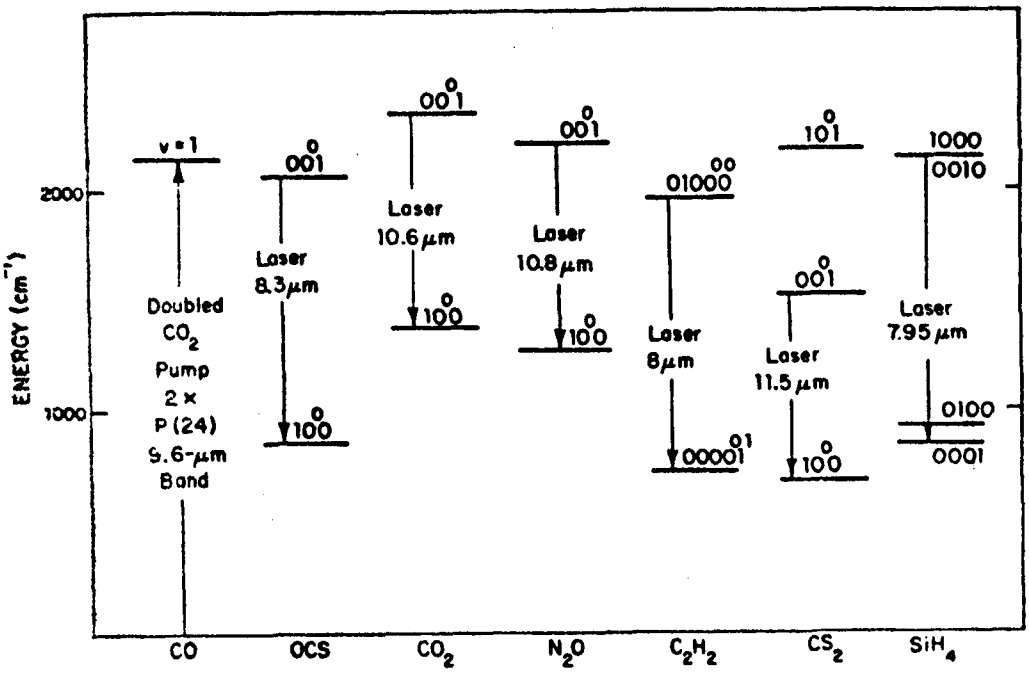

Fig. 3. Simplified energy level diagram for CO and the molecules pumped by nearly resonant energy transfer

Table I

Summary of performance of optically pumped lasers

System	Maximum Pressure (Torr)*	Minimum Threshold		Maximum Efficiency (Percent)	Maximum Output (mJ)
		Focused (mJ)	Unfocused (mJ)		
OCS (direct-pumped)	55	0.1	0.6	19.0	5.2
CO-OCS	420	0.1	1.0	7.6	1.3
CO-CO_2	12,400 (16.3 atm)	-	1.6	34.0	13.0
CO-C_2H_2	610	-	2.0	3.5	0.12
CO-CS_2 (11.5 μm)	20	-	2.5	0.5	0.03
CS_2 (6.6 μm)	25	-	6.3	0.1	0.03
CO-SiH_4	35	1.7	-	0.6	0.03

*With H_2 or He buffer

Fig. 4.9 Eight laser systems. (After Kildal and Deutsch [12])

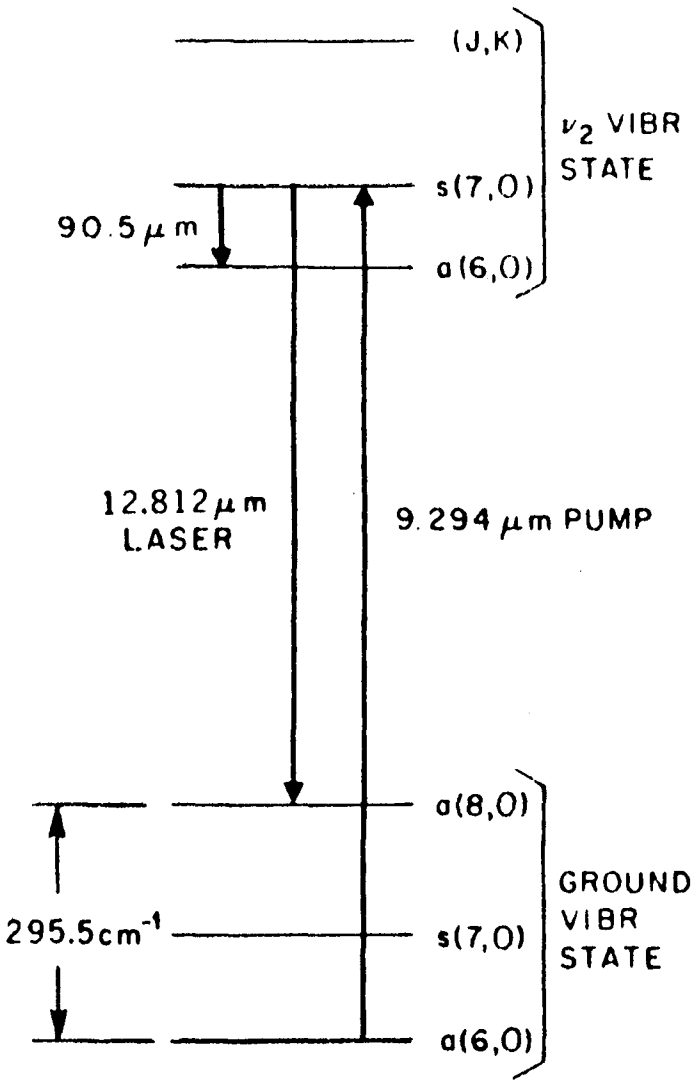

FIG. 1. Relevant energy levels of NH_3 for the 12.812-μm laser.

Fig. 4.10 The transitions of NH_3. (After Chang and McGee [13])

TABLE I. Summary of observed laser lines.

Gas	Vib. band	Emission line (μm)	Absorption line (μm)	CO_2 line	$\nu_p - \nu_a$ (cm^{-1})	$\nu_p - \nu_e$ (cm^{-1})	Rel. pol.	Opt. p (Torr)	Thresh. ϵ_p (J)
NH_3	ν_2	$sP(7,0)$-12.08	$sR(5,0)$-9.22	$R(30)$	0.026 [a]	256.9	∥	1.2	0.09
	ν_2	$aP(8,0)$-12.812	$aR(6,0)$-9.29	$R(16)$	−0.021 [a,b]	295.5	∥	5	0.08
	ν_2	$aP(3,1)$-11.46	$aR(1,1)$-10.29	$R(14)$	0.048 [c]	99.3	∥	2	0.09
	ν_2	$sP(6,4)$-11.80	$sQ(5,4)$-10.35	$R(6)$	−0.012 [c]	118.7	⊥	0.8	0.12
	ν_2	$aP(6,3)$-12.28	$aQ(5,3)$-10.72	$P(32)$	−0.032 [c]	118.7	⊥	1.2	0.09
C_2H_4	?	10.98	10.27	$R(16)$		62.2	⊥	3—5	0.12
	ν_7 or	$^RP(10,2)$-10.53 $^RQ(10,0)$	$^RQ(9,2)$-10.32 $^RR(9,0)$	$R(10)$		19.7	⊥	2	0.11

[a] From Ref. 7. [b] From Ref. 6. [c] From Ref. 8.

Fig. 4.11 Observed laser lines of ammonia and ethylene.
(After Chang and McGee [16])

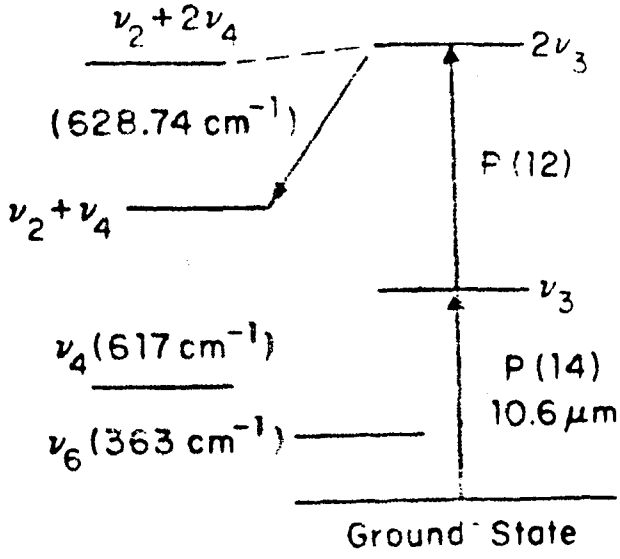

Fig. 3. Energy level diagram showing the proposed two-photon pumping model.

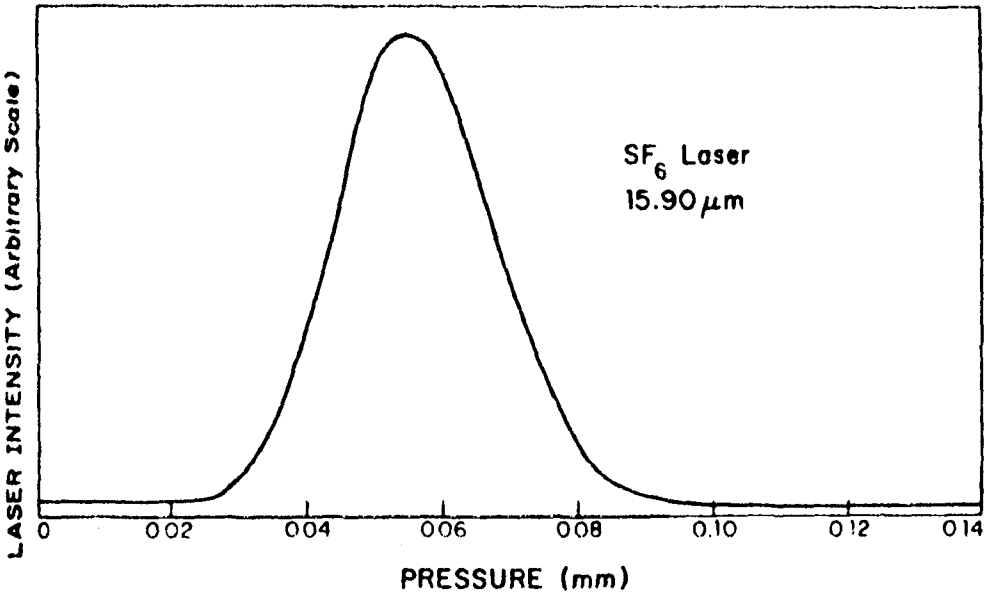

Fig. 2. SF_6 laser power versus pressure. The vertical axis is the output of a boxcar integrator while a capacitive manometer drove the horizontal axis.

Fig. 4.12 The transitions of SF_6 and the laser operating pressures. (After Barch et. al. [18])

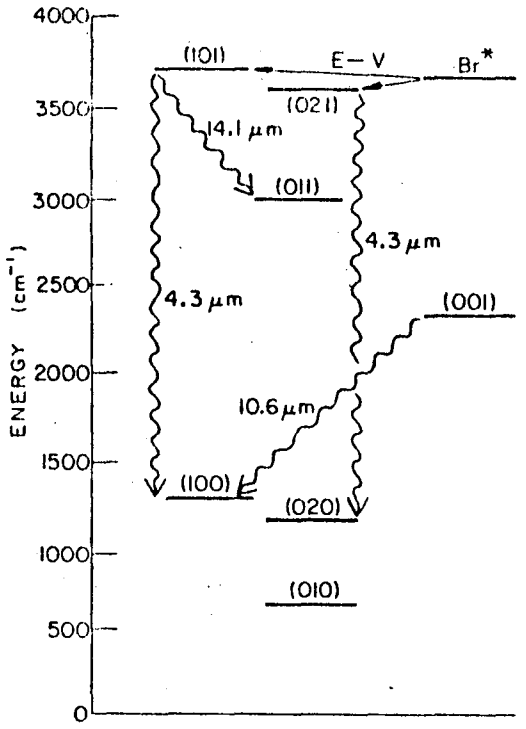

FIG. 3. Simplified energy-level diagram of the Br*-CO_2 system showing E-V energy-transfer path and laser transitions.

Fig. 4.13 A Br*-CO_2 system. (After Petersen et. al. [20])

Peterson et al. (1975) Peterson et al. (1977)

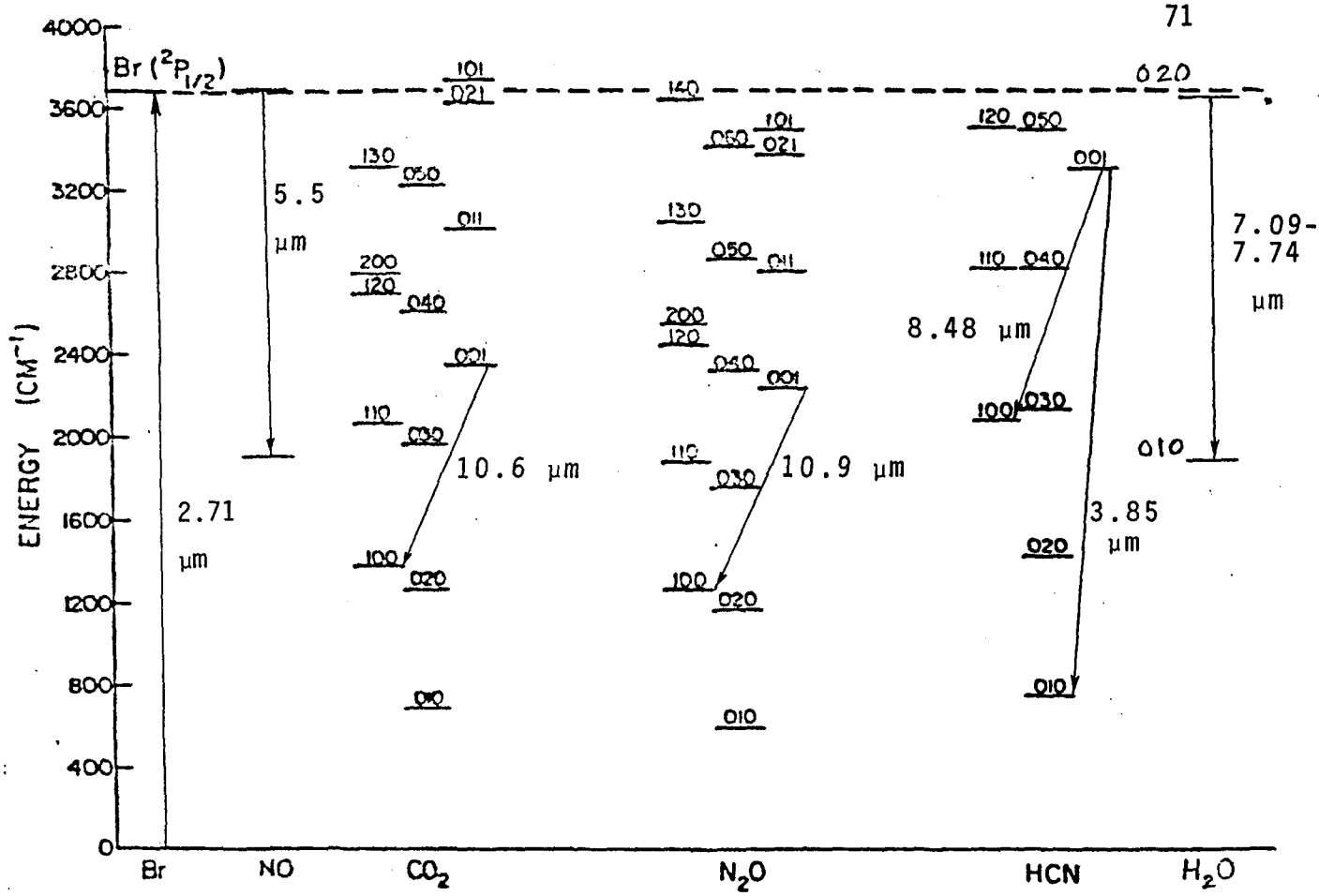

FIG. 1. Partial energy level diagram showing the first excited spin-orbit state of bromine and vibrational states of four poly- atomic molecules. For simplicity, vibrational angular momentum quantum numbers have been omitted,

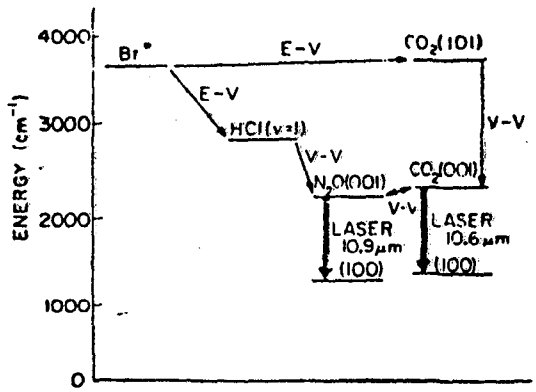

FIG. 2. Simplified energy-level diagram of the Br*-N_2O laser system. Energy transfer processes are shown, which are important in the indirect pumping of N_2O via HCl or CO_2.

Fig. 4.14 Laser transitions with electronic-vibrational transfer of energy from Br*. After Petersen et. al. (After Petersen et. al. [19] and Petersen et. al. [21])

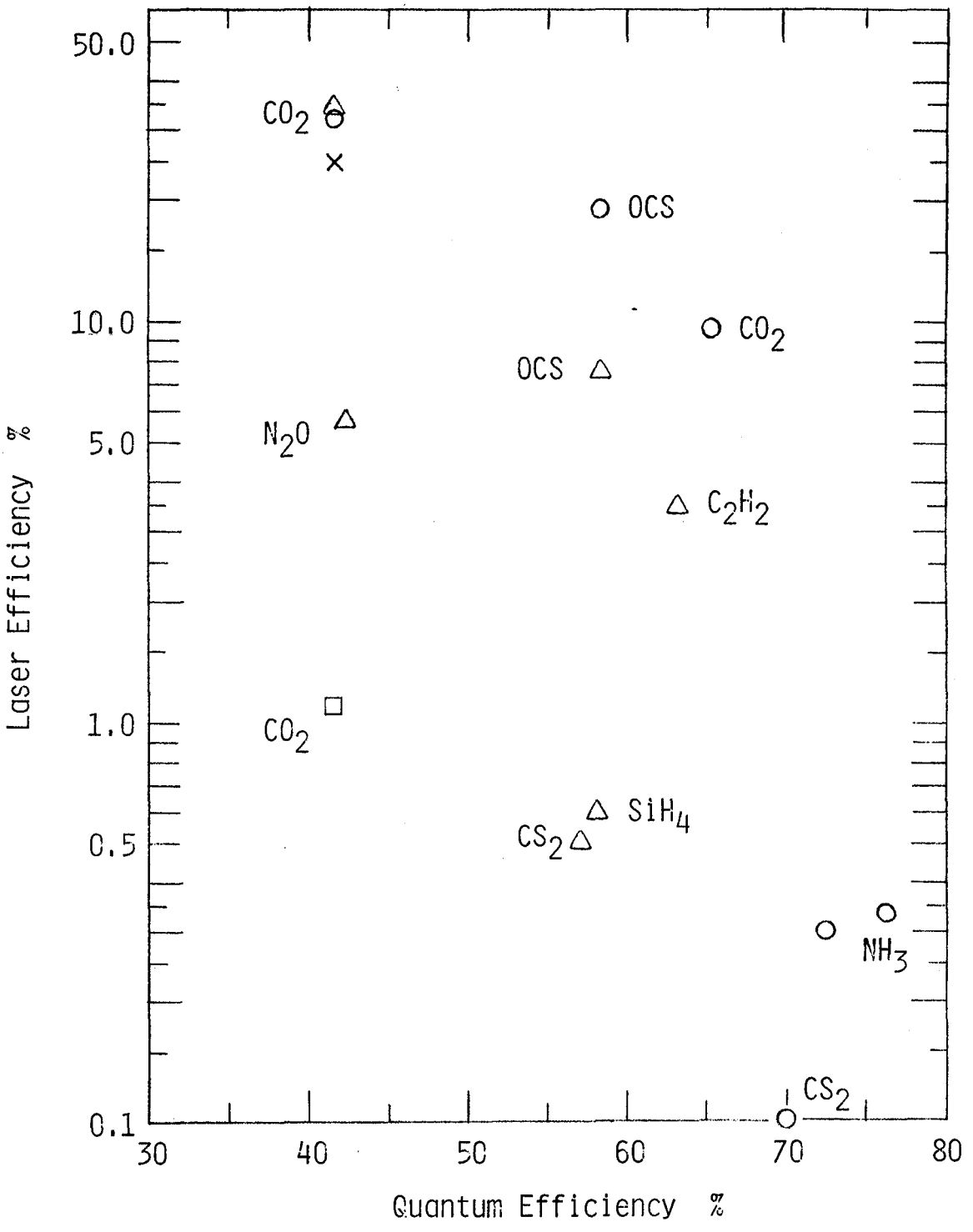

Fig. 4.15 Efficiency plot; triangles represent indirect-pumped, circles direct-pumped, square CW indirect-pumped, and cross blackbody direct-pumped systems.

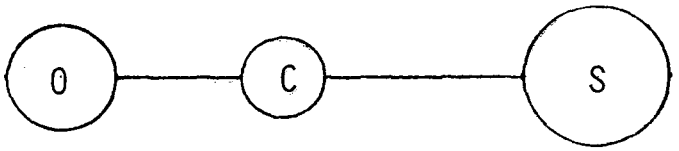

Carbonyl sulfide

859 520 2062 cm^{-1}

Linear

Acetylene

3374 1974 3287 612 729 cm^{-1}

Linear

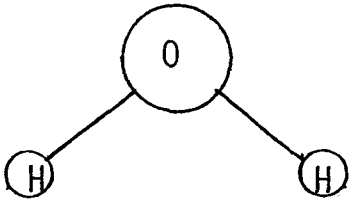

Water

3657 1595 3756 cm^{-1}

Asymmetric-top

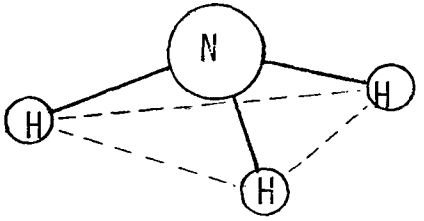

Ammonia

3337 950 3444 1627 cm^{-1}

Prolate symmetric-top

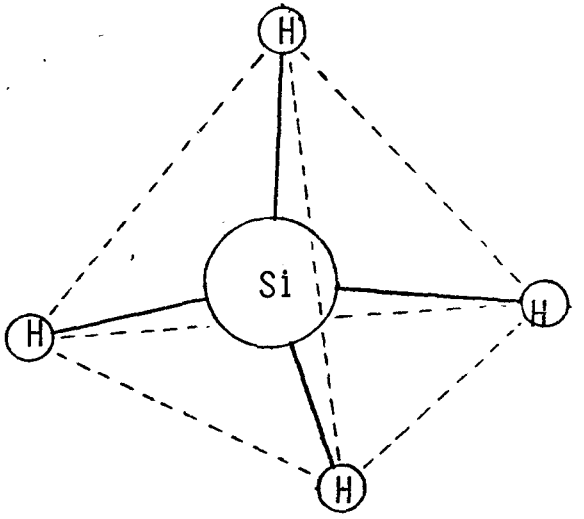

Silicane

2187 975 2191 914 cm^{-1}

Spherical-top tetrahedral

Fig. 4.16 Structures of some representative molecules.

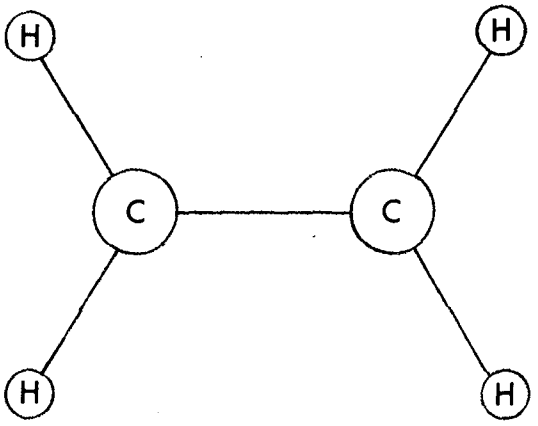

Ethylene

3026	1622	1342	1023	3102	1222	
949	943	3105	826	2989	1443	cm^{-1}

Asymmetric-top

Fig. 4.17 Molecular structure of ethylene.

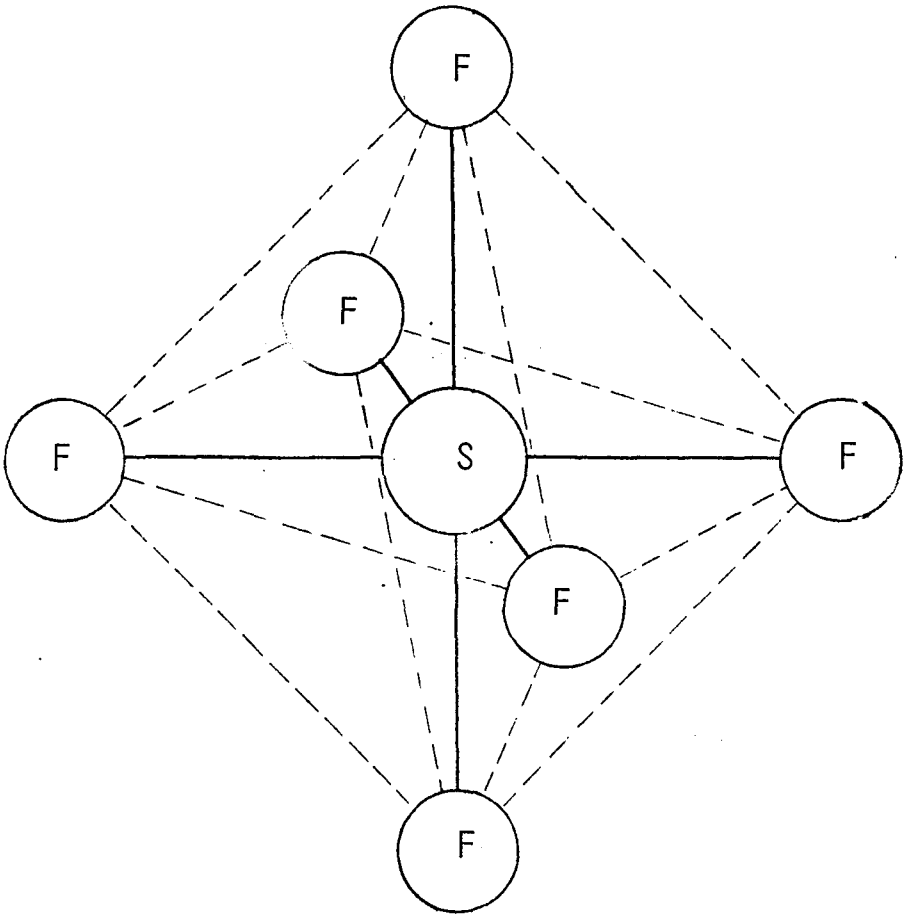

Sulfur hexafluoride

770 640 948 617 522 363

Spherical-top octahedral

Fig. 4.18 Molecular structure of sulfur hexafluoride.

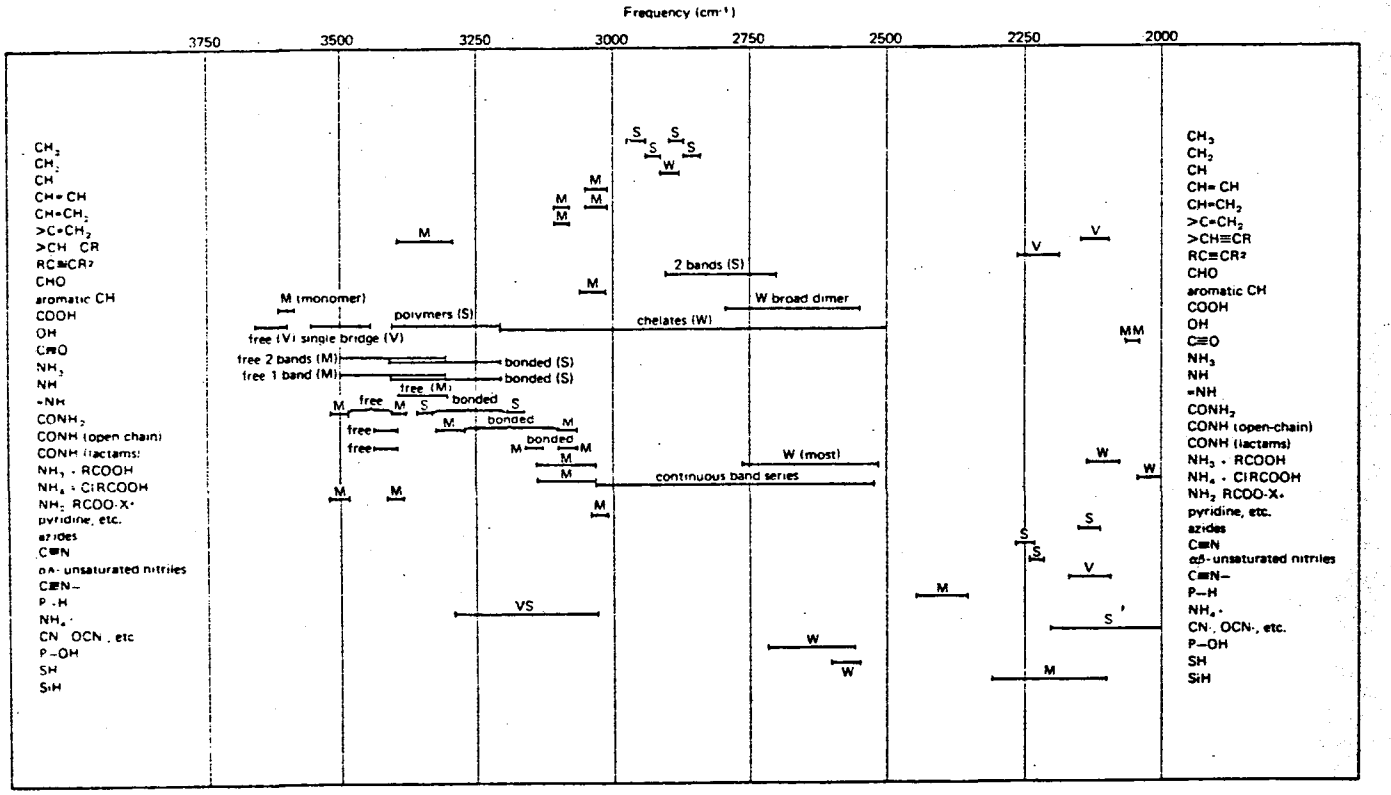

Correlation Chart No. 1. Hydrogen stretching and triple-bond vibrations. 3750—2000 cm^{-1}

Fig. 4.19a Correlation charts; S=strong, M=medium, W=weak, and V=variable. (After Bellamy [23])

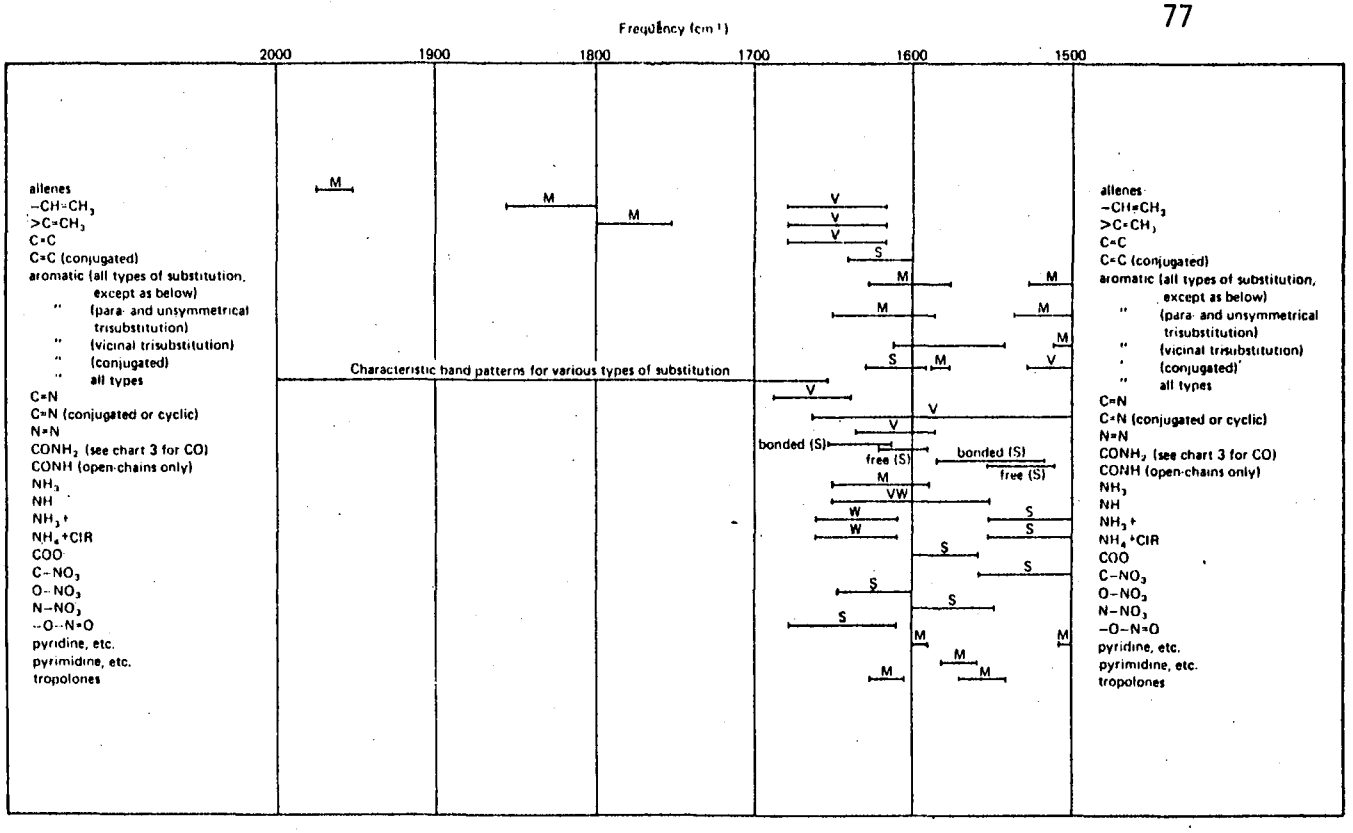

Correlation Chart No. 2. Double-bond vibrations etc. 2000–1500 cm^{-1}

Fig. 4.19b

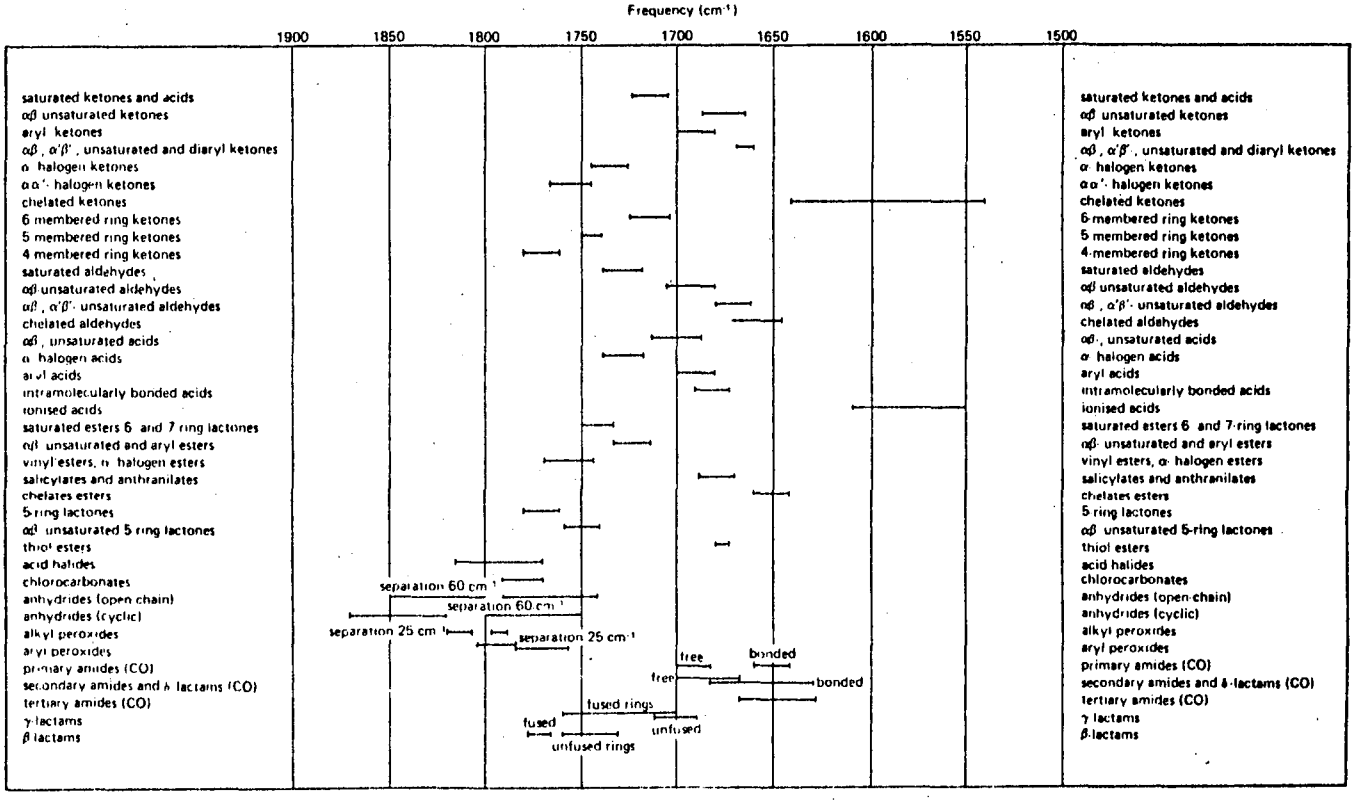

Correlation Chart No. 3. Carbonyl vibrations. 1900–1500 cm^{-1}

Fig. 4.19c

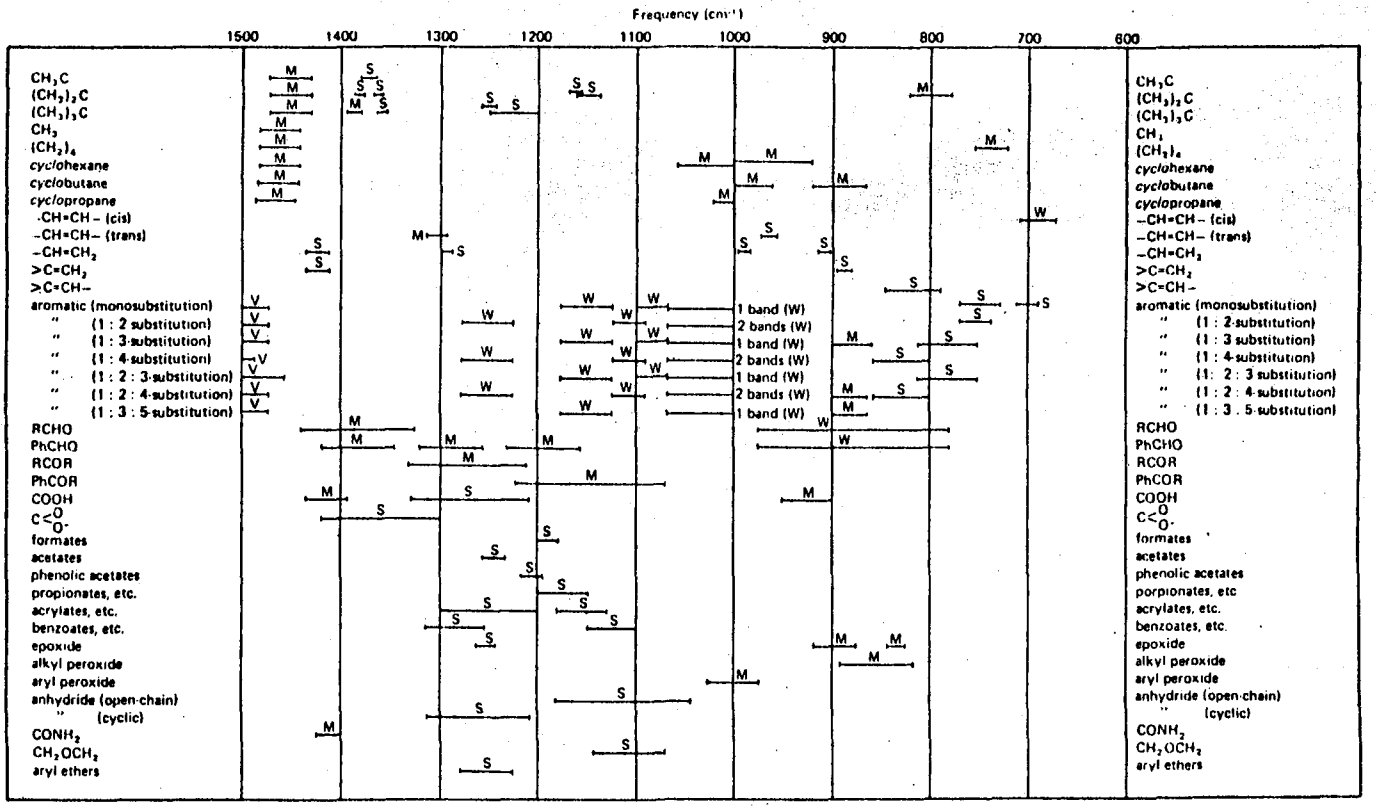

Correlation Chart No. 4. Single-bond vibrations etc. (I) 1500–650 cm^{-1}

Fig.4.19d

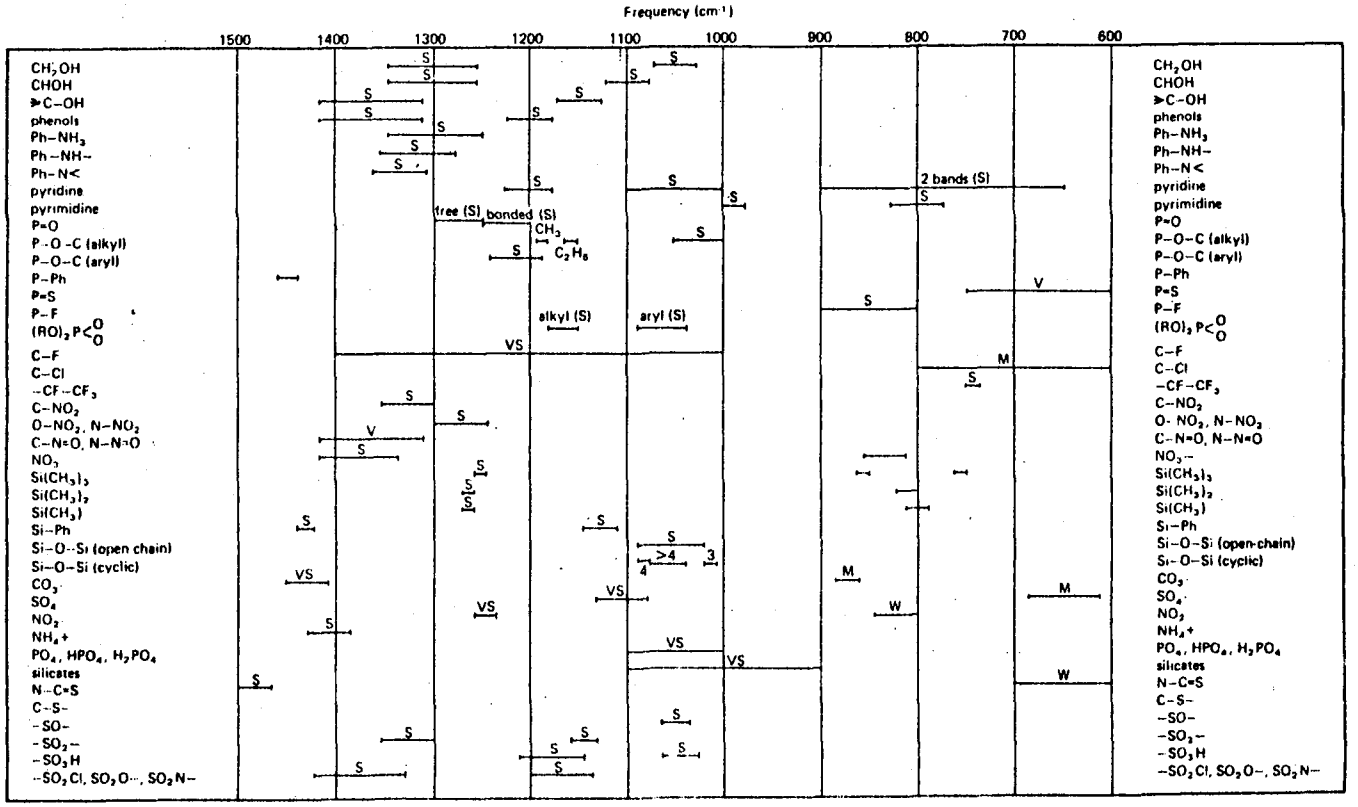

Correlation Chart No. 5. Single-bond vibrations etc. (II) 1500–650 cm^{-1}

Fig. 4.19e

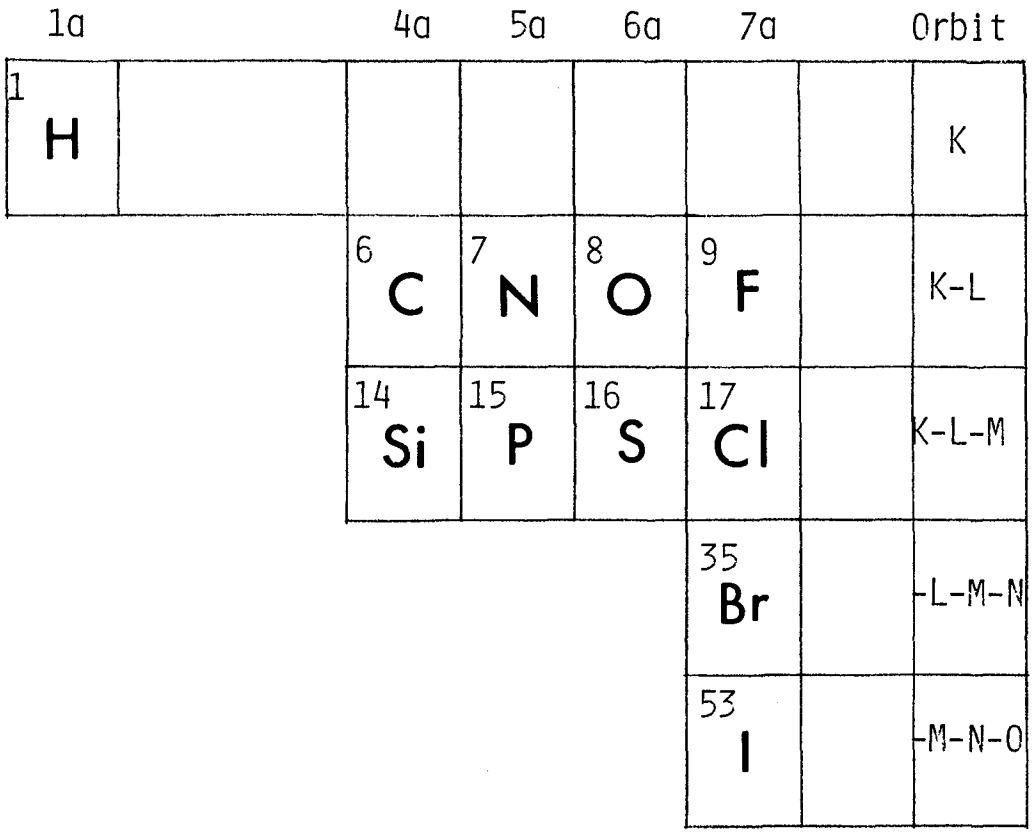

Fig. 4.20 The atoms of lasing molecules in the partial periodic table.

LASANTS FOR TRANSFER BLACKBODY-PUMPED LASERS

R. De Young
Space Technology Branch
NASA Langley Research Center

I. Introduction

This paper will outline the concept of transfer blackbody-pumped lasers, present recent research results concerning these lasers and expand into the search for new lasant materials for transfer blackbody-pumped lasers. Presently these lasers appear to have the best potential for scaling to multimegawatt power levels.[1]

There are two basic concepts for the blackbody-pumped transfer laser which are schematically drawn in figure 5.1. The first concept is called the translational heating concept, an example being $N_2:CO_2$. Here the blackbody cavity is heated to approximately 2000°K by collected sunlight in space. An absorbing molecule would come in contact with the blackbody walls thus coming into equilibrium with the blackbody temperature. The gas vibrational and blackbody temperature would be roughly equal, and thus a Boltzmann distribution of vibrational states would be excited at the blackbody temperature. The gas would then flow out of the cavity through a nozzle then into the laser cavity. The nozzle allows a pressure differential between the blackbody and laser cavity and also extracts the translational heat from the gas without substantially reducing the vibrational excitation. In the laser cavity, the absorbing and lasant gases are mixed creating a population inversion and subsequent lasing. The gases emerge from the laser cavity and are then cooled by a radiator. A separator directs the lasant molecule back to the laser cavity and the

absorbing molecule to the blackbody cavity. A typical example of this system is the N_2:CO_2 system in which the N_2 is translationally heated in the blackbody cavity creating $N_2(v)$ excited vibrational states. At the exit of the nozzle the translational temperature drops but the vibrational temperature remains high. The N_2 ($v = 1$) efficiently transfers its energy to the (001) mode of CO_2 creating lasing at 10.6 μm. This system has been demonstrated experimentally and will be reviewed subsequently. The major limitation of this concept is its relatively low system efficiency. In figure 5.2 is shown the N_2:CO_2 ideal efficiency as a function of the blackbody temperature (equal to the N_2 gas temperature). The efficiency is the quantum efficiency 41 percent multiplied by the thermal efficiency, that is the ratio of the energy in the $N_2(v=1)$ state to the N_2 gas enthalpy. At 2000°K the efficiency is approximately 4 percent. The overall system efficiency would be lower than this value--perhaps 1 percent.

An alternative concept shown in figure 5.1 is called the vibrational heating transfer laser. Here the absorbing molecule is not translationally heated. Energy is coupled to the molecule only by optical absorption creating a high density of vibrational states. Thus the gas temperature is near room temperature whereas the vibrational temperature comes into equilibrium with the blackbody temperature. The vibrationally excited gas is mixed with an appropriate lasant in the laser cavity from which lasing is extracted. This system is not limited by the thermal efficiency; the limitation being the quantum efficiency (41 percent for CO_2).

Figure 5.3 shows an example of such a system. CO gas would absorb energy at 4.6 μm in the blackbody cavity and subsequently transfer its vibrational energy to $CO_2(001)$ creating lasing at 10.6 μm. The CO absorbs

in a narrow band within the 2000°K blackbody cavity, but the blackbody radiation outside the CO absorption band remains in the cavity, thus in an ideal cavity the energy extracted by vibrationally excited CO would be equal to the sunlight energy entering the blackbody cavity. Under these conditions the laser efficiency would approach the quantum efficiency of 41 percent.

II. Present Research Status

Lasing of N_2-CO_2 has been achieved by heating N_2 in an electrically-heated oven to approximately 1500°K and then translating it to a laser cavity into which CO_2 is mixed with the nitrogen establishing lasing in CO_2 at 10.6 μm.[2] Figure 5.4 shows a schematic diagram of the experimental setup which was used to demonstrate blackbody pumping of nitrogen and subsequent lasing of CO_2. Nitrogen passing through the electrically-heated oven comes into equilibrium with the oven temperature. After passing out of the oven it goes through a nozzle which allows the lasing region to be at a lower pressure than the oven region. Also the nozzle reduces the translational temperature without substantially reducing the vibrational excitation. Vibrationally excited nitrogen passes through the nozzle which is water cooled and enters the laser cavity where CO_2 and helium are mixed together creating lasing between the laser cavity mirrors. The gases are extracted through vacuum pumps and expelled. Figure 5.5 shows the CO_2 laser power and efficiency as a function of nitrogen oven temperature. As the oven temperature increases lasing also increases to over 1 watt of CW power at 10.6 μm. The efficiency is plotted as a function of oven temperature and increases as the oven temperature

increases. A maximum intrinsic efficiency is shown at approximately 1500°K where it is a factor of 4 less than the maximum intrinsic efficiency. In figure 5.6 is plotted the CO_2 laser power and intrinsic efficiency as a function of N_2 oven pressure. Again, laser power increases to approximately 1.4 watts CW power at 700 torr N_2 pressure and the experimental efficiency is again shown to peak at about one-fourth the maximum intrinsic efficiency. The experimental intrinsic efficiency is here defined as the amount of laser power measured divided by the N_2 gas enthalpy.

Lasing has recently been achieved in N_2-N_2O mixtures. Laser output was substantially less than with CO_2; this has also been noted in electric discharge and gasdynamic lasers using N_2O. Lasing has also been achieved in N_2-CO_2 with the addition of CO. Presently, however the addition of CO tends to quench CO_2 lasing and further research is needed to understand the reasons for the quenching. Eventually through fluorescent studies we hope to replace the nitrogen and pump the CO_2 directly from vibrationally excited CO.

III. Characteristics of Transfer Blackbody Lasants

Figure 5.7 gives in outline form the pitfalls on the path to new blackbody lasants. The laser system in operation now is the N_2-CO_2, but this system has fundamental efficiency limitations which make it uninteresting and eventually we would like to replace this system with one that is purely optically pumped. To do this several considerations must be addressed. The absorption of the blackbody radiation is important, not

that the molecule be a strong absorber but that it sould be as broadband as possible. V-T relaxation of the absorber should be kept to a minimum since this is a loss of vibrational excitation. A finite time is needed to translate the optically pumped molecule into the laser cavity and V-T relaxation could substantially reduce the excitation density. The V-V transfer rate should be high between the vibrationally excited absorbing molecule and the lasant molecule within the laser cavity. Here the energy resonance, between the absorbing-lasant molecular states, is of utmost importance. Within the lasing molecule, V-V relaxation should be kept to a minimum for the upper laser level, but for the lower laser level V-V relaxation may play a beneficial role in rapidly depopulating the state. Quantum efficiency is also a consideration in that we would like to have this higher than 41 percent achievable with CO_2. Some chemically reactive species may be used and this compounds the quenching phenomena and must be addressed in certain molecular mixtures. If we have optimized all these considerations then we can feel assured that we have achieved the near ideal lasant molecule.

1. Absorbing Molecule

The first consideration in the transfer blackbody laser is the absorbing molecule which will optically absorb energy without gas heating. There are a number of modes in which energy can be coupled to a gas. One is through electronic states, either electronic atomic or molecular states. Rotational states could be involved and also vibrational states of polyatomic as well as diatomic molecules. Of these modes, the electronic states generally are very high in energy and are unaccessible through pumping by blackbody radiation. Also, atomic states tend to be very narrow in their absorption bands and radiatively relax very quickly. Conversely,

rotational states are generally too low in energy and thus of little interest. Presently, most consideration is being given to vibrational states of molecules since they have energies accessible by blackbody radiation and of these diatomic molecules appear to have the lower V-T relaxation rates with long vibrational lifetimes.

For a heteronuclear diatomic molecule the rate of absorption from state K to M can be written as

$$\frac{dN_M}{dt} = N_K \cdot B_{MK} \cdot \rho(\omega_{MK}) \tag{5.1}$$

where N_K is the number density of excited absorbers, B_{MK} is the Einstein absorption coefficient (cm^2/Erg-sec) and $\rho(\omega_{MK})$ is the blackbody radiation density per wavelength interval (Erg/cm^3 cm^{-1}). The Einstein coefficient can be written as

$$B_{MK} = \frac{8\pi^3}{3h^3C} (\mu)^2_{MK} \tag{5.2}$$

where $(\mu)_{MK}$ is the transition moment integral and can be written as

$$(\mu)^2_{MK} = \frac{3hQ^2}{8\pi^2 C\ M_E\ \omega_{MK}} \tag{5.3}$$

for a three dimensional harmonic oscillator. Here Q is the electric charge, M_E the electron mass and ω_{MK} is the transition frequency. The electric charge can be approximated by

$$Q = \frac{\mu}{R_e} \tag{5.4}$$

where μ is the dipole moment (esu-cm) and R_e is the equilibrium

internuclear distance (cm). Thus, looking at equation 5.3 we would like to maximize the quantity

$$\frac{\mu^2}{\omega_{MK} R_e^2} \tag{5.5}$$

This has been done for a number of diatomic molecules of interest and are listed, table 5.1, in order of decreasing value of the quantity 5.5. Also shown in table 5.1 are the calculated radiative lifetimes of each molecule from the fundamental vibrational state. It is interesting to note that CO, based on this criteria, is the best absorber. It also has a reasonably long radiative lifetime of 50 msec.

A number of candidate absorbers exist over a wide range of fundamental energies. Plotted in figure 5.8 is the blackbody spectrum as a function of wavelength for different temperatures running from 1500 to 2500°K. Also shown are some heteronuclear diatomic absorbing molecules of interest. Molecules other than CO which absorb closer to the peak of the blackbody spectrum are shown. Of particular interest is OH(ν = 2) which absorbs near the peak of the 2000°K blackbody spectrum. In general, we would like molecules which absorb at the peak of the blackbody spectrum over as wide a bandwidth as possible.

In general the radiative lifetimes of heteronuclear molecules are fairly long, and the loss of vibrational energy takes place through V-T relaxation rather than through radiative decay. Thus, it is important to consider the V-T loss process in detail. Before looking at the experimental data, some parameters need to be defined. Z_{10} is defined as the average number of collisions for a V-T deactivation from the first vibrational level. $P_{\tau V}$ is equal to the V-T vibrational relaxation time

and is usually given in atmosphere-seconds. This can be approximated by

$$P\tau_V = \frac{Z_{10}}{Z} = \frac{Z_{10}}{4N\sigma^2(\pi KT/M)^{1/2}} \tag{5.6}$$

where Z is the gas kinetic collision rate, N is the number density, σ is the collision cross section, T is the gas temperature and M is the molecular mass. Thus, for an ideal absorbing molecule we would like to have Z_{10} very high. For example, in figure 5.9 the vibrational V-T loss for CO is shown as a function of gas temperature.[3] CO has the very advantageous characteristic of having a slow V-T loss rate and as the figure shows at 300°K the rate approaches 10^{10} collisions per V-T relaxation. Figure 5.10 shows for other molecules the V-T relaxation lifetime plotted as a function of gas temperature.[4] CO is again shown having a very long lifetime at room temperature; it is interesting to note that when argon is mixed with CO, the V-T relaxation can be substantially reduced. Conversely, if a light atom is mixed with CO the V-T rate is increased as shown with helium-CO mixtures. Also shown in the figure are the halogens which have substantially higher V-T rates. Figure 5.11 shows, in the upper plot, the V-T loss again as a function of temperature for HF, DF, HCl, HBr, and DCl.[3] Note the substantially higher V-T loss rates for these molecules which would tend to make them difficult to use as blackbody absorbing molecules. In the lower graph of figure 5.11 is shown the V-T loss rates for polyatomic molecules and in general these molecules would not be good absorbers because of their fast V-T relaxation.

Thus, some general statements can be made concerning absorbing gas molecule characteristics. First of all they would tend to be heteronuclear

diatomic molecules which have a reasonable dipole moment, absorbing at as broad a bandwidth as possible (this may be possible by mixing isotopes of the diatomic molecule together). Secondly, it should have a small V-T rate approaching that of CO at 300°K. A carrier gas could be mixed with the absorbing molecule thus decreasing the V-T loss. Thirdly, we would like to have a high energy fundamental transition as this would tend to couple better to the blackbody spectrum.

2. Lasant molecules

There are some considerations that must be addressed when looking at the potential lasant molecule. In particular the upper laser level should have relatively low V-T and V-V loss rates. If the molecular structure is complex the energy transferred into the lasant molecule may V-V to a variety of other states, thus there would be no state selected inversion, thus, relatively simple molecules would appear to be best. The energy resonance between the absorbing and lasing molecules is important so that efficient transfer of energy can take place and we would generally tend to be dealing with IR active states.

Conversely, in the lower laser level we would like to have fast V-T and V-V rates to depopulate this level. Shown in figure 5.12 is the collision number for vibrational relaxation as a function of ν_{min} which is the energy of the lowest energy state of the molecule.[3] From the figure we can see that vibrational relaxation is inversely proportional to the energy that must be converted into translation from the lowest vibrational level. In the chart of figure 5.12, CO_2 is shown to be the

least deactivated in collisions due to its high (010) state. Also shown are molecules containing hydrogen and in general molecules which contain hydrogen deactivate with higher probability. These considerations are important in the lower laser level of the lasant molecule where rapid deactivation would be very important. Thus, molecules that deactivate quickly should be considered and these molecules are indicated on the chart in figure 5.12. Shown in figure 5.13 is the deactivation collision number, again versus the energy of the minimum energy state of the molecule.[3] In this figure molecules are shown which contain greater than two hydrogen atoms and it can be seen that when compared to figure 5.12, these molecules deactivate very rapidly. Such molecules may be important if they have a high deactivation of the lower laser level without affecting the upper laser level. The lower laser level should be higher than the lowest molecular energy, V_{min}, state to reduce the effect of thermal pumping the lower laser level.

Another consideration in the transfer blackbody pumped laser is the vibrational energy transfer from the absorbing molecule to the lasant molecule. This is shown in figure 5.14 which shows the parameters of two molecular systems CO_2 and N_2O. Note that CO at 2143 cm^{-1} is approximately resonant with the ν_3 modes of CO_2 and N_2O. The reaction of vibrationally excited CO on CO_2 is off resonance by about 206 cm^{-1}. Thus, it takes a collision number for transfer of 1580. Alternatively, if vibrationally excited CO is reacted with N_2O, where the energy off resonance is 80 cm^{-1}, then the collision number is only 40, demonstrating the importance of near resonant V-V transfer. Also of importance is the necessity for infrared active states, for instance, in figure 5.14 if vibrationally excited Cs is

reacted with CO_2 the transfer is to an IR inactive state and thus takes a collision number of 2700. Alternatively, if Cs is reacted with N_2O the transfer affects a IR active state (both of these states are identically 13 cm^{-1} off resonance) but in this case the collision number is only 26. Thus, for efficient energy transfer the energy mismatch must be a minimum and the transfer must be into IR active states. In figure 5.15 is plotted the vibrational transfer collision number versus the energy mismatch of the states involved in the V-V transfer.[3] The upper figure shows transfer for hydrogen containing heteronoculear molecules and the lower figure is for vibrationally excited CO. In general it can be seen that as the energy mismatch decreases the number of collisions to affect the V-V transfer substantially decreases. There are several systems that appear interesting from these diagrams, from an energy transfer standpoint, vibrationally excited HCl with CO_2, HCl with CH_4, HF with H_2S and HF with CO_2. Although the mismatch in energy is high with HF the collision number for V-V transfer is still relatively low. Also CO with N_2O or DCℓ appears to have a very low collision number for V-V transfer.

One way to evaluate potential blackbody-pumped transfer-laser systems is to look for resonance between heteronuclear diatomic absorbing molecules and polyatomic lasant molecules. This is shown in figure 5.16 and 5.17 where the energy levels of potential heteronuclear diatomic molecules are shown on the left and fundamental energies of potential lasant molecules of varying complexity are plotted on the right. The lines showing wavelengths are known laser transitions, in general pumped by other infared lasers. The energy levels are just the fundamental energies for each

particular molecule; harmonics and combination bands are not shown. From these charts, one can see that the absorbing molecule of highest energy would be HF. Of these aborbing molecules OH, NH, CH, SH, NS, and SO are reactive and thus would present some difficulty in using them as the absorbing molecule. In general we would like to have a high upper laser level (see fig. 5.8) with a near resonance with an absorbing molecule for fast V-V transfer. Also, we would like to have a relatively low lower laser level which could quickly V-T relax or, through multiple other levels, V-V its population away. We would like to have a large energy gap between the upper and lower laser level for the highest quantum efficiency and shortest wavelength. It must be stressed that this chart only shows the fundamental energy states. With all possible energy states, including both combination and harmonic levels, the energy level diagram would be extremely congested. For most all cases, energy transfer involving fundamental levels proceeds with the highest rate. From figure 5.16 and 5.17 potential systems of interest are CH-H_2S, CO-OCS, CO-C_2H_2, CO-N_2O, OH-HCN, HF-H_2O, NH-CH_3X where X is equal to F, Cl, BR, or I .

V. Conclusions

Many molecular systems appear to be potential candidates for transfer blackbody pumping. The V-V and V-T transfer rates are generally unknown for most of these systems making modeling these systems extremely difficult. In general for the absorbing molecule we would like a heteronuclear diatomic which has a V-T relaxation collision number of approximately 10^{10}, we would need a fundamental vibrational state which is

IR active and we would like the energy of that fundamental to be between 3000 and 4000 cm^{-1}. For the lasant molecule, the simple polyatomics seem to be the most appropriate. The energy transfer off resonance should be as small as possible (<200 cm^{-1}) and there should be few levels near the energy resonance with the absorbing molecule. Conversely, with the lower laser level it is advantageous to have many levels for effective V-V and V-T depopulation. Studies involving overtones or harmonics should be investigated. Systems involving HF and OH are chemically reactive, yet because of their high fundamental energy they are still of interest as absorbing molecules. Further research is needed to quickly evaluate potential absorbing-lasant molecular systems. This potentially could be done with IR laser excitation, and may become a valuable tool for quickly diagnosing the potential systems outlined here.

VI. References

1. R. J. De Young, "Scaling Blackbody Lasers to High Powers," NASA TM 86395, March 1985.

2. R. J. De Young and N. S. Higdon, "A Blackbody-Pumped CO_2-N_2 Transfer Laser," NASA TP 2347, Aug. 1984.

3. J. D. Lambert, Vibrational and Rotational Relaxation in Gases, Clarendon Press, Oxford, 1977.

4. R. C. Millikan and D. R. White, "Systematics of Vibrational Relaxation," J. of Chem. Phys., 39, 15, Dec. 1963, pp. 3209-3213.

CHARACTERISTICS OF HETRONUCLEAR MOLECULES

MOLECULE	ω_{01} (CM $^{-1}$)	DIPOLE MOMENT (ESU-CM)	R_E (CM)	γ_{RAD} (SEC)
1) CO	2143	2.7×10^{-18}	1.13×10^{-8}	50×10^{-3}
2) IF	603.3	1.95×10^{-18}	1.9×10^{-8}	8.2
3) HF	3961.4	1.9×10^{-18}	0.92×10^{-8}	2.7×10^{-3}
4) OH	3569.6	1.667×10^{-18}	0.97×10^{-8}	4.7×10^{-3}
5) NH	3125.6	1.39×10^{-18}	1.04×10^{-8}	10.2×10^{-3}
6) IBR	267.1	0.737×10^{-18}	2.47×10^{-8}	1442
7) CH	2732.5	0.88×10^{-18}	1.12×10^{-8}	37.3×10^{-3}
8) HCℓ	2885	1.08×10^{-18}	1.28×10^{-8}	33.5×10^{-3}
9) HBR	2558.5	0.83×10^{-18}	1.41×10^{-8}	83.2×10^{-3}
10) SH	2591.8	0.758×10^{-18}	1.35×10^{-8}	21.7×10^{-3}

Table 5.1

BLACKBODY-PUMPED TRANSFER LASER CONCEPTS

I. Translational heating

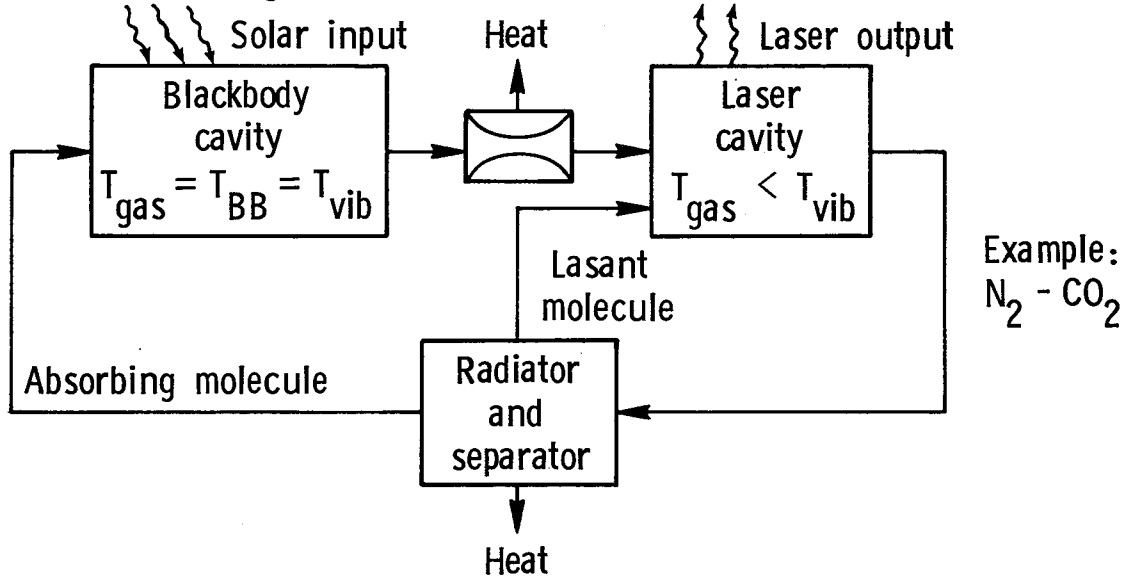

II. Vibrational heating

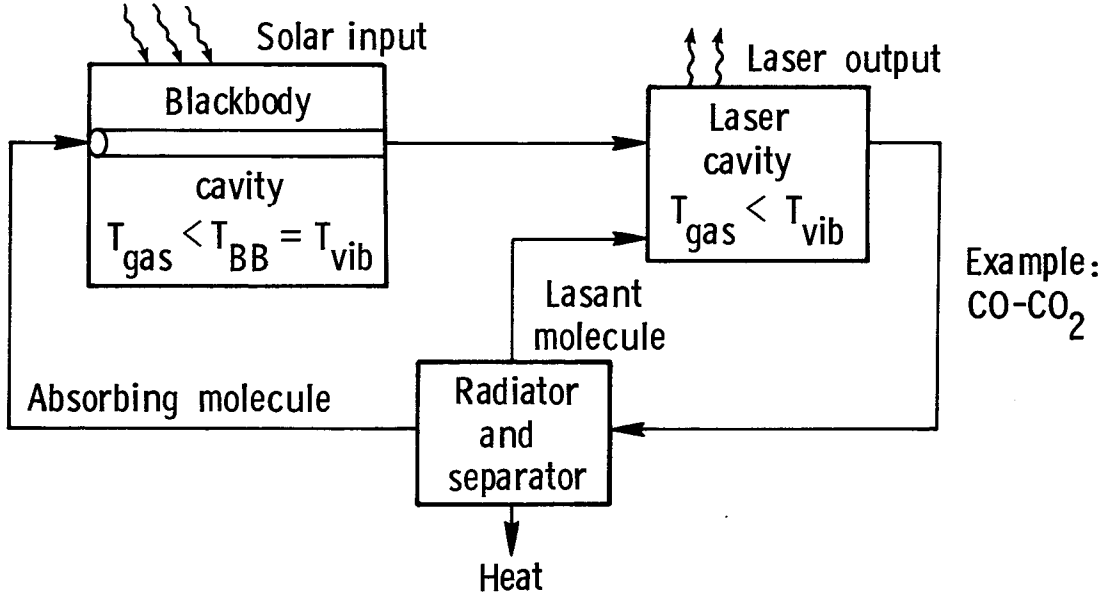

Fig. 5.1

Quantum—Thermal CO_2 Laser Efficiency

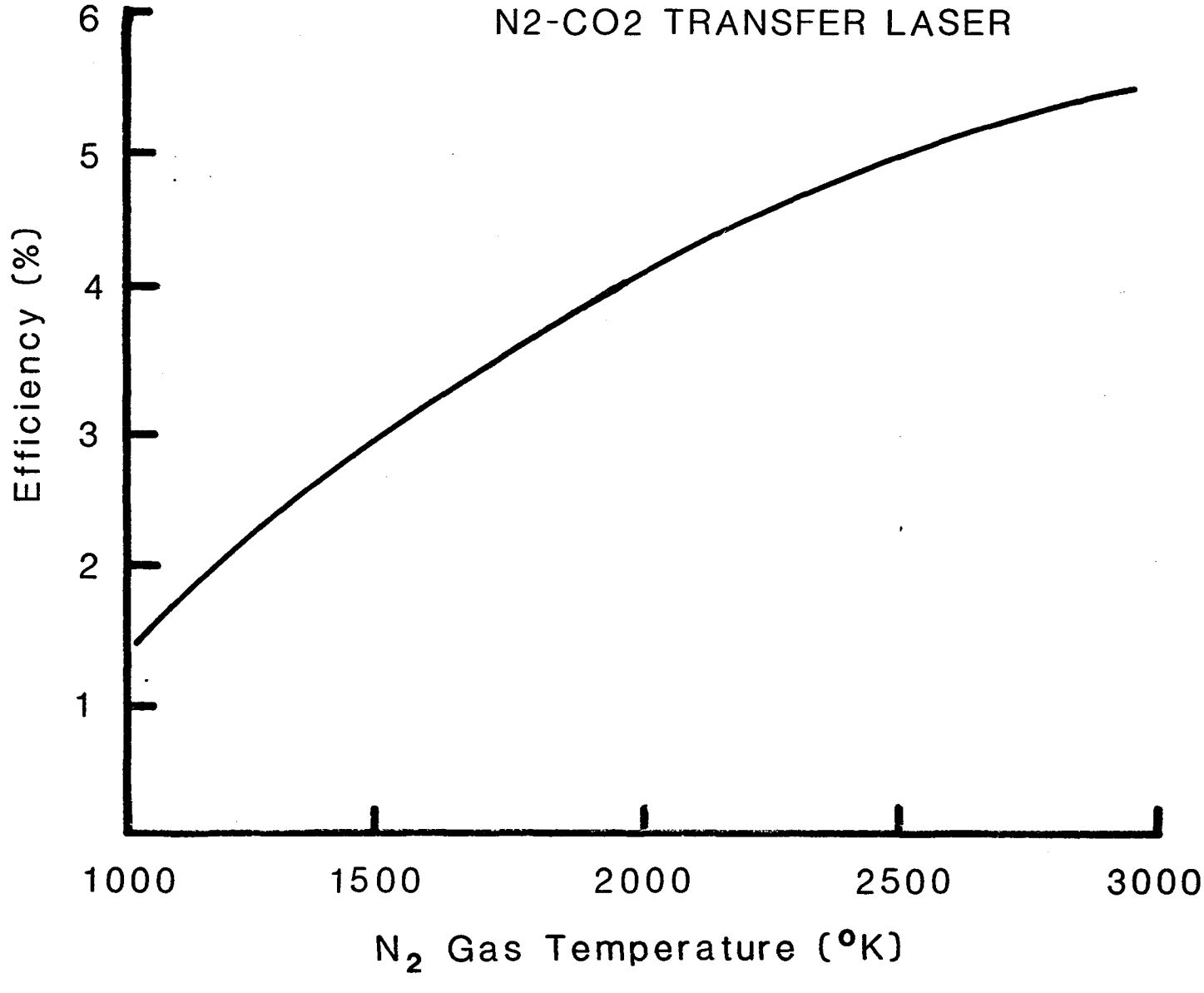

Fig 5.2

BLACKBODY PUMPED TRANSFER LASER

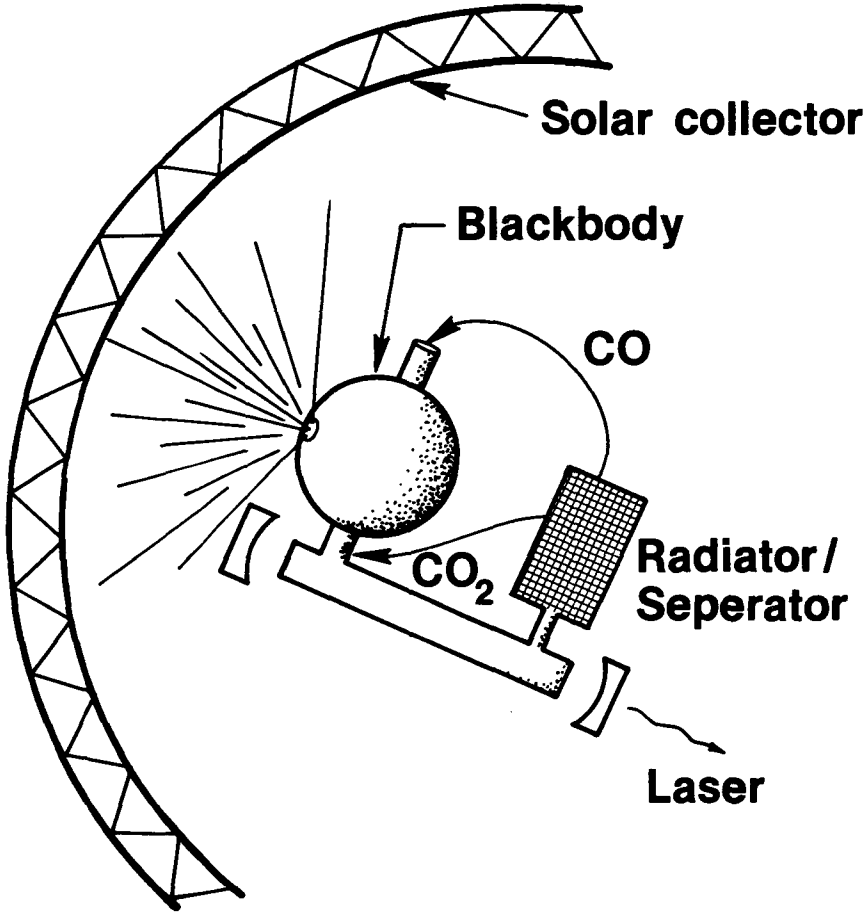

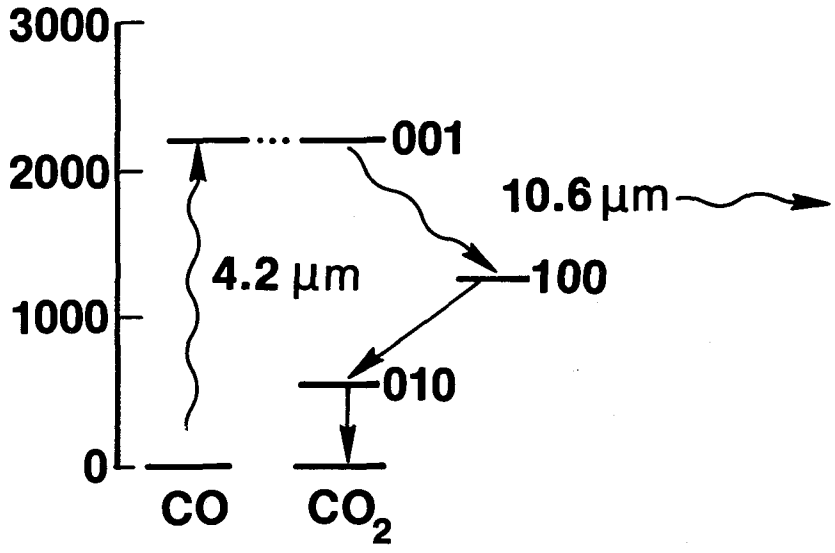

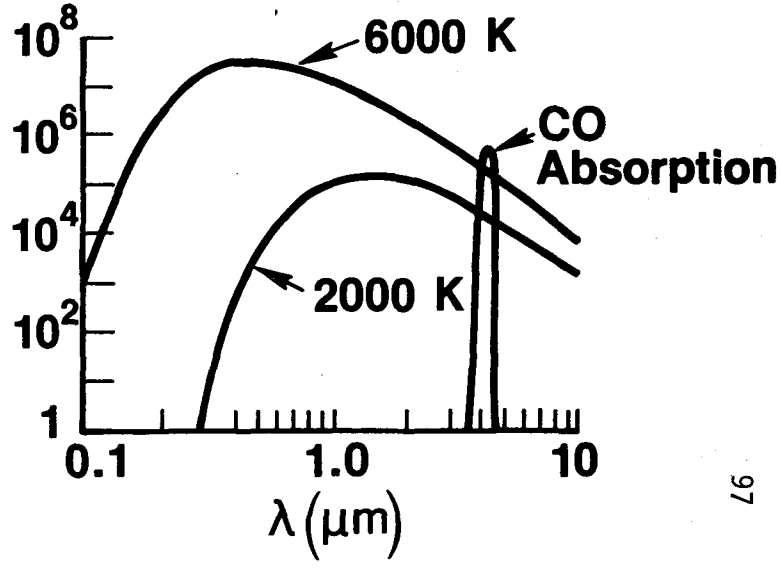

Fig 5.3

Blackbody Pumped Transfer Laser

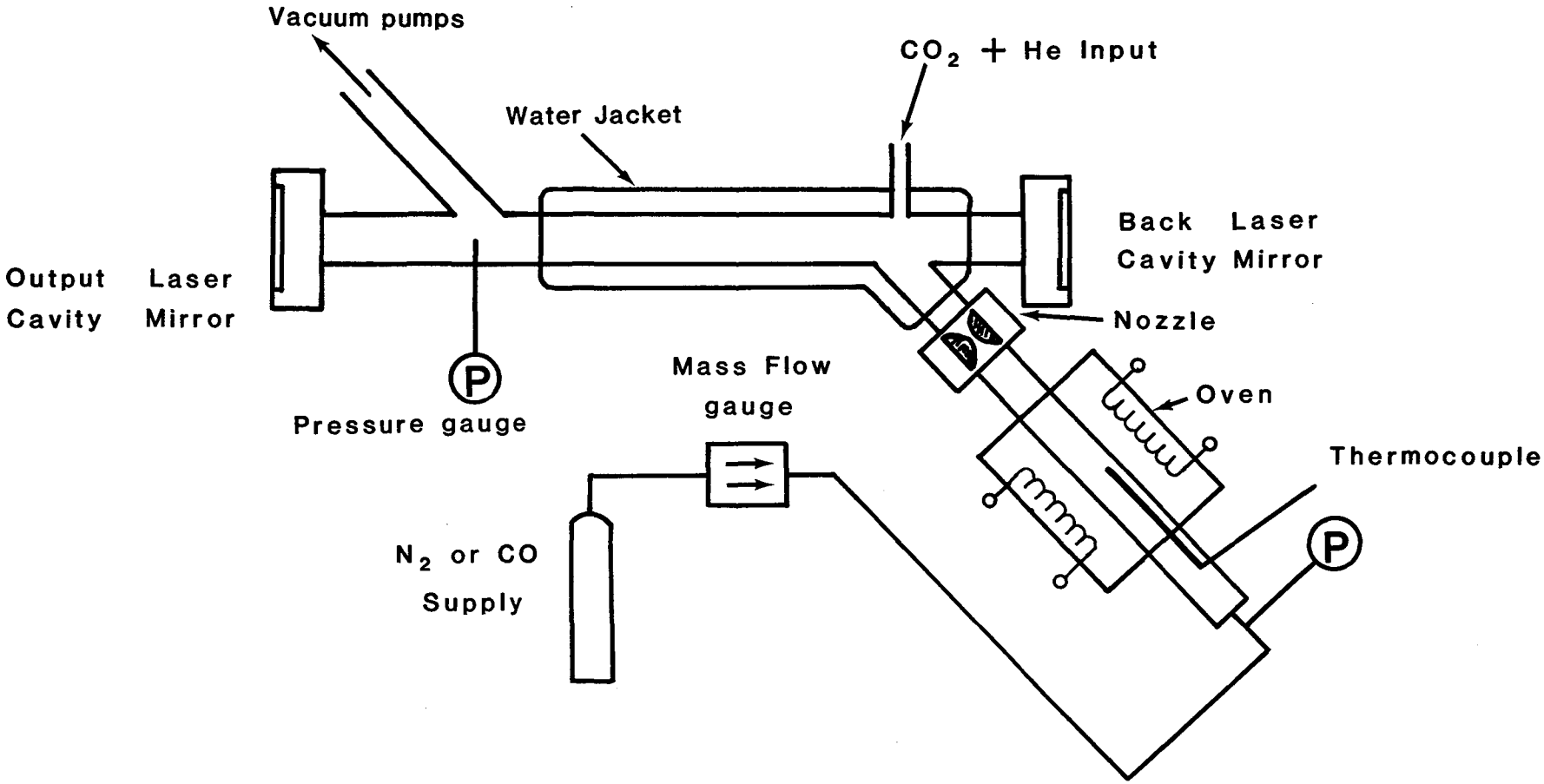

Fig 5.4

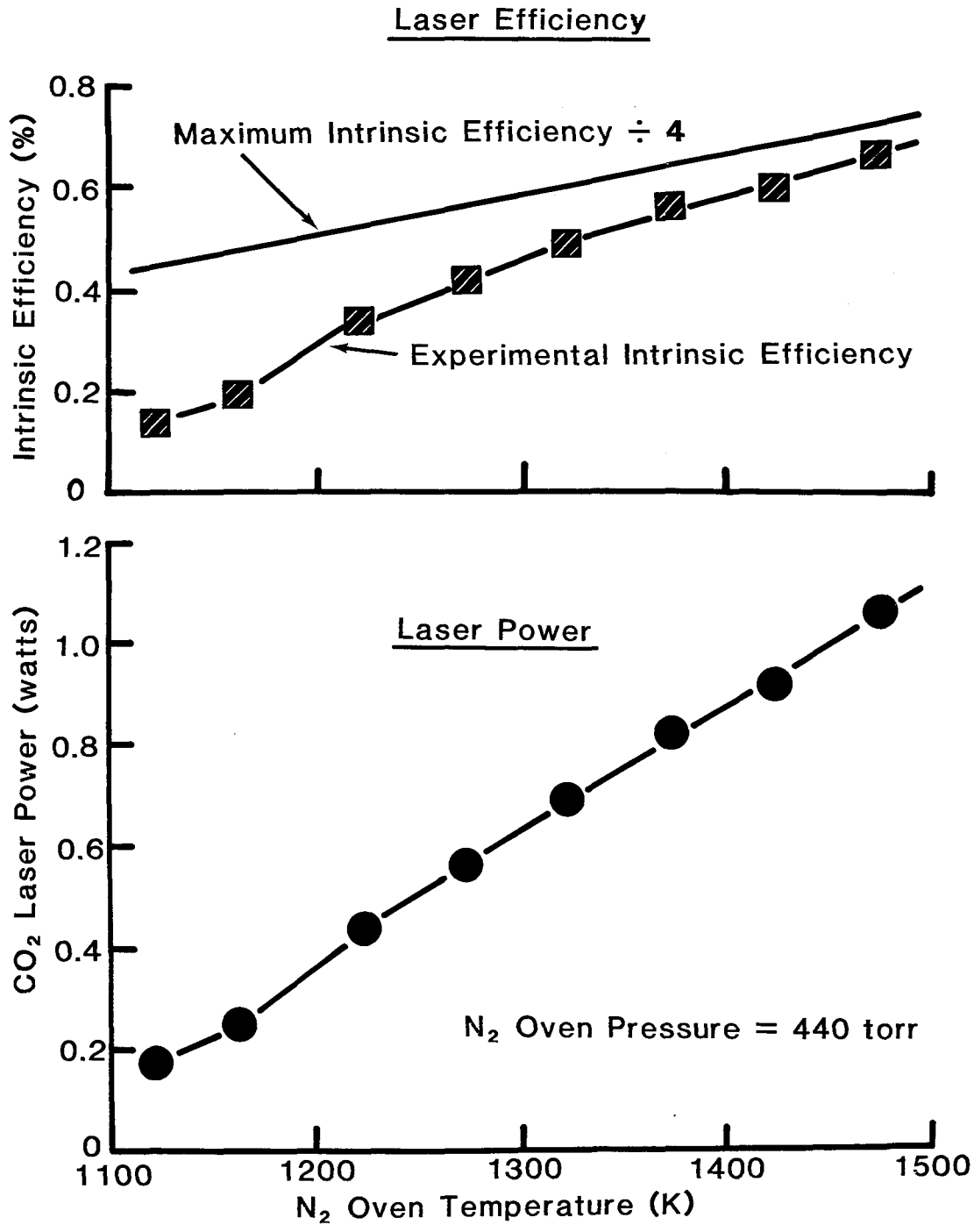
Laser Efficiency
Intrinsic Efficiency (%)
0.8
0.6
0.4
0.2
0
Maximum Intrinsic Efficiency ÷ 4
Experimental Intrinsic Efficiency
Laser Power
CO_2 Laser Power (watts)
1.2
1.0
0.8
0.6
0.4
0.2
0
N_2 Oven Pressure = 440 torr
1100
1200
1300
1400
1500
N_2 Oven Temperature (K)

Fig 5.5

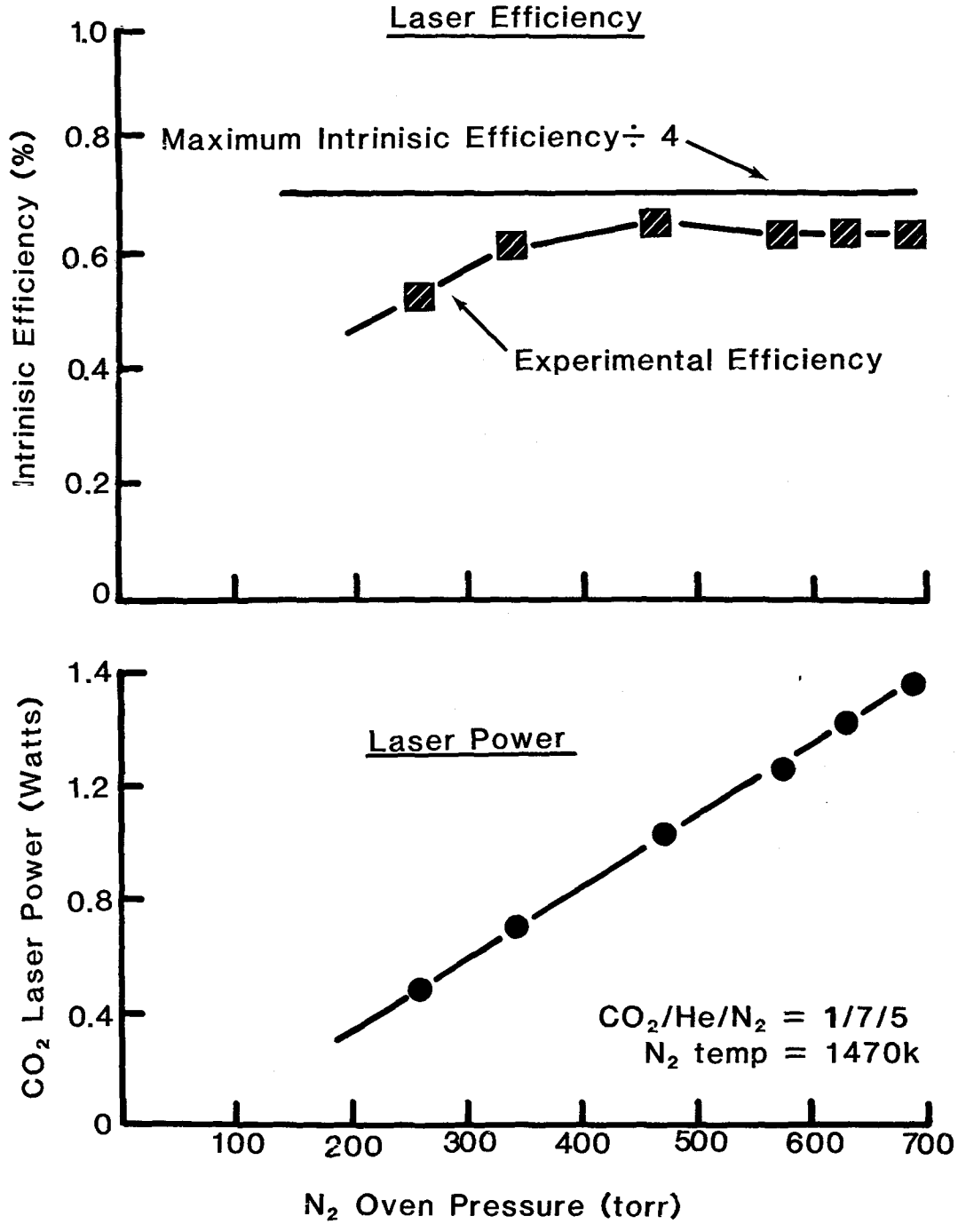
Laser Efficiency
1.0
0.8
0.6
0.4
0.2
0
Intrinisic Efficiency (%)
Maximum Intrinisic Efficiency÷ 4
Experimental Efficiency
Laser Power
1.4
1.2
0.8
0.4
0
CO_2 Laser Power (Watts)
CO_2/He/N_2 = 1/7/5
N_2 temp = 1470k
100
200
300
400
500
600
700
N_2 Oven Pressure (torr)

Fig 5.6

PITFALLS ON THE PATH TO

NEW BLACKBODY LASANTS

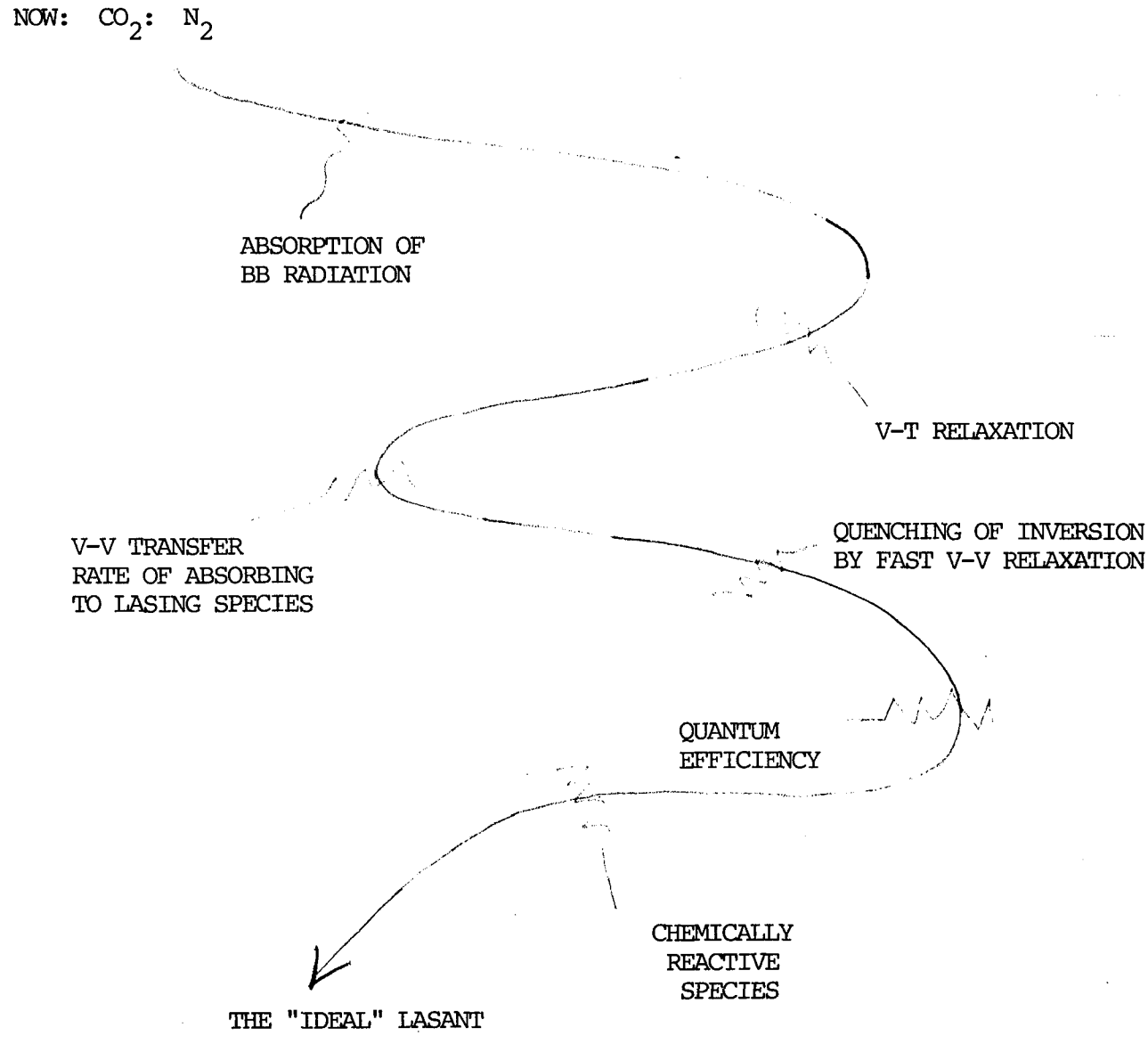

Fig 5.7

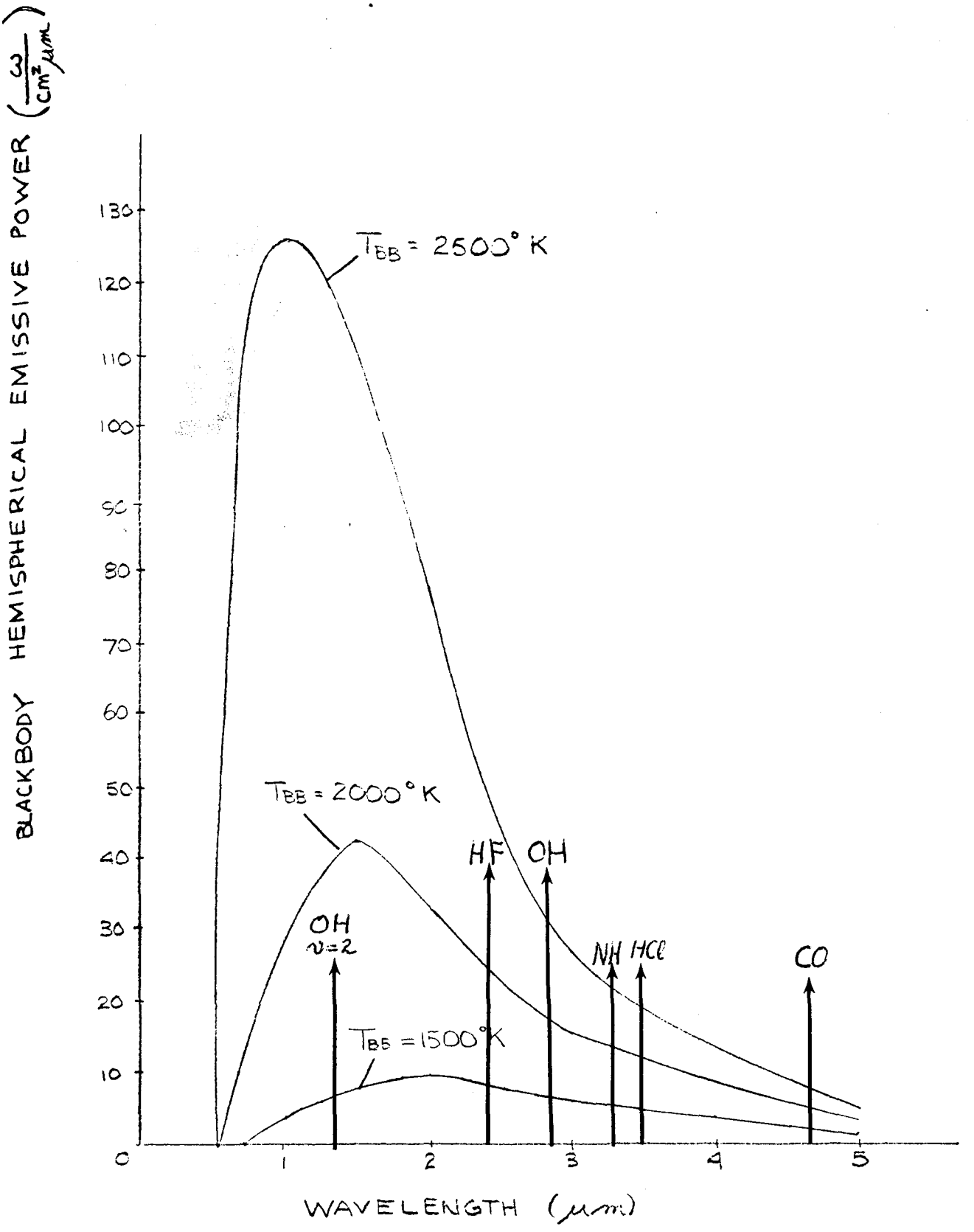
BLACKBODY SPECTRAL EMISSIVE POWER
BLACKBODY HEMISPHERICAL EMISSIVE POWER (w/cm²μm)
130
120
110
100
90
80
70
60
50
40
30
20
10
0
1
2
3
4
5
T_BB = 2500° K
T_BB = 2000° K
T_BB = 1500° K
HF
OH
OH ν=2
NH
HCl
CO
WAVELENGTH (μm)

Fig 5.8

CO

VIBRATION-TRANSLATION TRANSFER

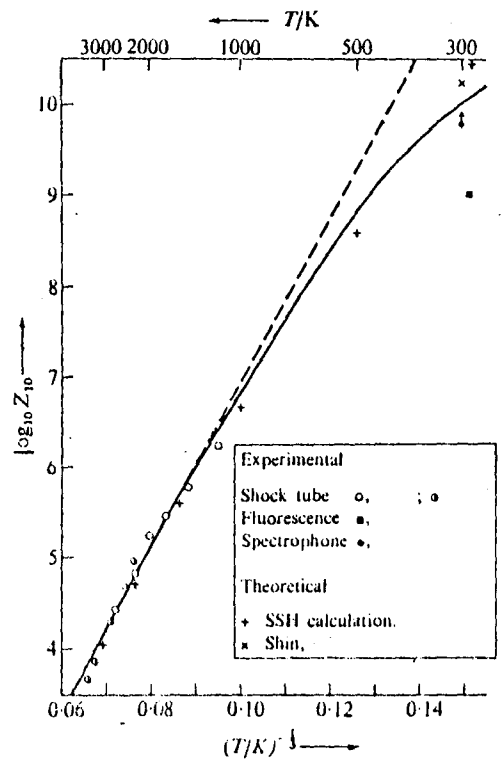

Landau-Teller plot for CO

Fig 5.9

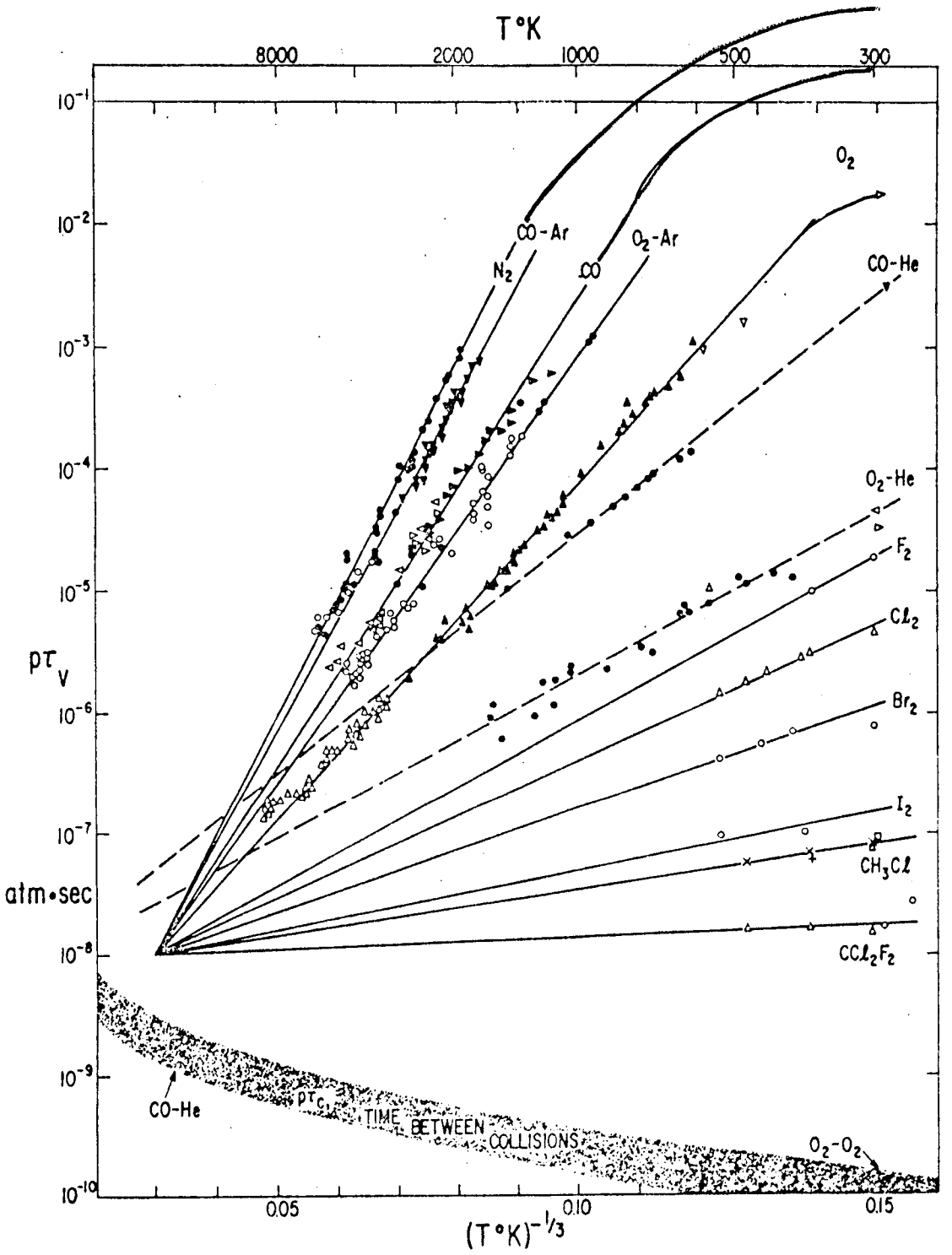

Common-origin plot of vibrational relaxation times. See Fig. 2 for sources of diatomic data. Polyatomic data from ultrasonics: CH_3Cl, ×, +, □, △; CCl_2F_2, △, ○

Fig 5.10

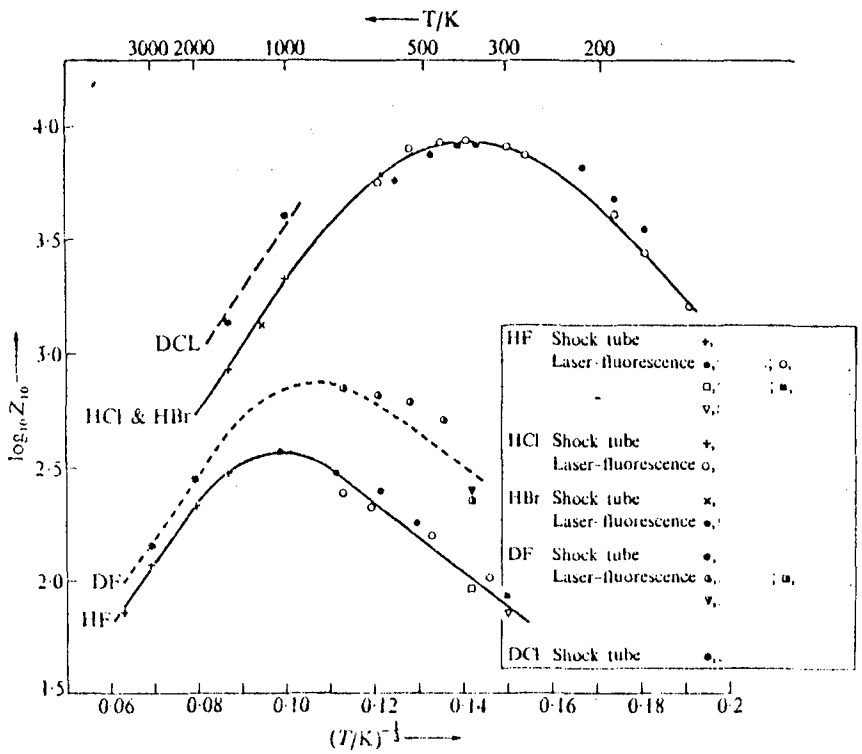

Experimental Landau-Teller plots for HF, HCl, HBr, DF, and DCl

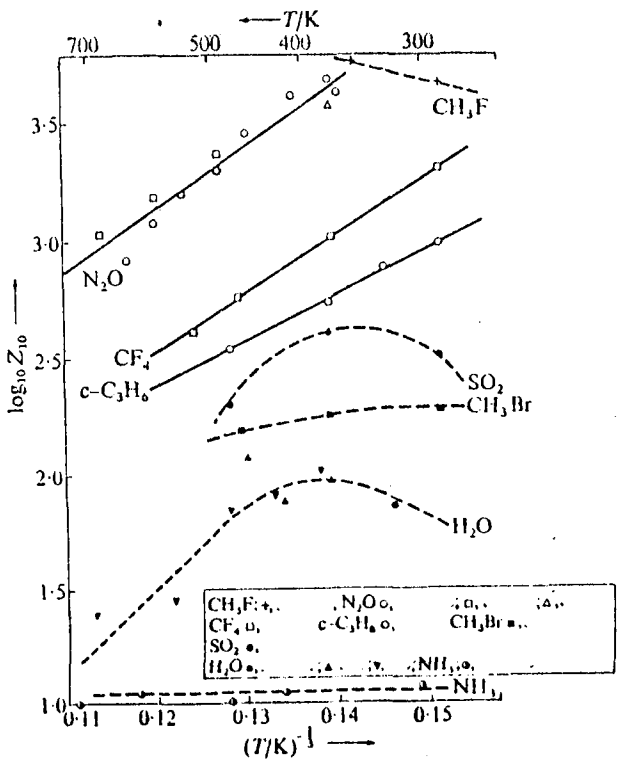

Experimental Landau-Teller plots for polyatomic gases

Fig 5.11

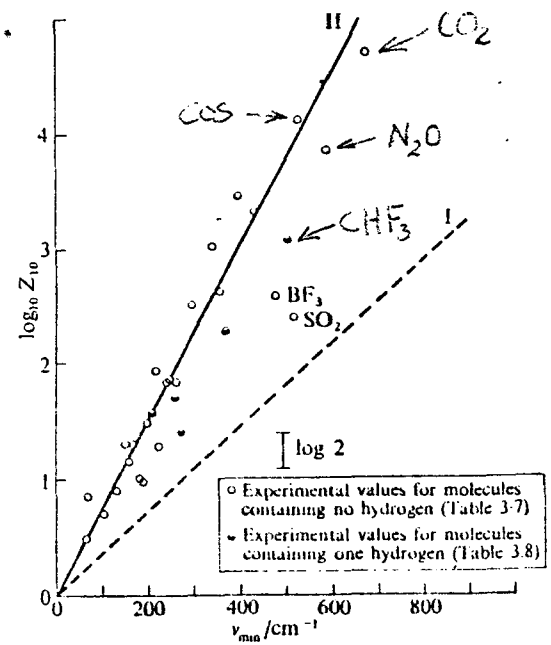

Lambert-Salter plot for molecules containing ≤ 1 hydrogen atom

Fig 5.12

Vibrational relaxation data at 300 K for polyatomic molecules containing no hydrogen atoms

Molecule	ν_{min} (cm^{-1})	β (ns)	Z_{10}	$\log_{10} Z_{10}$	Reference
CO_2	673	6370	53000	4·70	180
COS	527	1670	13000	4·12	147
N_2O	589	990	7320	3·86	181
CS_2	397	727	2950	3·47	168
CF_4	437	853	2070	3·32	68
SF_6	344	860	1005	3·02	182
CF_3Cl	356	239	427	2·63	169
BF_3	480	90	380	2·58	35
CF_3Br	297	196	316	2·50	169
SO_2	519	50*	250	2·40	183
CCl_4	218	19	86	1·93	184
$CFCl_3$	248	40	72	1·86	169
CF_2Cl_2	261	78	68	1·83	169
C_2Cl_4	237	57	68	1·83	185
CF_2BrCl	200	50	30	1·48	169
$SiCl_4$	150	5·9	20	1·30	184
C_2N_2	226	4·15*	18	1·28	183
CF_2Br_2	165	29	14	1·15	169
CF_3CN	187	3·18*	10	1·0	183
C_2F_4	190	17	9·6	0·98	171
$GeCl_4$	134	3·4	8	0·90	184
C_2F_6	68	28	7	0·85	165
$SnCl_4$	104	2·5	5	0·70	184
C_3O_2	63	1·0*	3	0·48	33

*values of β_1 for molecules showing multiple relaxation

TABLE 3.8.

Vibrational relaxation data at 300 K for Polyatomic molecules containing one hydrogen atom

Molecule	ν_{min} (cm^{-1})	β (ns)	Z_{10}	$\log_{10} Z_{10}$	Reference
CHF_3	507	479	1230	3·09	169
$CHClF_2$	369	95	191	2·28	169
$CHCl_3$	260	13·5	52	1·72	175
$CHBrCl_2$	215	9·8	37	1·57	186
$CHCl_2F$	276	25	26	1·42	169
$CHBr_2Cl$	168	6·3	20	1·30	186

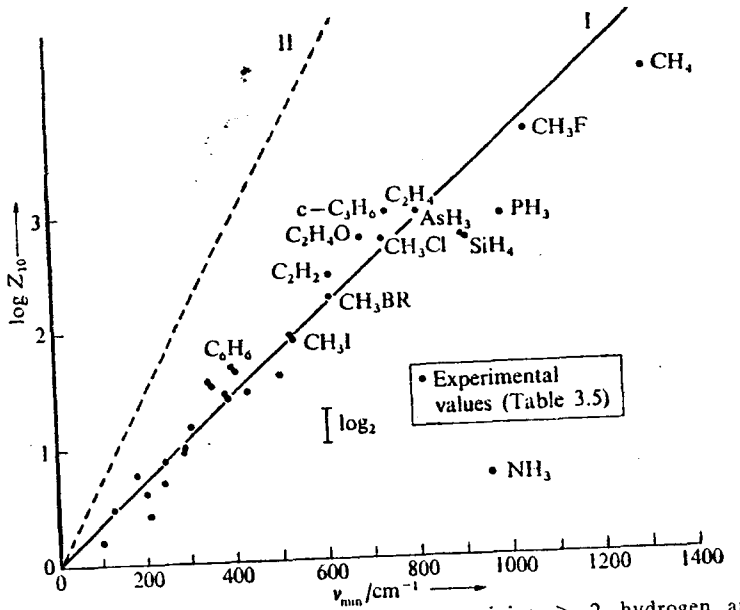

Lambert-Salter plot for molecules containing ⩾ 2 hydrogen atoms.

Fig 5.13

Vibrational relaxation data at 300 K for polyatomic molecules containing ⩾ 2 hydrogen atoms

Molecule	ν_{min} (cm^{-1})	β (ns)	Z_{10}	$\log_{10} Z_{10}$	Reference
CH_4	1306	2030	15160	4·18	151
CH_3F	1048	1900	4800	3·68	68
$c\text{-}C_3H_6$	740	311	990	2·99	68
C_2H_4	810	391	970	2·99	68
PH_3	991	196	890	2·95	167
C_2H_4O	685	360	603	2·78	168
AsH_3	905	310	605	2·78	131
CH_3Cl	732	204	575	2·76	169
SiH_4	914	115	570	2·76	151
C_2H_2	612	72·8	280	2·45	165
CH_3Br	611	34·3	190	2·28	68
CH_2F_2	529	30·0	83	1·92	169
CH_3I	533	37·0	78	1·89	170
CH_2CHCl	395	23·0	48	1·68	171
C_6H_6	404	29·0*	43	1·63	172
CH_2CHF	500	25·0	41	1·61	171
CH_2CHBr	345	24·0	36	1·56	171
$CH_2{:}C{:}CH_2$	354	5·2	33	1·52	33
C_2H_5OH	431	3·5	29	1·46	173
$CH_3COOC_2H_5$	376	8·5	29	1·46	173
CH_2CIF	385	10·0	26	1·42	169
CH_3COOCH_3	303	4·9	15	1·18	173
C_2H_6	290	15·0*	10	1·0	174
CH_2Cl_2	283	1·95*	9·6	0·98	175
C_3H_7OH	243	4·0	8	0·90	173
$CH_3CH{:}CH_2$	177	15·0	6	0·78	174
CH_3CHCl_2	240	5·35	5	0·70	176
NH_3	950	0·74	5	0·70	177
$C(CH_3)_4$	200	4·4	4·2	0·62	178
CH_2ClCH_2Cl	125	4·25	3	0·48	176
$c\text{-}C_5H_{10}$	207	1·9	2·6	0·42	178
$n\text{-}C_4H_{10}$	102	1·3	1·6	0·20	178
$(n\text{-}C_5H_{12}$	88	1·1	0·88	~0	178)
$(n\text{-}C_6H_{14}$	61	1·2	0·66	~0	178)

*values of β_1 for molecules showing multiple relaxation

LONG RANGE DIPOLE FORCES RESULT IN EFFICIENT V-V TRANSFER BETWEEN IR ACTIVE STATES WITH SMALL ΔE

CO_2		
$\nu_2(010)$	667 cm^{-1}	I.R. ACTIVE
$\nu_1(100)$	1388	I.R. INACTIVE
$2\nu_2(020)$	1285	I.R. INACTIVE
$\nu_3(001)$	2349	I.R. ACTIVE

N_2O		
$\nu_2(010)$	589	I.R. ACTIVE
$\nu_1(100)$	1285	I.R. ACTIVE
$\nu_3(001)$	2223	I.R. ACTIVE

CO
ν_{10} = 2143 cm^{-1}

ENERGY MATCH EFFECT

$$CO(\nu = 1) + CO_2(000) \xrightarrow{Z \approx 1580} CO(\nu = 0) + CO_2(001) - 206\ cm^{-1}$$

$$CO(\nu = 1) + N_2O(000) \xrightarrow{Z \approx 40} CO(\nu = 0) + N_2O(001) - 80\ cm^{-1}$$

I.R. ACTIVE SPECIES EFFECT

$$CS(\nu = 1) + CO_2(000) \xrightarrow{Z = 2700} CS(\nu = 0) + \underbrace{CO_2(020)}_{\text{I.R. INACTIVE}} - 13\ cm^{-1}$$

$$CS(\nu = 1) + N_2O(000) \xrightarrow{Z = 26} CS(\nu = 0) + \underbrace{N_2O(100)}_{\text{I.R. ACTIVE}} - 13\ cm^{-1}$$

Fig 5.14

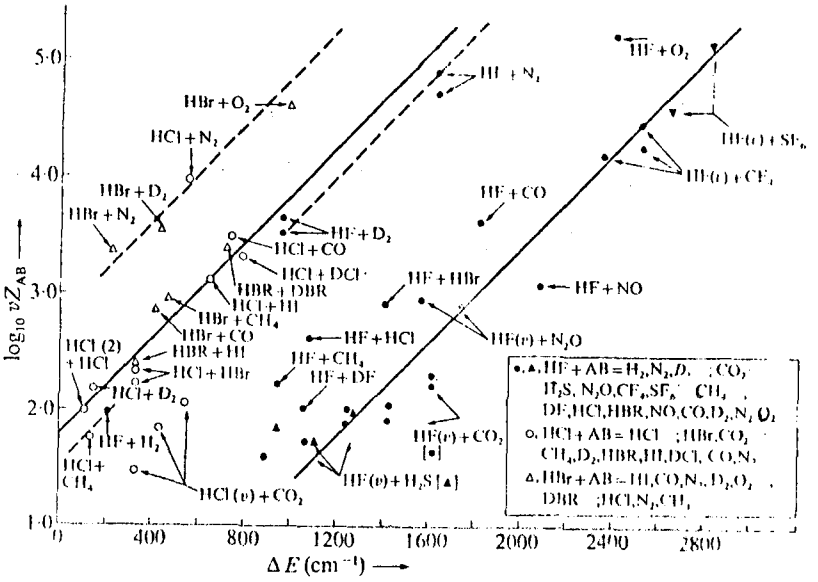

Reduced collision numbers for V-V transfer at 300 K
$HX(v) + AB(0) \leftrightarrow HX(v-1) + AB(v=1) \pm \Delta E$.
All values calculated for transition in the exothermic direction. Transitions are fo $HX(v=1)$ unless labelled $HX(v)$. Solid lines, transitions to infrared-active modes Dashed lines, transitions to infrared-inactive modes

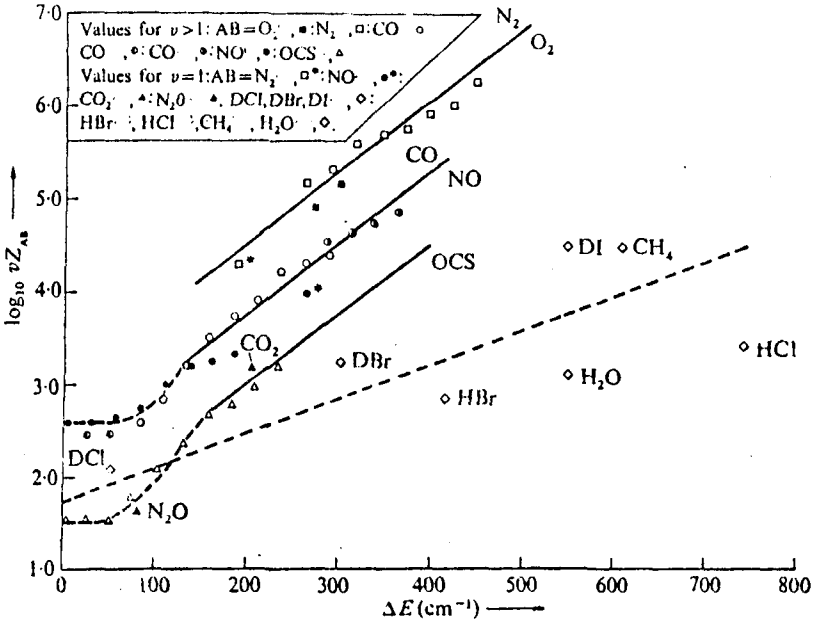

Reduced collision numbers for V-V transfer at 300 K $CO(v) + AB(0) \rightarrow CO(v-1) + AB(v=1) \pm \Delta E$.
All values calculated for transition in the exothermic direction. Solid line is the slope of Lambert-Salter plot II . Dashed line is the slope of Lambert-Salter plot I

Fig 5.15

FUNDAMENTAL ENERGY LEVELS OF DIATOMIC AND POLYATOMIC MOLECULES I

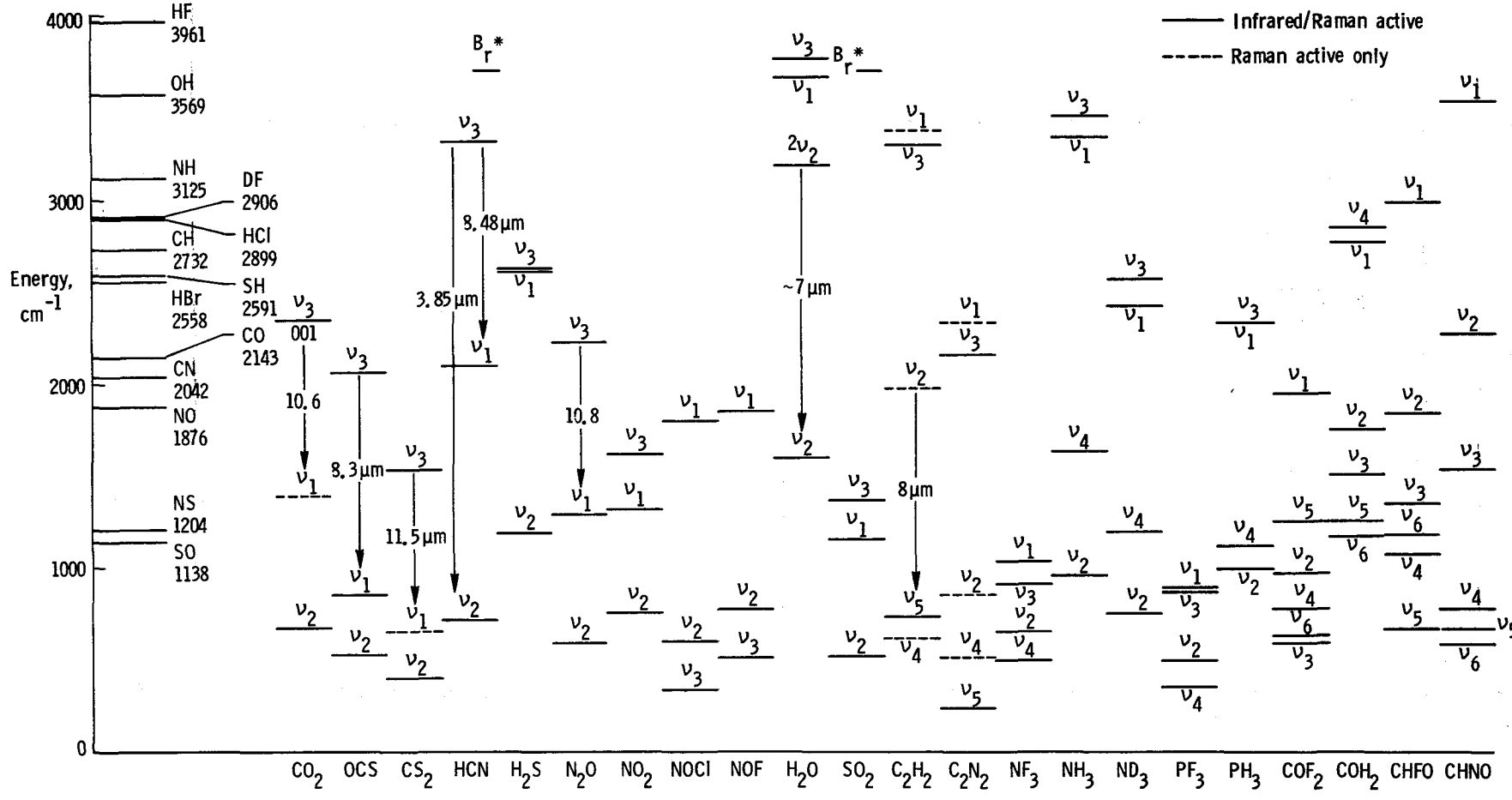

Fig 5.16

FUNDAMENTAL ENERGY LEVELS OF DIATOMIC AND POLYATOMIC MOLECULES II

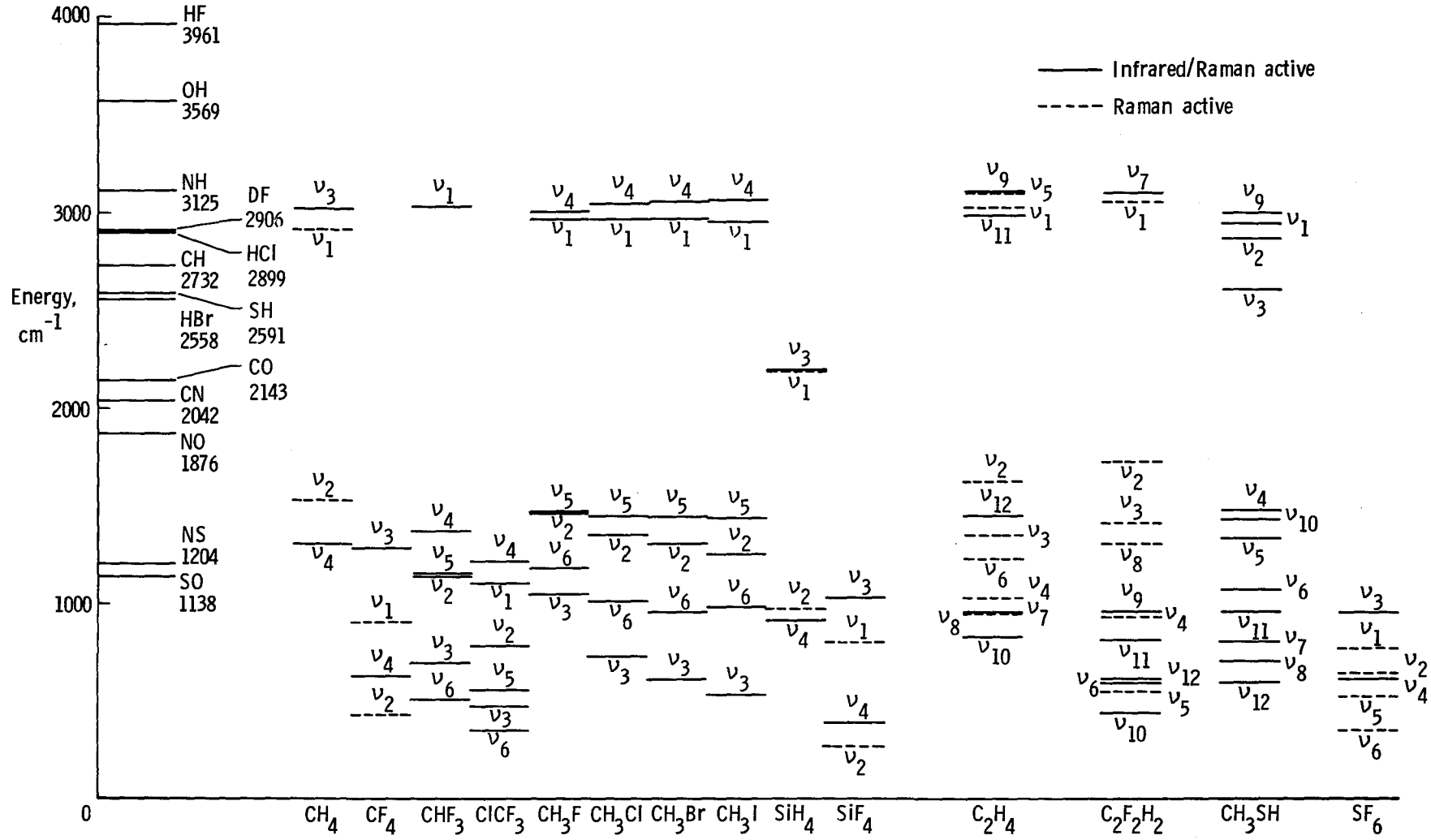

Fig 5.17

Energy Transfer Mechanisms Between Molecules

W. E. Meador
Space Technology Branch
NASA Langley Research Center

I. Introduction

The ability of light-absorbing molecules to transfer their energy to a second gas (lasant) is one of the keys to solar-pumped blackbody transfer lasers. Vibrational relaxation of the lasing gas is important for depopulating the lower laser level and maintaining population inversion. Therefore, reliable rate coefficients for energy transfer and relaxation phenomena are needed in order to do the theoretical modeling which is necessary for accomplishing the following objectives: understanding and justifying proposed laser systems, determining limitations, identifying control parameters, and scaling to space-power requirements. Modeling will also establish, to some extent, the criteria to be followed for lasant selection.

Lack of knowledge of rate coefficients is invariably the biggest obstacle to successful modeling. The purposes of this presentation are to discuss existing theoretical methods, identify sources of error, and list transfer laser criteria suggested by the theory. The emphasis is on vibrational-vibrational (V-V) energy transfer caused by both short-range (hard collisions) and long-range (dipole-dipole) interactions between molecules. Special attention is given to the importance of near-resonant collisional and dipole-dipole transfer. Finally, a technique is proposed

for perhaps significantly improving the theoretical predictions of rate coefficients.

II. V-V Rate Coefficients (Computational Methods)

V-V energy transfer can be represented by the reversible reaction

$$A^* + B \underset{k'}{\overset{k}{\rightleftarrows}} A + B^* + \Delta E \quad , \tag{1}$$

where A and B are interacting molecules, the asterisk superscript denotes vibrational excitation, k and k' are forward and reverse rate coefficients, and ΔE is the energy mismatch satisfying

$$\Delta E = E(A^*, B) - E(A, B^*) \quad . \tag{2}$$

Positive ΔE means an exothermic forward reaction, with the excess energy assumed to be converted to translational motion. Of fundamental importance to transfer lasers is the dependance of k on ΔE.

The rate coefficient k is given by

$$k = \sigma\left(\frac{8kT}{\pi\mu}\right)^{1/2} P(T, \Delta E, \mu) \quad , \tag{3}$$

where σ is the rigid-sphere cross-section, the second factor is representative of the collision frequency, μ is the reduced mass, and P is the transfer probability. The theoretical task is to compute P, which is known to peak at resonance ($\Delta E = 0$). As mentioned previously, the decay of P with increasing ΔE is a prime consideration for lasant selection.

For purposes of outlining the steps normally followed in computing P, we consider a hard collision of two diatomic molecules interacting along the line of their molecular axes. The first step is selecting an interaction potential, the simplest being exponential repulsion between nearest-neighbor atoms of the two molecules. Numerous variations have been used, including Morse and Lennard-Jones 6-12 potentials. This V(x) is then converted to V(t) through x(t) found by solving Lagrange's equations of motion. Unfortunately, most authors have followed the lead of Rapp[1] in 1965 and effectively solved these equations for elastic encounters resulting in a time-symmetrical V(t) symbollically illustrated as follows:

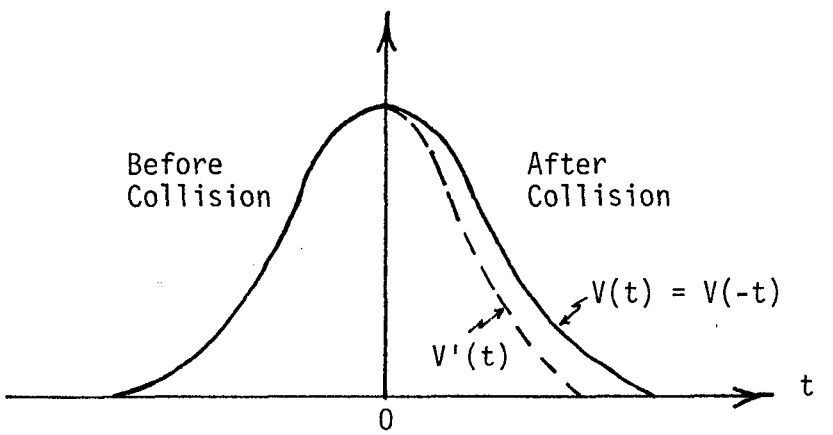

Figure 6.1

In actual fact, if $\Delta E > 0$ and transfer occurs, $V(t > 0)$ should look something like the dashed curve $V'(t)$ in order for the receding molecules to be farther apart at some time t, compared with what they were at the corresponding time - t before collision, and thereby see a reduced potential. Repercussions of this failure to conserve energy and a proposed remedy are discussed subsequently.

The next step in the determination of k is to use V(t) in time-

dependant perturbation theory (Born approximation) to find $P_{if}(v)$, the probability that colliding molecules with initial relative velocity v result in a transition from initial state i to final state f. This expression, which involves the usual transition matrix elements evaluated using linear harmonic oscillator wave functions for the two molecules, is integrated over the velocity distribution to yield the transition probability for collisions along the molecular axes. Finally, steric factors of the form $\langle\cos^2\theta\rangle$ are introduced for generalization to other impact geometries and to give the $P(T, \Delta E, \mu)$ appearing in Eq. (3).

What are the sources of error implicit in such calculations and how serious are they? Four can be identified immediately: (1) choice of the form of V(x); (2) choice of parameters in V(x); (3) failure to conserve energy by using t-symmetrical V(t); (4) use of steric factors to generalize collisional geometries. Whether steric factors can be used in this manner is certainly subject to question. The alternative, of course, is to deduce quantum mechanical potential energy surfaces with as many dimensions as necessary to completely define the geometry, and then to apply absolute reaction rate theory. Such a procedure is extremely difficult for complex molecules, but is surely needed for bench-marking the use of steric factors. There are theories and there are theories, and the ones currently being used may simply be too naive. That something is wrong is dramatically illustrated in comparisons[2] of calculated and experimental transition cross-sections, the ratios being sometimes as large as three and four orders of magnitude.

Nevertheless, and even though existing calculations of absolute rate

coefficients are generally unreliable, the relative magnitudes are useful for rating V-V channels, comparing proposed transfer lasers, and establishing trends with regard to variation of key parameters. These will be discussed in subsequent sections.

III. Detailed Balance

The first and most important result of using a t-symmetrical V(t) in perturbation theory for finding transition probabilities is

$$k = k' \quad . \tag{4}$$

That is, $P(T, \Delta E, \mu) = P(T, -\Delta E, \mu)$, which makes sense only for $\Delta E = 0$. In particular, the detailed balance relation

$$\frac{k'}{k} = \exp(-\Delta E/kT) \tag{5}$$

is not satisfied for non-resonant transfer.

Although previous authors[2] have recognized this deficiency, I see no evidence that any of them have traced it back to the failure to conserve energy. Equation (5) should come automatically from the theory. What they do, instead, is achieve detailed balance by arbitrarily adding the factor $\exp(\alpha\Delta E/kT)$ to k and the factor $\exp[-(1-\alpha)\Delta E/kT]$ to k', with 0.5 being the most common value of α. This is by no means satisfactory. In the first place, it is certainly not evident that the bad physics can be so corrected. Secondly, analysis of the integration over the velocity distribution (especially with recognition of the nonzero lower integration limit in the endothermic direction of the reaction) strongly suggests that $\alpha = 0$ would be by far the best choice.

IV. Proposed Correction

In consequence of the preceding discussion, it would seem that the very least one should do in calculating reliable rate coefficients is to impose energy conservation and satisfy detailed balance. This means using the double-valued V(t) shown in figure 6.1, with appropriate weights for V(t>0) and V'(t>0) according to whether transfer does or does not occur. In particular, the perturbation potential should be written

$$(1 - P_{if})\ V(t) + P_{if}\ V'(t)$$

if it can be ascertained that transfer predominantly occurs at minimum intermolecular separation.

That the calculations will be significantly more complex is immediately obvious. The unknown P_{if} appears in the perturbation and so requires a comparatively lengthy numerical iteration procedure for solution. We have developed the method and are currently writing the computer code. Comparison of the results with existing theories should answer the questions of how important strict energy conservation really is and whether differences between experimental and theoretical transfer cross-sections can be significantly reduced by this correction alone.

Meanwhile, we continue the present discourse with discussion of the results and predictions of existing theories as they pertain to selection of transfer lasant materials.

V. Identification of Key Parameters in Transfer Lasers

As mentioned in the Introduction, there are short-range and long-range interactions between molecular vibrators and either or both can cause V-V

transfer. For example, dipole-dipole forces create initial-final state coupling because molecular charge distributions change with nuclear coordinates. In general, it is found that long-range forces dominate transfer for small ΔE, but decrease faster than the influence of direct collisions with increasing ΔE. The short-range influence takes over for $\Delta E \gtrsim 250$ cm^{-1}. I know of no theory that includes both effects simultaneously in the perturbation, which it should for many transfer reactions.

Apart from these differences in magnitude, most of the theoretical predictions show the same general trends in k with variations of key parameters (excepting temperature), regardless of the type of interaction potential. These trends are listed as follows;

(1) Multiple quantum transitions are somewhat forbidden, constituting almost a selection rule. Squares of transition matrix elements decrease by about two orders of magnitude for every quantum transfer exceeding unity.

(2) V-V transfer is usually very rapid compared with V-translational because of greater initial-final state coupling through the perturbation potential. This often leaves vibrational excitation concentrated in a few particular levels, which is detrimental to lasing because only the ground state likely remains below the upper laser level and cannot be depopulated to maintain an inversion.

We need at least a tri-level system, with the upper level being relatively metastable to vibrational relaxation. An excellant example is transfer to the 001 (asymmetric stretching) mode of CO_2, which has the 100 (symmetric stretching) and 010 (bending) modes between it and the ground state.

(3) The transfer probability P falls off by roughly a factor of 10 for each 100 cm^{-1} of energy mismatch. As near resonance as possible is obviously the place to be for transfer lasers. However, this calculated rate of decay might be changed dramatically with a more accurate model. I expect it to be more rapid for both exothermic and endothermic transfer (i.e. a much narrower bandwidth than currently predicted).

(4) The transfer probability P increases with increasing temperature for hard collisions, but goes like T^{-1} for long-range dipole-dipole interactions. The latter dependence follows from the longer interaction times at the lower temperatures.

(5) Energy transfer is most effective when

$$\frac{\hbar}{\Delta E} \sim \text{interaction time} \sim \langle v \rangle^{-1} \sim \mu^{1/2}$$

That is, P versus $\mu^{1/2}$ goes through a maximum corresponding to this condition.

(6) Whereas the resonance value of P is usually $\lesssim 10^{-3}$ for collisions, it can approach and even exceed unity for dipole-dipole interactions. The latter is possible because long-range forces can result in effective transfer cross-sections larger than the geometrical dimensions of the molecule.

VI. V-V Energy Transfer in Polyatomics

The theory for interacting polyatomics is a straightforward extension of that for diatoms and yields the same general trends discussed previously. The main difference is that collisions may induce energy transfer among all of the vibrational degrees of freedom of both oscillators. Many types are possible, including intramolecular V-V transfer, intermolecular V-V transfer, and vibrational energy sharing. Examples involving single-quantum transfer are

$$CO_2(001) + M \rightarrow CO_2(100) + M \quad ,$$

$$CO_2(001) + N_2O(000) \rightarrow CO_2(000) + N_2O(001) \quad ,$$

and

$$CO_2(001) + SF_6 \rightarrow CO_2(100) + SF_6^* \quad ,$$

respectively.

Because of the multiplicity of modes in large polyatomics and the resulting large number of vibrational relaxations, which are therefore

quite rapid, such molecules as a class are not very promising candidates for the lasing gas. We cannot have a rapid decay to the lowest excited state because there would be no way to depopulate the ground state as the lower laser level. It would seem that linear and perhaps planar molecules, with their fewer degrees of freedom, would be the types to consider as potential lasants. However, they would have to be at least triatomics to permit single-quantum transfer and simultaneously have the lower laser level above the ground state.

Another difficulty with large polyatomics is the virtual impossibility of unraveling relaxation channels. There are few, if any, unambiguous experimental rate constants, even for triatomics, although theory does provide some useful guides: (1) V-V is most efficient for small ΔE and when the net number of quantum number changes is smallest, (2) individual processes with small ΔE are usually available, (3) V-V >> V-translational, and (4) V-translational and rotational usually proceed through the lower lying vibrational state because V-V often yields vibrational excitation concentrated in a few particular levels.

VII. Criteria for Blackbody Transfer Lasants

These may be summarized as follows from the foregoing discussion:

(1) Small polyatomics, preferably linear or planar, for the lasing gas, but at least triatomic. Dipole-dipole interactions should exist for efficient transfer of energy from the absorbers.

(2) Near-resonant energy transfer from the light-absorbing gas to the

lasing gas, provided not too many quantum number changes are required.

(3) ΔE positive in forward transfer reaction to maximize rate coefficient.

(4) "Metastable" upper laser level for inversion, at least with respect to radiative and V-V decay; good V-V relaxation of lower laser level. Might not do better than CO_2.

(5) Good absorber of blackbody radiation at 1500-2000°K; excited state sufficiently long-lived to transport to lasing gas located outside of cavity and at room temperature.

VIII. Suggested Procedure

(1) Use criteria in section VII to select potential absorbers and lasants.

(2) Use laser pumping of potential candidates to aid in this selection.

(3) Seek rate coefficients in literature for modeling of final candidates.

(4) If rate coefficients cannot be found, and they probably will not be, investigate possibilities of experimental determination.

(5) Should experimental determination not be feasible, consider theory. As it stands, theory is useful for relative rates, but probably not for absolute rates. It is useful for selecting

reasonable relaxation channels. Perhaps the changes proposed in section IV will improve the situation; if not, we should not ignore the possibility of a university grant for developing rigorous quantum mechanical methods.

References

1. D. Rapp, J. Chem. Phys. 43, 316 (1965).

2. J. J. Yardley, Introduction to Molecular Energy Transfer (Academic Press, NY, 1980).

VIBRATIONAL EXCITATION OF CO BY BLACKBODY RADIATION

L. Arriola and J. W. Wilson
Space Technology Branch
NASA Langley Research Center

I. Introduction

Lasers excited by blackbody radiation are of interest for power beaming applications in Space. In such a system sunlight is collected and focused into a blackbody cavity, heating it to approximately 2000°K. An appropriate absorbing molecule is vibrationally heated but not translationally heated when passed through the blackbody cavity. The vibrationally excited gas is then mixed with a lasant resulting in laser emission. This paper calculates the number density of CO(υ=1,2) molecules within a blackbody radiation field of a given temperature and pressure. Such calculations show the degree of excitation achievable, under ideal conditions, from blackbody pumping.

Carbon monoxide (CO) gas in the ground state is introduced into an ideal blackbody cavity. Radiant energy is absorbed by the ground state exciting it into higher vibrational levels. Once in the higher levels, processes such as vibrational to vibrational (V-V), vibrational to translational (V-T), and radiative decay tend to depopulate the upper levels. After a sufficient period of time, steady state conditions are attained.

The CO in ground state, CO(0), is assumed to be at 300°K, while the blackbody temperature is assumed to be between 1500-2000°K. The pressure

of the CO(0) can be varied from 1 to 10^4 torr. It is also assumed that the only molecular levels of importance are CO(0), CO(1) and CO(2). Figure 7.1 shows an energy level diagram, indicating the dominant kinetic process involved.

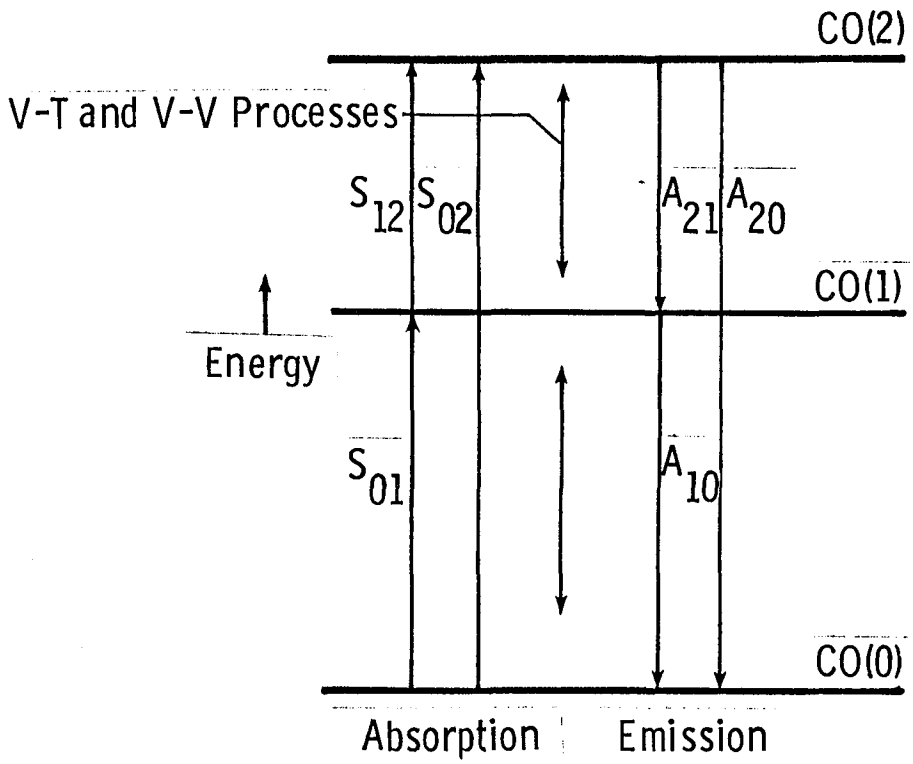

Figure 7.1 Energy Level Diagram for Molecular Levels of CO

II. Calculation of the Absorption Cross Sections

The absorbtion cross section for any material in a radiant flux is given by

$$\sigma_{ij} = \frac{A_{ij}\,\lambda^2}{8\pi}\, g(\nu) \qquad (1)$$

where A_{ij} is the Einstein coefficient associated with the transition from level i to level j, λ is the associated wavelength of the transition and

$g(\nu)$ is the lineshape including broadening effects. If we assume

$$g(\nu) = \frac{\Delta\nu}{2\pi[(\nu-\nu_0)^2 + (\frac{\Delta\nu}{2})^2]} \tag{2}$$

i.e. $g(\nu)$ is a Lorentz distribution, where ν_0 is the peak frequency. Furthermore, assume $\nu \approx \nu_0$, i.e. very small broadening effects. We see that $g(\nu)$ reduces to

$$g(\nu) = \frac{2}{\pi\ \Delta\nu} \tag{3}$$

substituting into (1) we get

$$\sigma_{ij} = \frac{A_{ij}\ \lambda^2}{4\pi^2\Delta\nu} \tag{4}$$

III. Rate Equation for Absorbtion and Relaxation

Consider now the ground state CO(0) when first introduced into the blackbody cavity. Radiant energy is absorbed by CO(0) which then raises it to CO(1) and CO(2). It is assumed to be a step function of fixed intensity at t = 0. The number of CO(0) leaving, i.e. absorbing energy, is equal to

$$\frac{d[CO(0)]}{dt} = -\sigma_{oj}\ \phi(\nu_{oj})\ \Delta\nu\ [CO(0)] \tag{5}$$

where $\phi(\nu_{oj})$ is the flux of photon at frequency ν_{oj}, σ_{oj} is the absorption cross section, and $\Delta\nu$ the absorption bandwidth. Since the radiant field is due to the blackbody we see that

$$\phi(\nu)\ \Delta\nu = \frac{2\pi}{\lambda^2}\ \frac{\Delta\nu}{e^{\frac{1.44}{\lambda T}} - 1} \tag{6}$$

and hence (5) reduces to

$$\frac{d[CO(0)]}{dt} = - (S_{01} + S_{02}) [CO(0)] \tag{7}$$

where

$$S_{ij} := \frac{A_{ij}}{2\pi} \quad \frac{1}{e^{\frac{1.44}{\lambda_{ij} T}} - 1} \tag{8}$$

Since we require conservation of mass, the formation rates for CO(1) and CO(2) are

$$\frac{dN_{CO(0)}}{dt} = - S_{01}N_{CO(0)} - S_{02}N_{CO(0)} + A_{10}N_{CO(1)} + A_{20}N_{CO(2)} \tag{9}$$

$$\frac{dN_{CO(1)}}{dt} = S_{01}N_{CO(0)} - S_{12}N_{CO(1)} - A_{10}N_{CO(1)} + A_{21}N_{CO(2)} \tag{10}$$

$$\frac{dN_{CO(2)}}{dt} = S_{02}N_{CO(0)} + S_{12}N_{CO(1)} - A_{21}N_{CO(2)} - A_{20}N_{CO(2)} \tag{11}$$

IV. Molecular Kinetics

Upon combining V-V and V-T losses to equations 9, 10, and 11, we get the complete system which model the rate of production and loss of CO(0), CO(1) and CO(2).

$$\begin{aligned}\frac{dN_{CO(0)}}{dt} = & - (S_{10} + S_{20})N_{CO(0)} + A_{10}N_{CO(1)} + A_{20}N_{CO(2)} \\ & - K_{V20}N_{CO(2)}N_{CO(0)} + K_{V11}N_{CO(1)}N_{CO(1)} \\ & + \sum_j K_{T_{j1}}N_{CO(j)}N_{CO(1)}\end{aligned} \tag{12}$$

$$\frac{dN_{CO(1)}}{dt} = S_{01}N_{CO(0)} - S_{12}N_{CO(1)} + 2K_{V20}N_{CO(2)}N_{CO(0)}$$

$$- 2K_{V11}N_{CO(1)}N_{CO(1)} - \sum_j K_{T_{j1}}N_{CO(j)}N_{CO(1)}$$

$$+ \sum_j K_{T_{j2}}N_{CO(j)}N_{CO(2)} - A_{10}N_{CO(1)} + A_{21}N_{CO(2)} \qquad (13)$$

$$\frac{dN_{CO(2)}}{dt} = S_{20}N_{CO(0)} + S_{12}N_{CO(1)} - A_{21}N_{CO(2)} - A_{20}N_{CO(2)}$$

$$- K_{V20}N_{CO(2)}N_{CO(0)} + K_{V1}N_{CO(1)}N_{CO(1)} - \sum_j K_{T_{j2}}N_{CO(j)}N_{CO(2)} \qquad (14)$$

V. Steady State Solutions

Numerical methods may be employed to generate the steady state solution to 12, 13, and 14, however, by inspection a much quicker way is possible.

Notice that the coefficients K_V's and K_T's are at least 10 orders of magnitude smaller than either the Einstein coefficients A_{ij}'s or the absorbtion coefficients S_{ij}'s (see table 7.1). We can see that eliminating them from 12, 13, and 14 will do no harm provided that the cross terms

$$\begin{matrix} K_V \\ T_{ij} \end{matrix} N_{CO(i)}N_{CO(j)}$$

are small. This assumption turns out to be true for CO.

Now upon setting 12, 13, and 14 equal to zero and eliminating the K_V and K_T terms we obtain

$$0 = -(S_{10} + S_{20})N_{CO(0)} + A_{10}N_{CO(1)} + A_{20}N_{CO(2)} \qquad (15)$$

$$0 = S_{10}N_{CO(0)} - S_{21}N_{CO(1)} - A_{10}N_{CO(1)} + A_{21}N_{CO(2)} \qquad (16)$$

$$0 = S_{20}N_{CO(0)} + S_{21}N_{CO(1)} - A_{21}N_{CO(2)} - A_{20}N_{CO(2)} \tag{17}$$

By (8) for 2000°K

$$S_{10} = 1.45$$

$$S_{21} = 2.74$$

$$S_{20} = .01$$

upon substitution of these values of S_{ij} and A_{ij} into (15)-(17) (see Table 7.1) we get

$$0 = -1.46N_{CO(0)} + 33.4N_{CO(1)} + .9N_{CO(2)} \tag{18}$$

$$0 = 1.45N_{CO(0)} - 36.14N_{CO(1)} + 62N_{CO(2)} \tag{19}$$

$$0 = .01N_{CO(0)} + 2.74N_{CO(1)} - 62.9N_{CO(2)} \tag{20}$$

From the conservation of species we get

$$\frac{N_{CO(1)}}{N_{CO(0)}} \leq .1 \tag{21}$$

and

$$\frac{N_{CO(2)}}{N_{CO(0)}} \leq .01 \tag{22}$$

Numerical solution of 12, 13, and 14 yield

$$\frac{N_{CO(1)}}{N_{CO(0)}} \approx .04 \tag{23}$$

and

$$\frac{N_{CO(2)}}{N_{CO(0)}} \approx 4(10^{-3}) \tag{24}$$

Time dependent numerical solutions of 12, 13, and 14 are shown in figures 7.2, 7.3, and 7.4. After approximately 10 msec the density approaches steady-state values. Figure 7.5 shows the CO(v = 1) density as a function of CO pressure for blackbody temperatures of 1500 to 2000°K.

VI. Conclusions

As shown in figure 7.4 steady-state CO(1) densities of 5×10^{17} per cm^3 can be obtained by blackbody pumping at 2000°K. The energy storage at such densities is 0.0215 joules/cm^3. If the CO had a volume of 1000 cm^3 and was transferred to a lasant within 10 msec, lasing on the order of 2 kW would be achieved.

It was also found that blackbody pumping the second harmonic, CO(2), is much less efficient than the fundamental. The CO(2) density is approximately 100 less than CO(1).

Table 7.1.- CO parameters.

$A_{10} = 33.4\ sec^{-1}$ [1]

$A_{20} = 0.9\ sec^{-1}$ [1]

$A_{21} = 62.0\ sec^{-1}$ [1]

$K_{V11} = 2.57\ (10^{-12})\ cm^3/sec$ [2]

$K_{V20} = 2.14\ (10^{-12})\ cm^3/sec$ [2]

$K_{T01} = 1.94\ (10^{-20})\ cm^3/sec$ [2]

$K_{T11} = 1.94\ (10^{-20})\ cm^3/sec$ [2]

$K_{T21} = 1.94\ (10^{-20})\ cm^3/sec$ [2]

$K_{T02} = 2.48\ (10^{-20})\ cm^3/sec$ [2]

$K_{T12} = 2.48\ (10^{-20})\ cm^3/sec$ [2]

$K_{T22} = 2.48\ (10^{-20})\ cm^3/sec$ [2]

$S_{10}\ (2000°K) = 1.45\ sec^{-1}$

$S_{21}\ (2000°K) = 2.74\ sec^{-1}$

$S_{20}\ (2000°K) = .01\ sec^{-1}$

$\lambda_{10} = 4.67\ (10^{-4})\ cm$

$\lambda_{20} = 2.35\ (10^{-4})\ cm$

$\lambda_{21} = 4.72\ (10^{-4})\ cm$

References

1. Blaver, J. A.; and Nickerson, G. R.: A Survey of Vibrational Relaxation Rate Data for Processes Important to CO_2-N_2H_2O Infrared Plume Radiation. AIAA 7th Fluid and Plasma Dynamics Conference, AIAA, c. 1974.

2. Javan, A.; and Gverra, M.: Photoexcitation of Lasers and Chemical Reactions for NASA Missions - A Theoretical Study. NASA CR-3428, 1981.

CO(υ=1,2) DENSITY VERSUS TIME

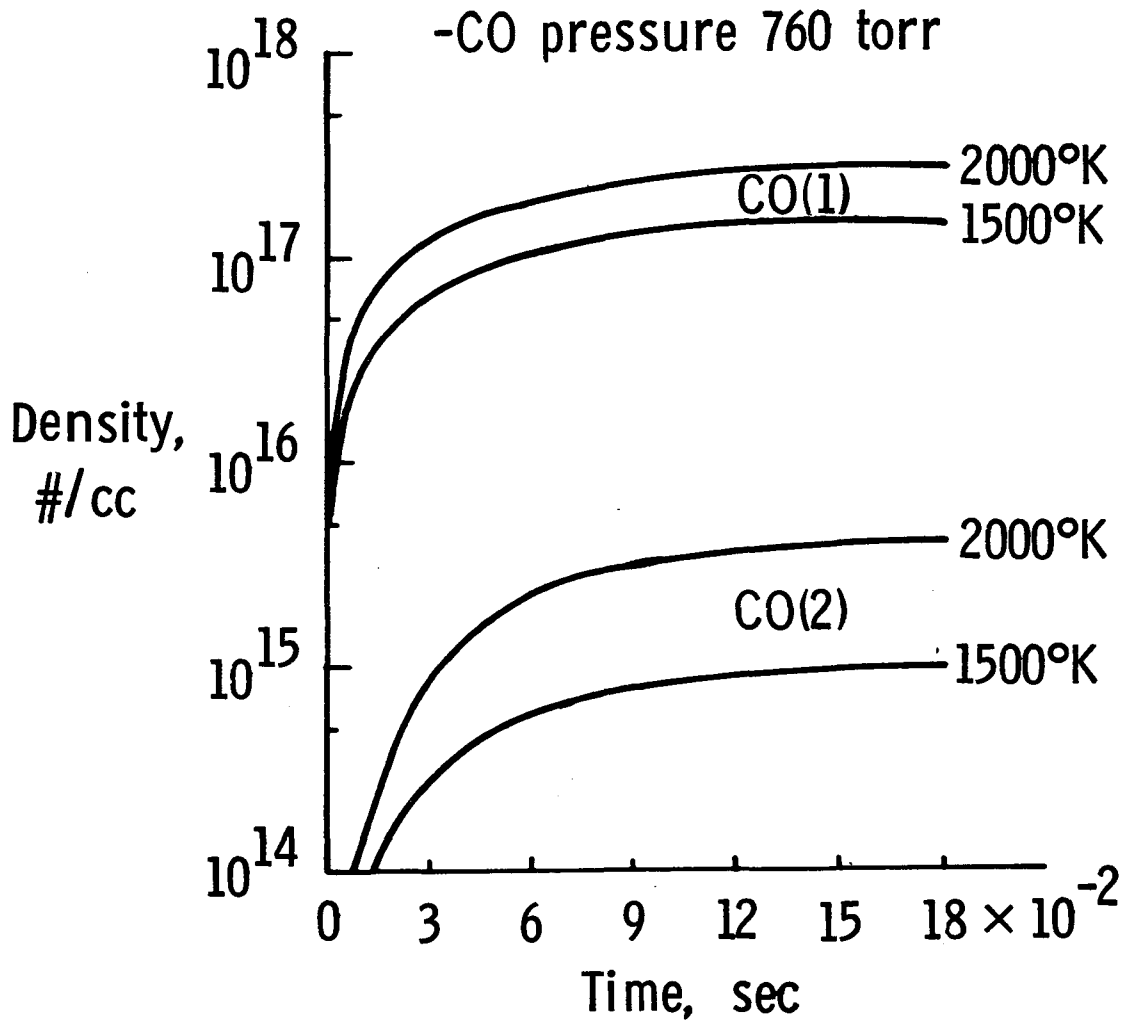

Fig. 7.2

CO(υ=1,2) DENSITY VERSUS TIME

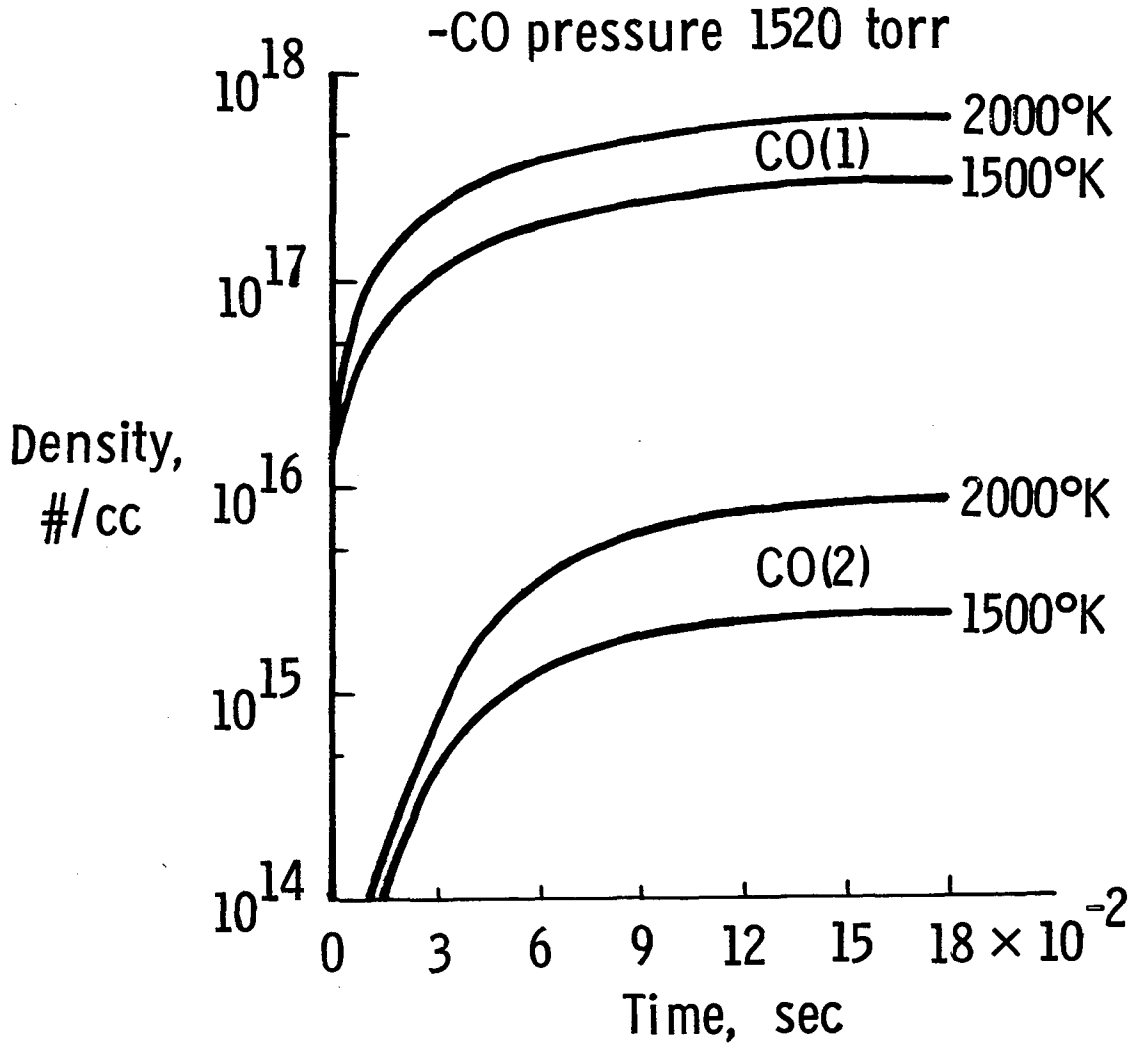

Fig. 7.3

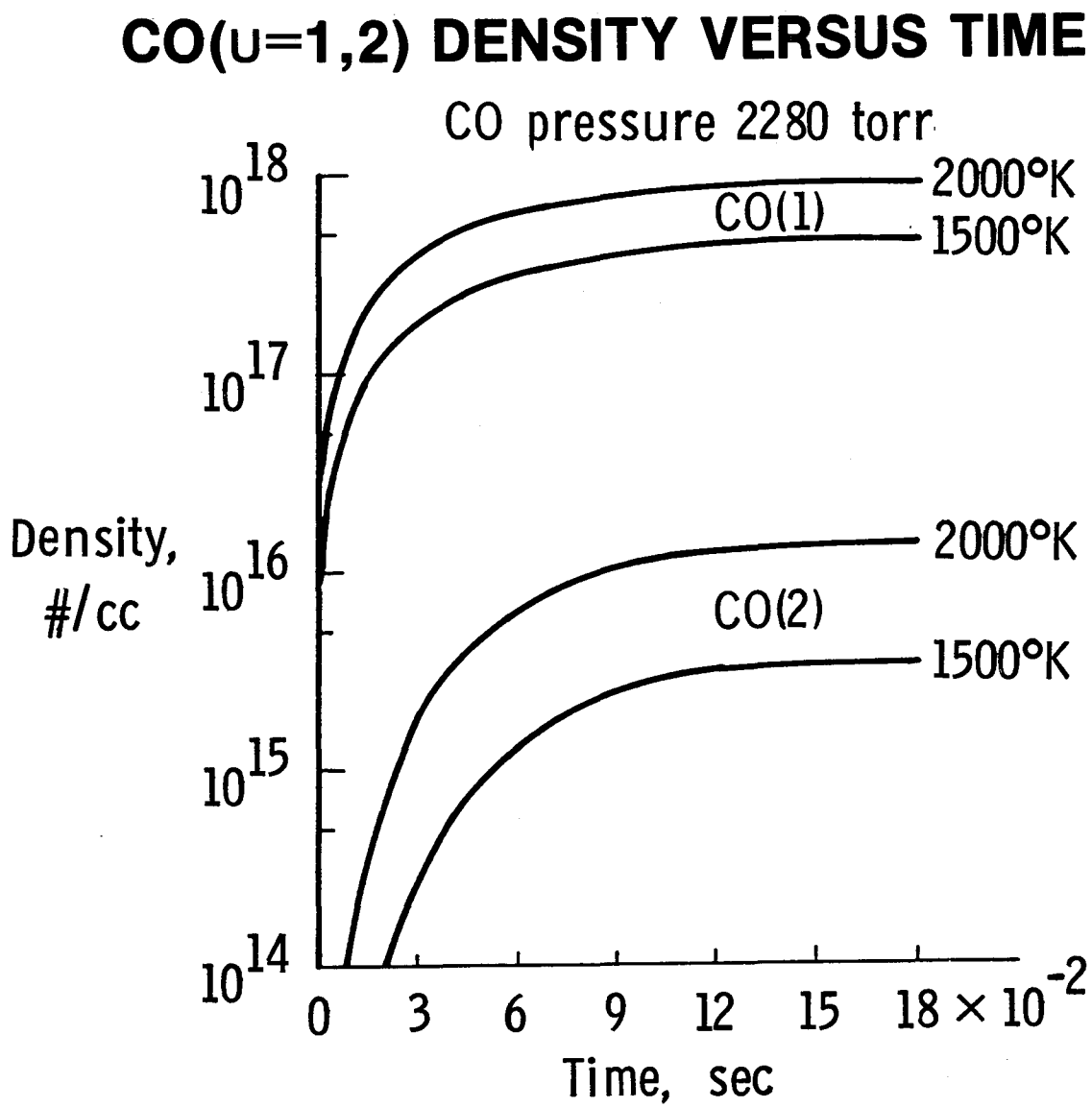
CO(U=1,2) DENSITY VERSUS TIME
CO pressure 2280 torr
Density, #/cc
10^{18}
10^{17}
10^{16}
10^{15}
10^{14}
CO(1)
2000°K
1500°K
CO(2)
2000°K
1500°K
0
3
6
9
12
15
18×10^{-2}
Time, sec

Fig. 7.4

CO(1) DENSITY VERSUS PRESSURE

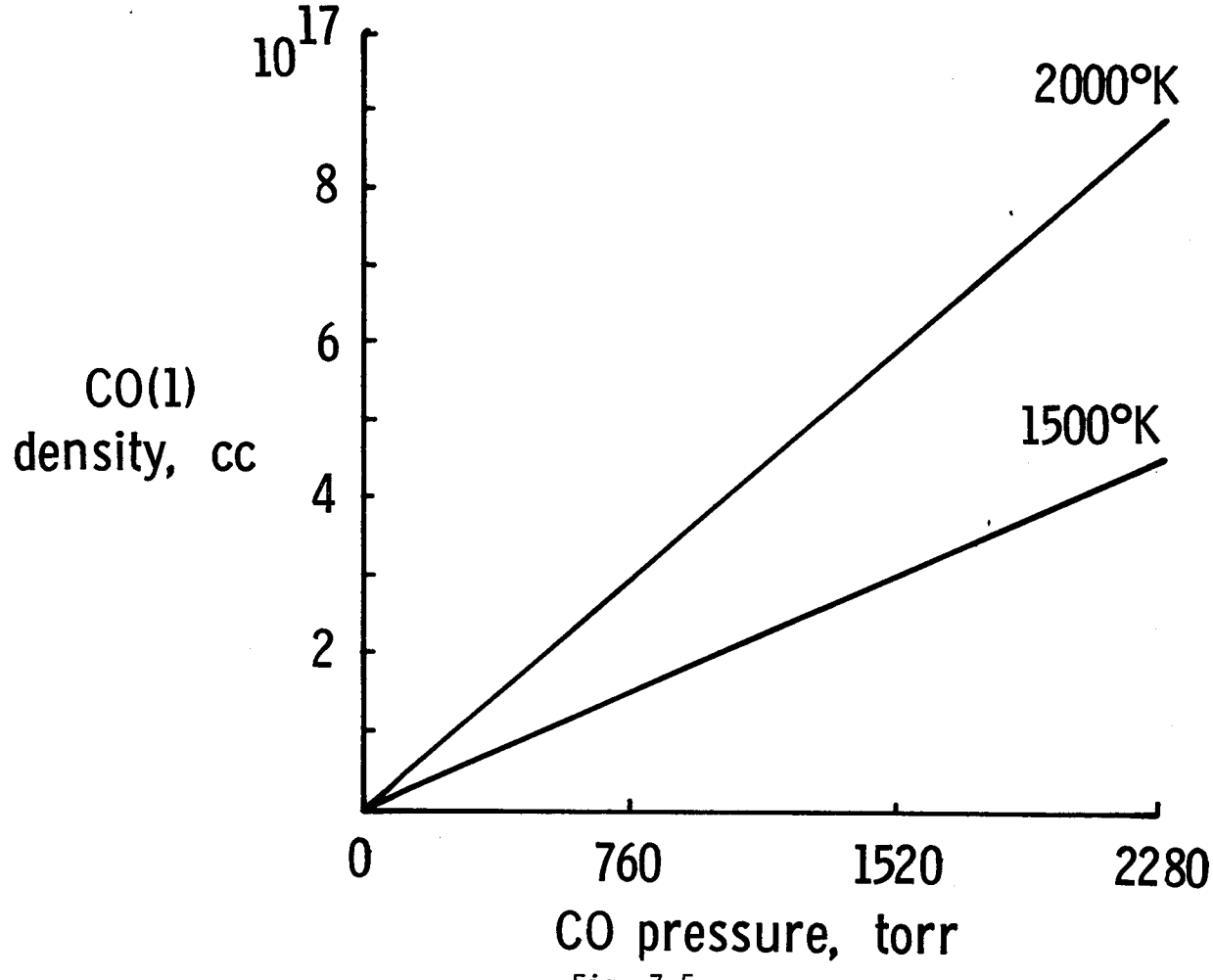

Fig. 7.5

A METHOD FOR ANALYSIS OF BLACKBODY DIATOMIC-TRIATOMIC LASERS

J. W. Wilson, K. Y. Chen, L. Arriola,
and J. H. Heinbockel
NASA Langley Research Center
Hampton, Virginia

A formalism is developed for analysis of performance of direct blackbody and blackbody transfer lasers. Application to the CO/CO_2 system is made.

We treat three cases:

1. Photoexcited triatomic laser
2. Photoexcited diatomic-triatomic laser
3. Photoexcited diatomic mixing triatomic laser

Each will be treated in a transverse flow geometry as illustrated in figure 8.1.

Case 1: Photoexcited Triatomic Laser

The triatomic molecule has three vibration modes denoted by $T(\nu_1, \nu_2, \nu_3)$ where ν_1 is quantum number of symmetric stretch, ν_2 of bending mode and ν_3 is for asymmetric stretch. The modes are approximately harmonic oscillator modes with allowed transitions as $\Delta\nu = \pm 1$. Only the lowest vibrational level of each mode is significantly excited by a radiation source.

The ν_3 mode is weakly coupled to ν_1 and ν_2 levels. The ν_1 and $2\nu_2$ are strongly mixed due to Fermi resonance in CO_2. The laser transition is taken as $T(001) \rightarrow T(100)$ corresponding to the 10.6 μ line in CO_2. The present model assumes a CO_2 like behavior.

The photoexcitation rate is

$$S = \int_0^\infty \sigma(\nu)\ \phi_T(\nu)\ d\nu$$

where $\sigma(\nu)$ is the absorption cross section and ϕ_T is a blackbody source flux at temperature T (exposure on one side and no attenuation in gas). This is approximated by

$$S \simeq \sigma(\nu_a)\ \phi_T(\nu_a)\ \Delta\nu$$

where ν_a is the band center, $\Delta\nu$ the bandwidth and

$$\sigma(\nu_a) \simeq \frac{\lambda_a^2\ A}{4\pi^2\ \Delta\nu}$$

where A is the spontaneous transition rate and

$$\lambda_a = c/\nu_a$$

with

$$\phi_T(\nu) = \frac{2\pi}{\lambda_a^2}\ \frac{d\nu}{e^{h\nu/kT}-1}$$

so that

$$S = \frac{A}{2\pi}\ \frac{1}{e^{1.44/\lambda_a T}-1}$$

We denote T(000) as T_o, T(001) as T_u and T(100) as T_L and write

$$\dot{T}_u = S_u T_o - \alpha_u T_u$$

$$\dot{T}_L = \alpha_T T_u - \alpha_L T_L$$

$$\alpha_u = \tau_u^{-1} = k_d^{'}\ T_o + A_u$$

$$\alpha_T = k_d' T_o$$

$$\alpha_L = \tau_L^{-1} = k_{d_L}' T_o$$

with kinetic coefficients given in table 8.1. The above equations can be solved for a steady light source as

$$T_u(t) = S_u T_o \tau_u [1-e^{-\alpha_u t}]$$

The maximum density for the upper level is

$$T_{max} = S_u T_o \tau_u$$

The excitation efficiency is given as the ratio

$$n^*(t) = T_u(t)/S_u T_o t$$

where $S_u T_o t$ is the number of photons absorbed by the gas. The equations for the lower level are

$$T_L(t) = \alpha_T T_{max} \{\tau_L(1-e^{-\alpha_L t}) - (\alpha_L-\alpha_u)^{-1} (e^{-\alpha_u t}-e^{-\alpha_L t})\}$$

The maximum extractable energy is

$$E_S(t) = h\nu_\ell [T_u(t) - T_L(t)]$$

and the laser energy storage efficiency is

$$n(t) = h\nu_\ell [T_u(t) - T_L(t)]/(h\nu_a S_u T_o t)$$

where ν_ℓ is the frequency of the laser transition.

First note that there is no inversion if $\alpha_L < \alpha_u$. In fact, $\alpha_L >> \alpha_u$ is a requirement to obtain adequate gain. One may rewrite as

$$n(t) \simeq h\nu_\ell T_{max}[1-e^{\alpha_u t} - \frac{\alpha_T}{\alpha_L} + \frac{\alpha_T}{\alpha_L} e^{-\alpha_u t}]/h\nu_a S_u T_o t$$

$$= \frac{h\nu_\ell}{h\nu_a \alpha_u t} (1 - \frac{\alpha_T}{\alpha_L}) (1 - e^{-\alpha_u t})$$

for which the energy storage efficiency approaches (ν_ℓ/ν_α) at $t \simeq 0$ and $0.63\ (\nu_\ell/\nu_a)$ at $t \simeq \tau_u$, which results in about 25 percent efficiency for CO_2 as is observed experimentally. The fraction of storable energy is

$$F(t) = E_S(t)/(h\nu_\ell\ T_{max})$$

$$\simeq (1 - \frac{\alpha_T}{\alpha_L}) (1 - e^{-\alpha_u t})$$

and rises from 0 at $t = 0$ to $0.63\ (1 - \alpha_T/\alpha_L)$ at $t_{opt} \simeq \tau_u$.

In terms of a flowing system a design in which pumping occurs over a period $t \simeq \tau_u$ before reaching the output mirrors would result in a reasonably high inversion without great sacrifice in efficiency.

Clearly the system parameters are to be chosen such that

$$\alpha_L >> \alpha_u \geq \alpha_T$$

This gives

$$k'_{d_L} T_o >> k'_d T_o + A_u \geq k'_d T_o$$

so that gas requirements are

$$k'_{dL} >> k'_d \quad \text{and} \quad T_o >> A_u/k'_d$$

which are clearly satisfied by CO_2 when

$$T_o >> 4 \times 10^{16}/cm^3$$

The maximum density achievable for the upper level is

$$T_u \simeq S_u/k_d' = 1.7 \times 10^{15}/cm^3$$

and is independent of the pressure range of ordinary operation above a few torr.

The fraction of maximum storable laser energy is shown in figure 8.2 along with the laser storage efficiency. The maximum storable laser energy is shown in figure 8.3 where the pressure independence above a few torr is clearly shown.

Case 2: Photoexcited Diatomic-triatomic Laser

The triatomic molecule of case 1 is now mixed with a diatomic molecule that has its first vibrational level in near resonance with the upper laser level. The rate equation for the first excited level of the diatomic molecules is

$$\dot{D}_1 = S_D D_o - \alpha_D D_1$$

where

$$\alpha_D = \tau_D^{-1} = k_T D_o + k_T' T_o + k_V T_o + A_D$$

where k_T', k_T are V-T transfer rate coefficients and k_V is the V-V transfer rate coefficient. The triatomic equations have added terms

$$\dot{T}_u = S_u T_o + \alpha_V D_1 - \alpha_u T_u$$

$$\dot{T}_L = \alpha_T T_u - \alpha_L T_L$$

$$\alpha_u = \tau_u^{-1} = k_d D_o + k_d' T_o + A_u$$

$$\alpha_v = k_V T_o$$

$$\alpha_T = k_d D_o + k_d' T_o$$

$$\alpha_L = \tau_L^{-1} = k_{d_L} D_o + k_{d_L}' T_o$$

The kinetic coefficients are given in table 8.1.

We first consider the steady state solution. In steady-state, we find

$$D_{ss} = S_D D_o \tau_D$$

$$T_{u_{ss}} = \left(S_u T_o + \frac{\alpha_V}{\alpha_D} S_D D_o\right) \tau_u$$

$$T_{L_{ss}} = \frac{\alpha_T}{\alpha_L} \left(S_u T_o + \frac{\alpha_V}{\alpha_D} S_D D_o\right) \tau_u$$

The steady state inversion density is then

$$\Delta T = \left(T_{u_{ss}} - T_{L_{ss}}\right) = \left(S_u T_o + \frac{\alpha_V}{\alpha_D} S_D D_o\right) \tau_u \left(1 - \frac{\alpha_T}{\alpha_L}\right)$$

The maximum gain is achieved when

$$\alpha_V \approx \alpha_D$$

$$\alpha_L >> \alpha_T$$

Noting that steady state is generally an inefficient mode of excitation we now consider the transient solution.

The transient solution is given as

$$D_1(t) = S_D D_o \tau_D \left(1 - e^{-\alpha_D t}\right)$$

$$T_u(t) = \left(S_u T_o + \frac{\alpha_V}{\alpha_D} S_D D_o\right) \tau_u \left(1 - e^{-\alpha_u t}\right)$$

$$+ \frac{\alpha_V}{\alpha_u - \alpha_D} S_D D_o \tau_D \left(e^{-\alpha_u t} - e^{-\alpha_D t}\right)$$

$$T_L(t) = \frac{\alpha_T}{\alpha_L} \left(S_u T_o + \frac{\alpha_V}{\alpha_D} S_D D_o\right) \tau_u \left(1 - e^{-\alpha_L t}\right)$$

$$- \frac{\alpha_T}{\alpha_L - \alpha_u} \left(S_u T_o + \frac{\alpha_V}{\alpha_D} S_D D_o\right) \tau_u \left(e^{-\alpha_u t} - e^{-\alpha_L t}\right)$$

$$+ \frac{\alpha_T}{\alpha_L - \alpha_u} \frac{\alpha_V}{\alpha_u - \alpha_D} S_D D_o \tau_D \left(e^{-\alpha_u t} - e^{-\alpha_L t}\right)$$

$$- \frac{\alpha_T}{\alpha_L - \alpha_D} \frac{\alpha_V}{\alpha_u - \alpha_D} S_D D_o \tau_D \left(e^{-\alpha_D t} - e^{-\alpha_L t}\right)$$

We first take $\alpha_V \simeq \alpha_D$ as optimum. To insure a large inversion

$$\alpha_L >> \alpha_u \geq \alpha_T$$

Using these requirements we get

$$T_u(t) \approx \left(T_{max} + D_{SS} \frac{\alpha_D}{\alpha_u}\right) \left(1 - e^{-\alpha_u t}\right)$$

$$+ \frac{\alpha_D}{\alpha_u - \alpha_D} D_{SS} \left(e^{-\alpha_u t} - e^{-\alpha_D t}\right)$$

Clearly $\alpha_V \approx \alpha_D >> \alpha_u$ will give large values to $T_u(t)$. Maximizing the upper level in time obtains

$$t_o \simeq \ell n \left[\frac{\alpha_u}{\alpha_D} + \frac{S_u T_o \alpha_u}{S_D D_o \alpha_D}\left(1 - \frac{\alpha_u}{\alpha_D}\right)\right]/(\alpha_u - \alpha_D)$$

where t_o is the time at which T_u is maximum.

Similarly,

$$T_L(t) \simeq \frac{\alpha_T}{\alpha_L}\left(T_{max} + D_{SS}\frac{\alpha_D}{a_u}\right)$$

$$- \frac{\alpha_T}{\alpha_L}\left(T_{max} + D_{SS}\frac{\alpha_D}{\alpha_u}\right) e^{-\alpha_u t}$$

$$- \frac{\alpha_T}{\alpha_L} D_{SS}\, e^{-\alpha_u t}$$

Finally, the inversion density is $(t > \tau_D, \tau_L)$

$$\Delta T = [T_u(t) - T_L(t)]$$

$$\approx \left(T_{max} + D_{SS}\frac{\alpha_D}{\alpha_u}\right)\left(1 - \frac{\alpha_T}{\alpha_L}\right)\left(1 - e^{-\alpha_u t}\right)$$

$$- D_{SS}\left(1 + \frac{\alpha_T}{\alpha_L}\right) e^{-\alpha_u t}$$

There seems to be no critical dependence on the relative magnitudes of α_L and α_D. There is a slight advantage of choosing $\alpha_L >> \alpha_D$ in the term

$$- \frac{\alpha_T}{\alpha_L - \alpha_D}\,\frac{\alpha_V}{\alpha_u - \alpha_D} S_D D_o \tau_u \left(e^{-\alpha_D t} - e^{-\alpha_u t}\right)$$

So the final requirement is

$$\alpha_L >> \alpha_D \approx \alpha_V >> \alpha_u \geq \alpha_T$$

although the requirement $\alpha_L >> \alpha_D$ is not critical. The above requirements lead to

$$k_{d_L} D_o + k'_{d_L} T_o >> k_T D_o + k'_T T_o + k_V T_o + A_D \approx k_V T_o$$

$$>> k_d D_o + k'_d T_o + A_u \geq k_d D_o + k'_d T_o$$

which are easily achieved for the CO/CO_2 system.

The time dependence of the fraction of maximum storable laser energy and storage efficiency are shown in figure 8.4. The maximum storable laser energy is shown in figure 8.5. There seems to be no real advantage in mixing the two gases. Although the photoabsorption rate is increased by the CO, the limited storage factor seems to be the relatively short lifetime of the upper laser level and the added CO gas even reduces it somewhat.

Case 3: Photoexcited Diatomic Mixing Triatomic Laser

(A) Energy storage in a diatomic gas

Neglecting the overlap of the wings of the rotational lines in absorption, the absorption rate is

$$S_D = \frac{A_D}{2\pi} \left(e^{1.44/\lambda_a T} - 1\right)^{-1}$$

where T is the photoexcitation source temperature ($\approx 2000°K$), λ_a is the absorption wavelength (cm) and A_D is the Eienstein A coefficient. Assuming the gas does not heat up from room temperature and that higher levels than the first vibration are negligible

$$\dot{D}_1 = S_D D_o - k_T D_o D_1 - A_D D_1$$

adequately define the kinetics so long as $D_1 << D_o$. The density of excited states is then

$$D_1(t) = S_D D_o \tau_o (1 - e^{-\alpha_o t})$$

where

$$\alpha_o = \tau_o^{-1} = k_T D_o + A_D$$

The maximum number of excited states that can be achieved is

$$D_{max} = S_D D_o \tau_o$$

which is a function of D_o and is largest when $k_T D_o >> A_D$ for which

$$D_{max} \simeq S_D / k_T$$

But an optimum pressure is indicated here as

$$D_o >> A_D / k_T \cdot$$

The efficiency of energy storage is

$$\eta(t) = D_1(t) / S_D D_o t = (1 - e^{-\alpha_o t}) \frac{\tau_o}{t}$$

while the fraction of energy stored is

$$F(t) = D_1(t) / D_{max} = (1 - e^{-\alpha_o t})$$

We see that there is a tradeoff between storage efficiency and stored density. A good compromise is probably

$$D_o \approx 2A_D / k_T \quad \text{at} \quad t \simeq \tau_o$$

(B) Mixing with triatomic gas

The diatomic gas is removed from the excitation region with an excitation level D_1 and mixed with a triatomic gas. The upper laser level is

$$T_u(t) = \frac{\alpha_V}{\alpha_u - \alpha_D} D_1[e^{-\alpha_D t} - e^{-\alpha_u t}]$$

and the lower laser level is

$$T_L(t) = \frac{\alpha_T}{\alpha_L - \alpha_D} \frac{\alpha_V}{\alpha_u - \alpha_D} (e^{-\alpha_D t} - e^{-\alpha_L t}) D_1$$

$$- \frac{\alpha_T}{\alpha_L - \alpha_u} \frac{\alpha_V}{\alpha_u - \alpha_D} (e^{-\alpha_u t} - e^{-\alpha_L t}) D_1$$

where D_1 is the value at the time mixing occurs. Suppose $\alpha_L >> \alpha_u$ so we only worry about maximizing $T_u(t)$

$$\frac{\partial}{\partial t} T_u(t) = \frac{\alpha_V}{\alpha_u - \alpha_D} D_1(-\alpha_D e^{-\alpha_D t} + \alpha_u e^{-\alpha_u t})$$

is stationary at

$$t_o = \ell n(\alpha_u/\alpha_D)/(\alpha_u - \alpha_D)$$

at which time

$$T_u(t_o) = \frac{\alpha_V}{\alpha_D} D_1[\frac{\alpha_u}{\alpha_D}]^{\frac{\alpha_u}{\alpha_D - \alpha_u}}$$

and can be approximated as

$$T_u(t_o) \approx \frac{\alpha_V}{\alpha_D} D_1 e^{-\alpha_u/\alpha_D}$$

Clearly the maximum occurs at $\alpha_D \approx \alpha_V >> \alpha_u$.

In this event

$$t_o \simeq \frac{\ell n(\alpha_D/\alpha_u)}{\alpha_D} \approx 2/\alpha_D$$

is on the order of the optimum mixing time before lasing.

Again

$$\alpha_L >> \alpha_u \geq \alpha_T$$

$$\alpha_D \approx \alpha_V >> \alpha_u \geq \alpha_T$$

as requirements for an optimum system.

The fraction of maximum storable laser energy and the energy storage efficiency are shown as a function of time in figure 8.6. The optimum time of energy extraction is somewhat less than τ_u in this case. The maximum storable energy is shown in figure 8.7. We first note that the optimum CO to CO_2 mixing ratios is about 9 : 1. Note also the much higher excitation levels achievable (nearly 2 orders of magnitude). This is because

$$D_{max} \simeq 4.8 \times 10^{18}/cm^3$$

is quite large.

Conclusions

The present formalism gives a basis for intercomparison of various diatomic/triatomic lasant mixtures in three laser configurations. It is seen from the present analysis that the mixing laser configuration has many advantages in that CO can achieve high excitation densities so that high power can be achieved on a relatively small scale.

Table 8.1.- CO/CO_2 parameters*

Au	425 sec^{-1}
Su	16.9 sec^{-1}
K_d'	1E-14 cm^3/sec
K_{d_L}'	4E-13 cm^3/sec
A_D	33.4 sec^{-1}
S_D	1.33 sec^{-1}
K_d	6.E-15 cm^3/sec
K_{d_L}	5.7E-12 cm^3/sec
K_V	5.7E-14 cm^3/sec
K_T	2.8E-19 cm^3/sec
K_T'	5.7E-18 cm^3/sec

*Data is from E. W. McDaniel et. al., Compilation of Data Relevant to Nuclear Pumped Lasers, volume IV, Technical Report H-78-1, Redstone Arsenal, Dec. 1978.

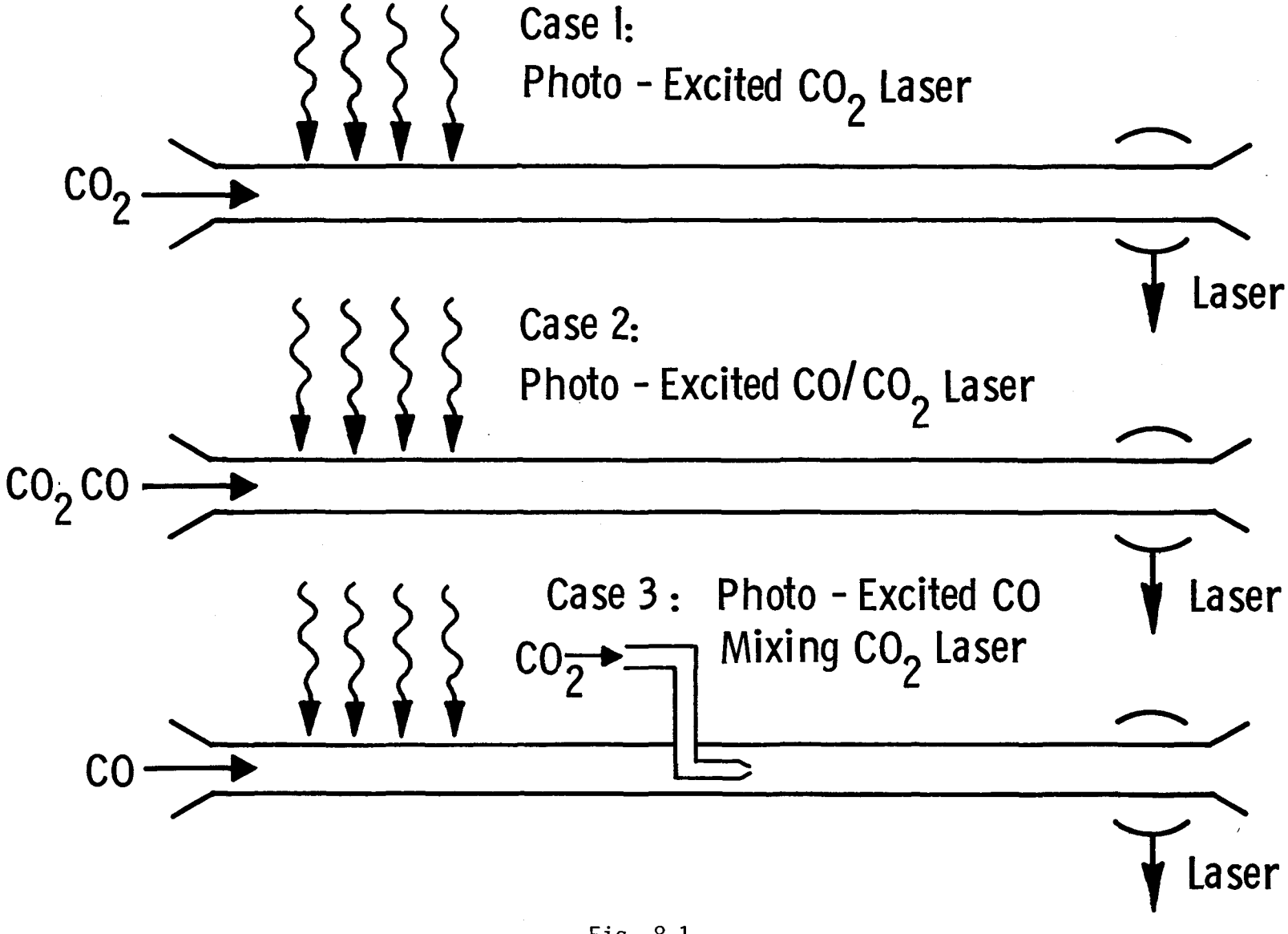
Case 1:
Photo - Excited CO_2 Laser
CO_2
Laser
Case 2:
Photo - Excited CO/CO_2 Laser
CO_2 CO
Laser
Case 3 : Photo - Excited CO
Mixing CO_2 Laser
CO_2
CO
Laser

Fig. 8.1

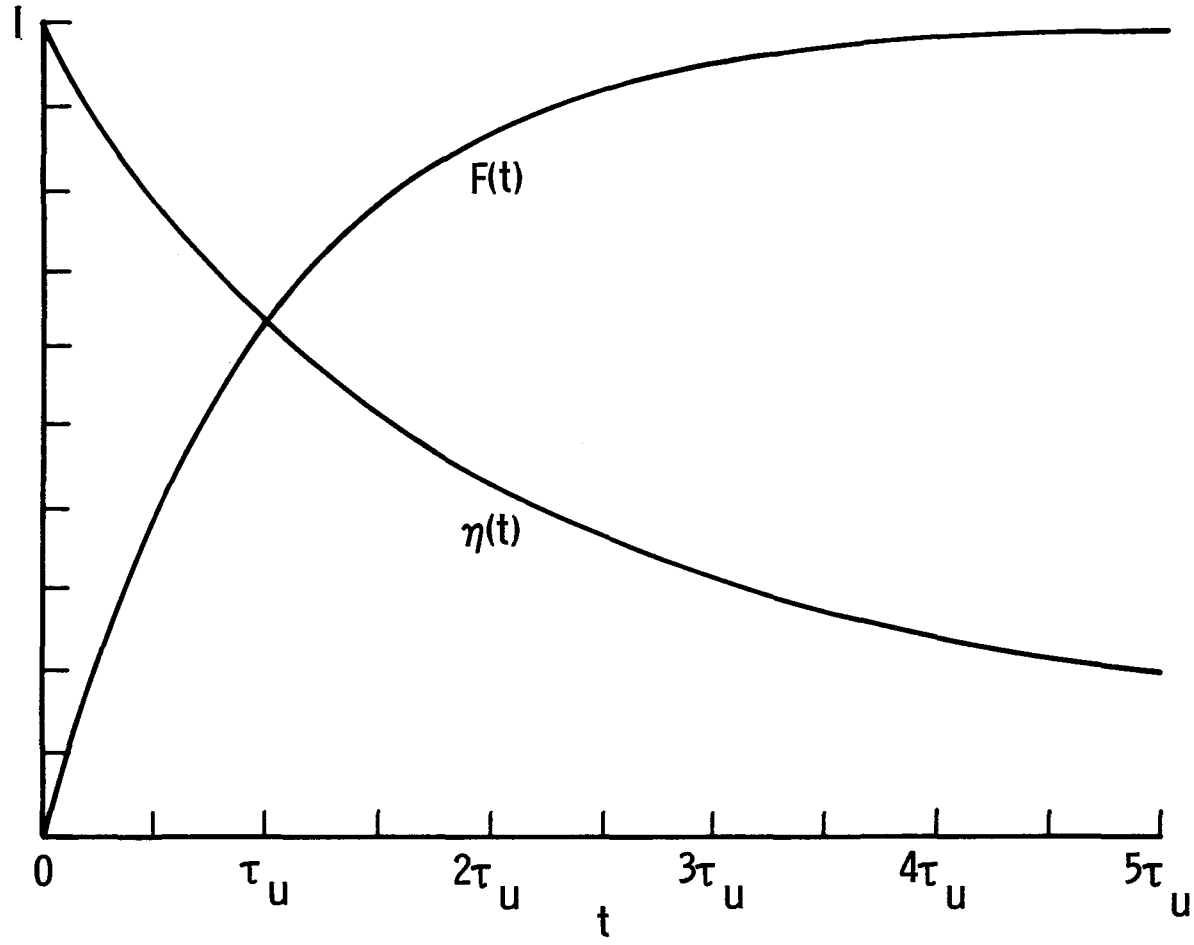

Fig. 8.2

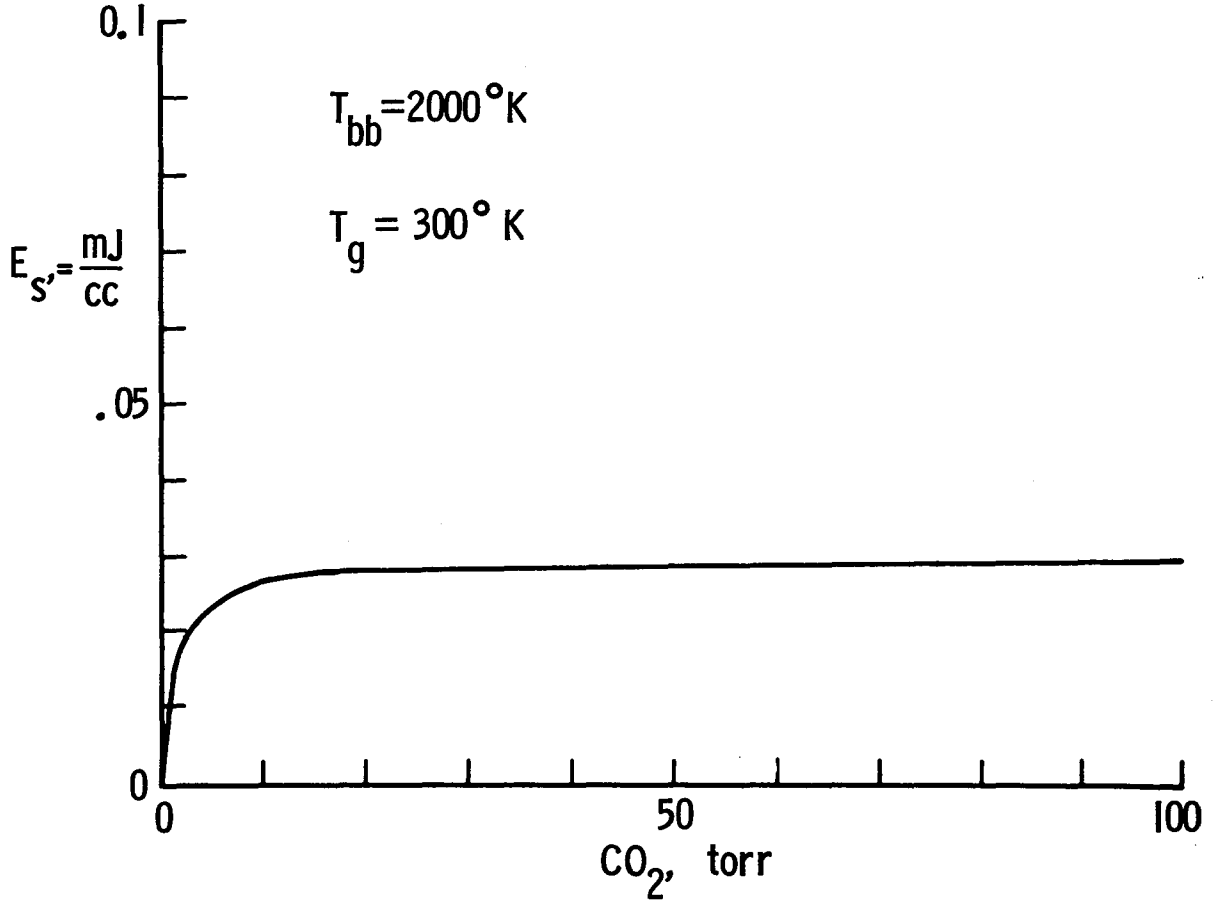

Fig. 8.3

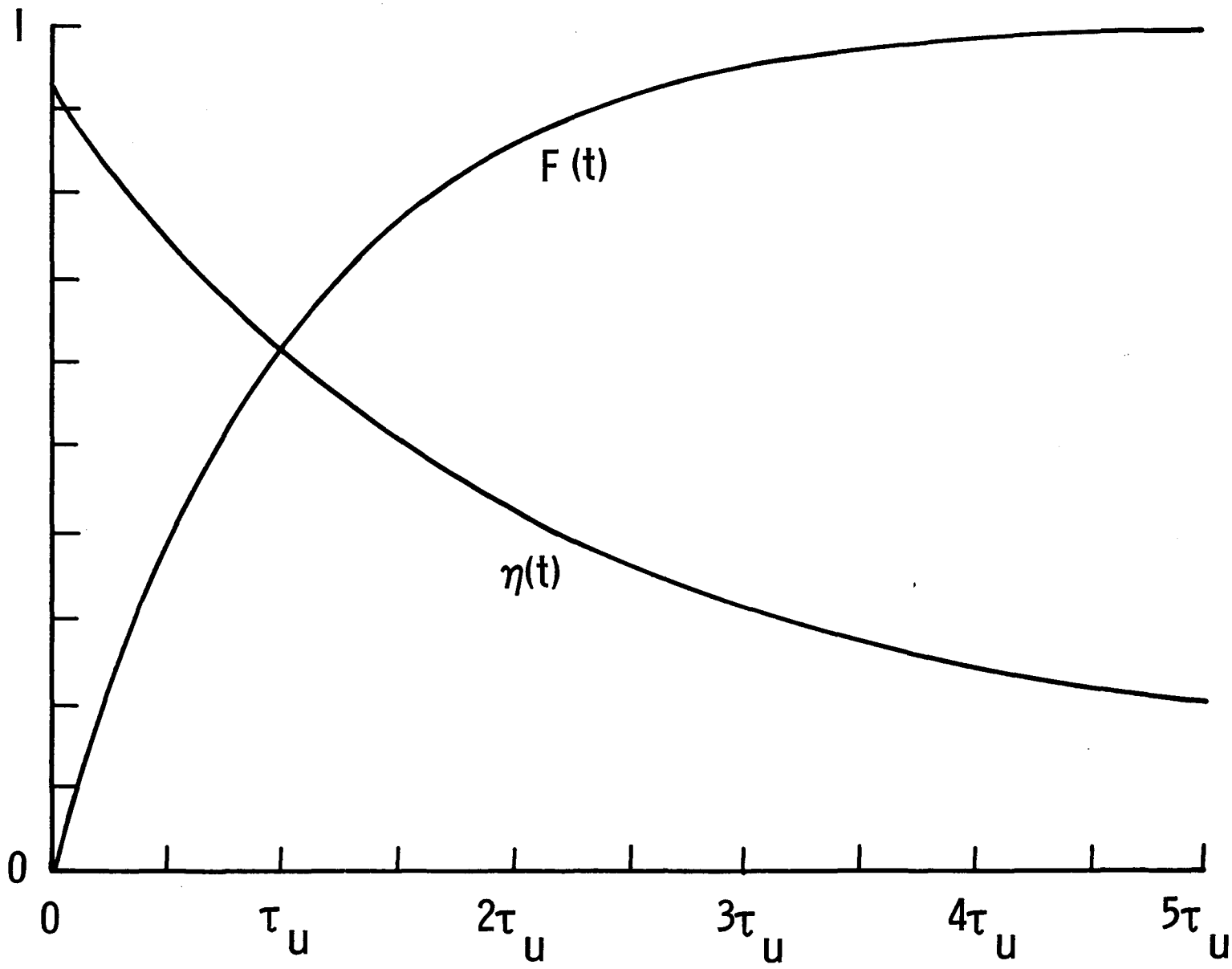

Fig. 8.4

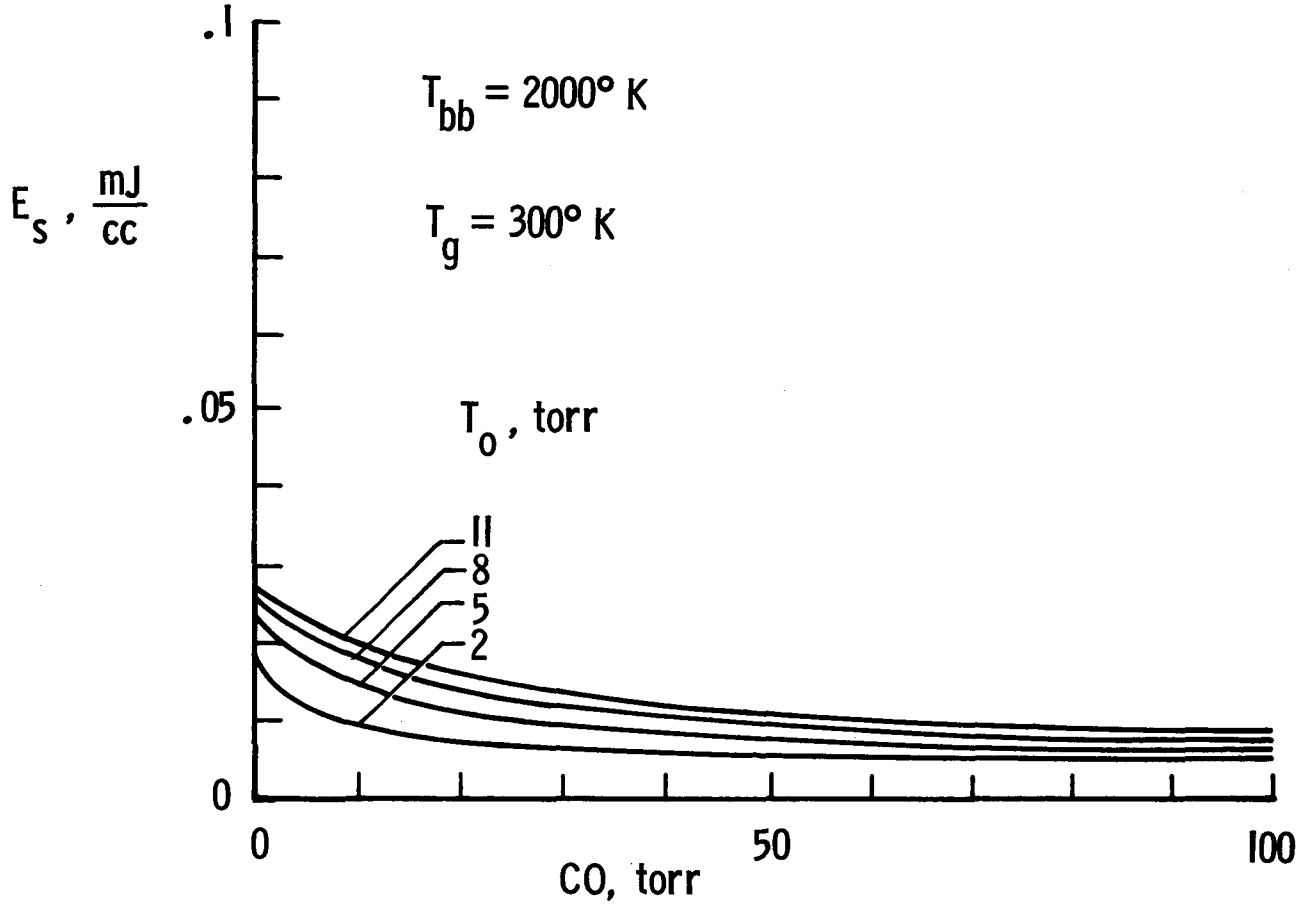
.1
.05
0
E_s, $\frac{mJ}{cc}$
T_{bb} = 2000° K
T_g = 300° K
T_o, torr
11
8
5
2
0
50
100
CO, torr

Fig. 8.5

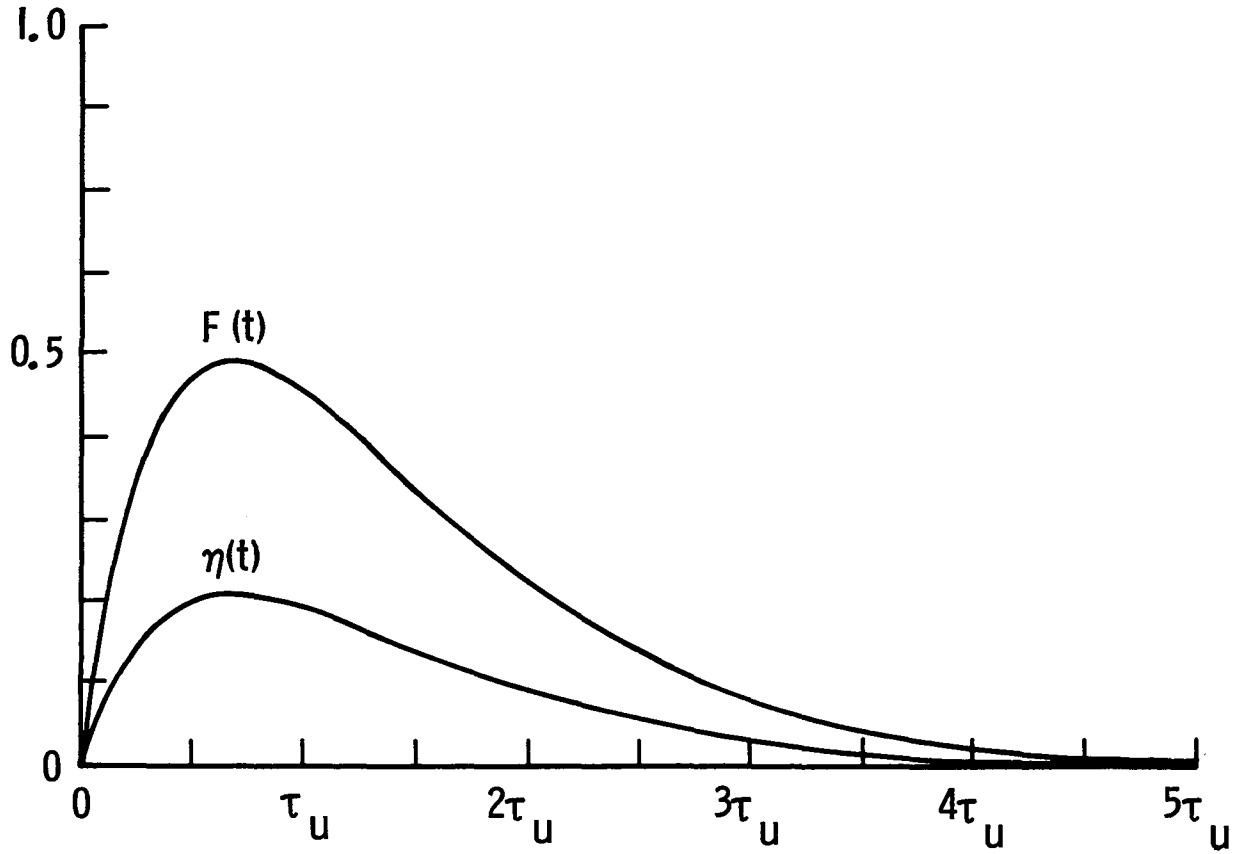

Fig. 8.6

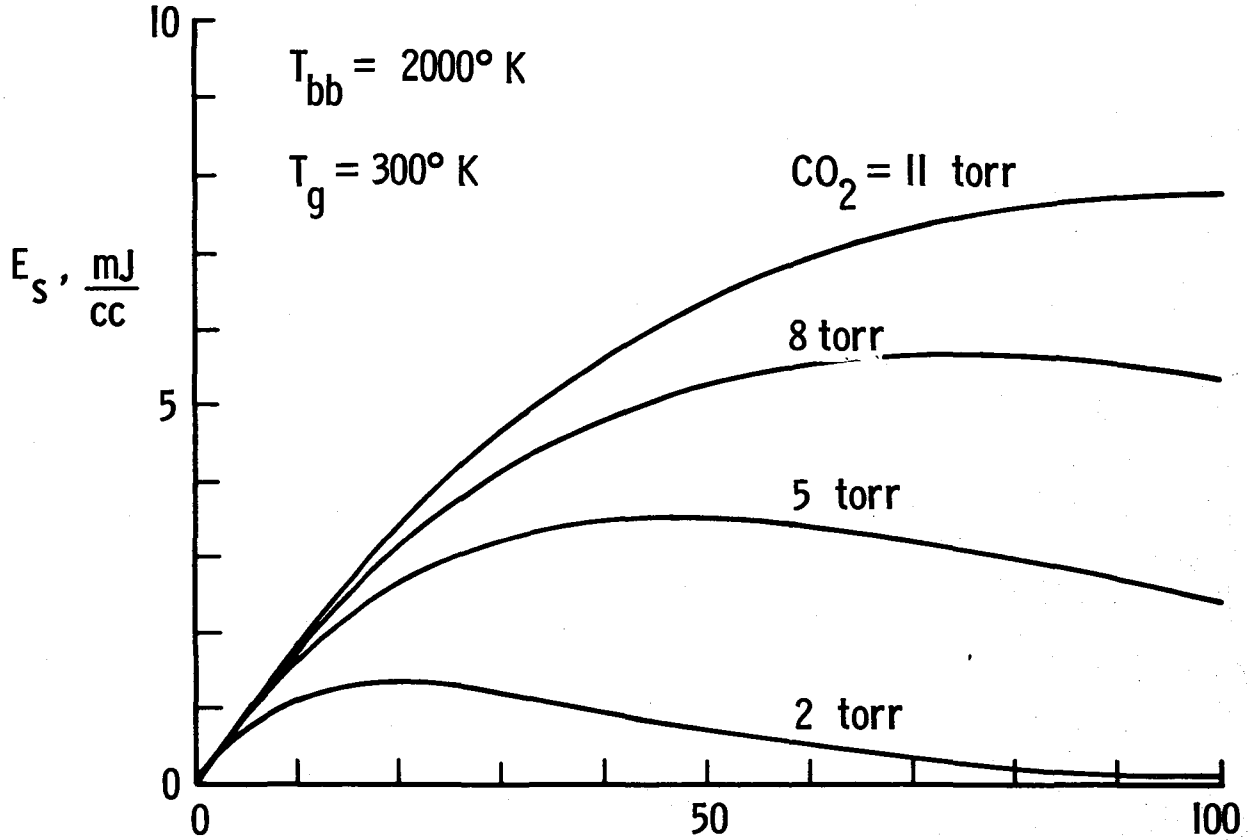
10
5
0
0
50
100
T_{bb} = 2000° K
T_g = 300° K
E_s, $\frac{mJ}{cc}$
CO_2 = 11 torr
8 torr
5 torr
2 torr

Fig. 8.7

Report from the Cavity-Laser Working Group

Edmund J. Conway
Space Technology Branch
NASA Langley Research Center

From the Workshop, a Cavity-Laser Working Group was formed with the attendees listed in table 9.1. The goal of this Cavity-Laser Working Group was to propose molecules which might be useful as lasants for blackbody cavity-lasers. The approach was to (a) define some rules for the identification of molecules, (b) consider molecules presented at the Workshop and (c) identify additional molecules through the suggestions of attendees. Some evaluation was to be attempted for each molecule considered.

A set of criteria was developed, however, sophisticated rules required detailed information which was not available for every molecule. The rules were:

1. The lasants should be polyatomic gases, generally with more than two atoms per molecule, permitting the lower laser level (LLL) to be above the ground state.

2. The molecule should be heteronuclear so that vibrational (V) transitions could lead to absorption of infrared (IR) radiation.

3. The physical structure of the molecule should be simple because simple molecules have the fewest vibrational modes which may divide or dissipate excitation energy. Linear molecules are the most desirable, planar are second, and non-planar molecules are third most desirable.

4. Generally, the first vibrational frequency ($\omega = \sqrt{k/m}$) of any mode is the most important. A calculation was discussed which showed that the IR absorption of the lowest harmonic was lower by more than a factor of 10 than that of the fundamental frequency.

5. Molecules providing a broad absorption band are desired. A broad absorption band means broader than that of CO_2, such as gas with two or more broadened and intercommunicating vibrational lines.

6. The absorption line should be at a shorter wavelength than the 4.3 μm absorption of CO_2 to take greater advantage of the intense blackbody fluxes occurring in the 1 to 3 μm range.

7. The laser emission should be shorter than 10.6 μm to provide higher quantum efficiency than CO_2.

8. The lower laser level (LLL) should be higher than that of CO_2 to limit the temperature sensitivity of laser emission.

Most of the potential lasant molecules mentioned during the Workshop presentations were identified by K. Y. Chen and R. De Young. A list of 36 are contained, with fundamental energy levels, in figures 5.16 and 5.17 of this report. An additional 16 were chosen by attendees primarily because they were gases or liquids with substantial vapor pressure at 300°K, and they exhibit relatively simple molecular structures, i.e. linear, planar, etc.

Some evaluation was attempted in table 9.2 for each molecule considered. The areas of evaluation were expected infrared absorption of the molecule, expected laser emission and general characteristics. These were areas of "expected" behavior because the only data used was that mentioned in the paragraph above. Generally, comparisons were made. For example, if IR absorption is "narrow strong, at X μm" then the highest energy fundamental absorption is similar to that of CO_2 but at a wavelength of X μm. Comments on whether likely lower laser levels (LLL) could or could not be populated by IR absorption were included.

Laser emission wavelength, if known, was listed along with likely temperature sensitivity as compared to that of CO_2. If laser wavelength was unknown, the wavelength for a transition from a high energy level to one or more lower levels was estimated. The terminology "unknown, Y μm possible" denotes unobserved laser transitions which would make this molecule a useful blackbody cavity lasant.

Comments on General Characteristics fell into three classes. First was a subjective rating of the likelihood that the molecule would be a useful blackbody cavity lasant. The likelihood ratings were Very Good, Good, Fair, and Poor. For some cases, the rating was replaced with the letters MDN (meaning More Detail Needed).

The second class of comments suggest which molecules should be investigated more thoroughly. These were labeled, High Priority. The last class of general comments specified the molecular structure as Linear, Planar or Non-Planar.

Molecules which are rated as High Priority candidates for cavity lasants include H_2O, NH_3, CH_4, BeH_2, $Be(CH_3)_2$, BH_3 and $B(OH)_3$. In approximately the order shown, these molecules deserve broader consideration, further literature search and more experimental work.

Table 9.1

Attendees at Cavity Laser Working Group

C. Blount, Texas Christian University
P. Brockman, Laser Systems and Measurements Branch, FED
W. Christiansen, University of Washington
E. Conway, Space Technology Branch, SSD
W. Harries, Old Dominion University
D. Humes, Space Technology Branch, SSD
J. Jones, Virginia Commonwealth University
M. Lee, Hampton University
G. Miner, Space Technology Branch, SSD
D. Phillips, Materials Characterization Instrumentation Section, IRD
J. Quagliano, Virginia Commonwealth University
L. Stock, Hampton University
W. Weaver, Space Technology Branch, SSD
L. Vallarino, Virginia Commonwealth University
L. Zapata, Miami University

Evaluative Comments for Potential Cavity Lasants

Molecule	IR Absorption	Laser Emission	General	
CO_2	• Narrow strong, at 4.3 μm • LLL IR inactive	• At 10.6 μm, strong, temp. sensitive • BB pumping achieved	Very Good	Linear mol.
OCS	• Narrow strong, near 5 μm • LLL IR active	• At 8.3 μm, temp. sensitive • Strong OCS quenching • Laser pumping, 19% efficient	Fair	Linear mol.
CS_2	• Narrow strong, near 6.5 μm • LLL IR inactive	• At 11.5 μm, strongly temp. sensitive	Poor	Linear mol.
HCN	• Narrow strong, near 3.5 μm • 2LLLs IR active	• At 8.5 μm, not thermally sensitive • At 3.85 μm, thermally sens. • Lases laser-pumped	Good	Linear mol.
H_2S	• Strong vib doublet near 3.8 μm • LLL pop. by IR abs.	• Unknown, 7.0 μm possible • Emptying of LLL may be slow	Fair	Planar mol.
N_2O	• Strong narrow, near 4.5 μm • LLL pop. by IR abs.	• At 10.8 μm, thermal sensitivity equal to CO_2 • BB pumping achieved	Good	Linear mol.

Table 9.2

Molecule	IR Absorption	Laser Emission	General
NO_2	• Strong narrow, near 6.2 μm • LLL pop. by IR abs.	• Unknown, 11.5 μm possible • Temperature sensitive	Poor — Planar mol.
NOCl	• Strong narrow, near 5.6 μm • LLL pop. by IR abs.	• Unknown, 6.9 μm possible • ν_2 & ν_3 thermally pop.	Poor — Planar mol.
NOF	• Strong narrow, near 5.5 μm • ν_2 & ν_3 pop. by IR abs.	• Unknown, 7.5 μm possible • ν_2 & ν_3 thermally pop.	Poor — Planar mol.
H_2O	• Two abs. lines between 2.6 μm and 2.8 μm • ν_2 pop. by IR abs. • $2\nu_2$ weak abs. near 3.1 μm	• At 7 μm, from overtones of ν_2 • Unknown, 4.9 μm possible	Good — Planar mol. High priority
SO_2	• Strong narrow, near 7.3 μm • ν_1 & ν_2 pop. by IR abs.	• Unknown, 11.8 μm possible • ν_2 temp. sensitive	Poor — Planar mol.
C_2H_2	• Strong narrow, near 3.0 μm • ν_5 pop. by IR abs.	• At 8 μm, ν_2 to ν_5 thermally sensitive • Others unknown, but 6.1 μm and 3.0 μm possible	Good — Linear mol.

Table 9.2(continued)

Molecule	IR Absorption	Laser Emission	General
C_2N_2	• Strong narrow, near 4.6 μm • ν_5 pop. by IR abs.	• Unknown, 6.2 μm possible • Some possible LLL IR inactive but very thermally sensitive	Fair — Linear mol.
NH_3	• Strong doublet between 2.9 μm and 3.0 μm • ν_2 & ν_4 pop. by IR abs.	• At 6.7 μm, ULL and LLL unknown • Unknown, but 4.7 μm and and 3.4 μm possible	Good, interesting laser wavelengths High priority Non-planar mol.
ND_3	• Strong doublet between 3.9 μm and 4.1 μm • ν_2 & ν_4 pop. by IR abs.	• Unknown, but 6.5 μm and 4.8 μm possible • As temp. sensitive as CO_2	Fair — Non-planar mol.
NF_3	• Strong abs. near 9.6 μm	• Unknown, 14.5 μm possible • Much more temp. sensitive than CO_2	Poor — Non-planar mol.
PH_3	• Strong doublet near 4.3 μm • ν_2 & ν_4 pop. by IR abs.	• Unknown, 6.0 μm possible • Temp. sensitivity similar to CO_2 • Good transfer from LLL	Good, interesting laser wavelength Non-planar mol.
PF_3	• Strong doublet near 11.3 μm • ν_2 & ν_4 pop. by IR abs.	• Unknown, 12.2 μm possible • ν_2 & ν_4 thermally pop.	Poor — Non-planar mol.

Table 9.2 (continued)

Molecule	IR Absorption	Laser Emission	General
COF_2	• Strong narrow, near 5.1 μm • ν_2 thru ν_6 pop. by IR abs	• unknown, 7.4 μm possible • ν_2 thru ν_5 thermally pop.	Poor — Planar mol.
COH_2	• Strong doublet between 3.5 μm and 3.6 μm • ν_2, ν_3, ν_5, ν_6 pop. by IR abs.	• Unknown, 6.2 μm possible • Less temp. sensitive than CO_2 • Good transfer from LLL	Fair — Planar mol.
COHF	• Strong narrow, near 3.4 μm • ν_2 thru ν_6 pop. by IR abs.	• Unknown, 8.7 to 4.3 μm possible • ν_3 thru ν_6 thermally sensitive • ν_2 less temp. sensitive than CO_2 LLL	Fair — Planar mol.
COHN	• Strong narrow, near 2.8 μm • ν_2 thru ν_6 pop. by IR abs.	• Unknown, but 8.0 to 3.4 μm possible • ν_2 & ν_3 less temperature sensitive than CO_2 LLL • Good transfer from LLL	Fair — Planar mol.
CH_4	• Strong narrow, near 3.3 μm • ν_1 & ν_2 not pop. by IR abs.	• Unknown, but 6.7 and 5.8 μm possible • ν_1, ν_2 & ν_4 less temp. sensitive than CO_2 LLL	Good — Non-planar mol. High priority

Table 9.2 (continued)

Molecule	IR Absorption	Laser Emission	General	
CF_4	• Strong narrow, near 7.8 μm • ν_1 & ν_2 not pop. by IR abs.	• Unknown, 11.6 μm possible • All modes temp. sensitive	Poor	Non-planar mol.
CHF_3	• Strong narrow, near 7.3 μm • All modes IR active	• Unknown, but 6.0 to 4.0 μm • ν_2, ν_3, ν_5 & ν_6 more temp. sensitive than CO_2 LLL	Fair	Non-planar mol.
CF_3Cl	• Strong narrow, near 8.2 μm • All modes IR active	• Unknown, 11.5 μm possible • Strongly temp. sensitive	Poor	Non-planar mol.
CH_3F	• Strong doublet, near 3.3 μm • All modes IR active	• Unknown, but 6.7 to 5.2 μm possible • ν_2 & ν_5 less temperature sensitive than CO_2 LLL	Fair	Non-planar mol.
CH_3Cl	• Strong doublet, near 3.3 μm • All modes IR active	• Unknown, but 6.6 to 4.4 μm possible • ν_5 & ν_2 less temperature sensitive than CO_2 LLL	Fair	Non-planar mol.
CH_3Br	• Strong doublet, near 3.3 μm • All modes IR active	• Unknown, but 6.6 to 4.2 μm possible • ν_5 less temp. sensitive than CO_2 LLL	Fair	Non-planar mol.

Table 9.2 (continued)

Molecule	IR Absorption	Laser Emission	General
CH_3I	• Strong doublet, near 3.3 μm • All modes IR active	• Unknown, but 6.6 to 4.1 μm possible • ν_5 less temp. sensitive than CO_2 LLL	Fair — Non-planar mol.
SiH_4	• Strong doublet, near 4.5 μm • ν_1 & ν_2 not IR active	• At 7.95 μm, laser-pumped • ν_2 & ν_4 more temperature sensitive than CO_2 LLL.	Good — Non-planar mol.
SiF_4	• Strong narrow, near 9.6 μm	• Unknown, 13.1 μm possible • All modes temperature sensitive	Poor — Non-planar mol.
C_2H_4	• Strong doublet, near 3.2 μm • Many modes not IR active	• Unknown, but 6.7 to 4.4 μm possible • Several modes not strongly temp. sensitive • V-V in ULL and LLL	• Fair, complex V spectrum • Interesting laser wavelengths Non-planar mol.
$C_2F_2H_2$	• Strong narrow, near 3.2 μm • Many modes not IR active	• Unknown, but 7.5 to 3.8 μm possible • Several modes not strongly temp. sensitive • V-V in ULL and LLL	• Fair, complex V spectrum • Interesting laser wavelengths Non-planar mol.

Table 9.2 (continued)

Molecule	IR Absorption	Laser Emission	General
CH_3SH	• Strong triplet, near 3.3 μm • All modes IR active	• Unknown, but 7.2 to 4.4 μm possible • Several modes not strongly temp. sensitive	• Fair, complex V spectrum • Interesting laser wavelengths Non-planar mol.
SF_6	• Strong narrow, near 10.5 μm • All modes IR active	• Unknown, 20.2 μm possible • All modes temperature sensitive	Poor Non-planar mol.
CO	• Strong narrow, at 4.7 μm	• Known • Requires low temperature operation	Good Linear mol.
NaK			MDN Linear mol.
NaLi			MDN Linear mol.
BeH_2			MDN, Linear mol. High priority
$BeCl_2$			MDN Linear mol.
BeF_2			MDN Linear mol.
BH_3;$(BH_3)_2$			MDN, Planar mol. High priority

Table 9.2 (continued)

Molecule	IR Absorption	Laser Emission	General
BF_3			MDN Planar mol.
$AlCl_3$			MDN Planar mol.
AlF_3			MDN Planar mol.
$SOCl_2$			MDN Planar mol.
$Be(CH_3)_2$			MDN, Approx. linear mol. High priority
$Be(C_2H)_2$			MDN Linear mol.
$B(OH)_3$			MDN, Planar mol. High priority
$Ni(CO)_4$			MDN Planar mol. Electron recombination site
$Ni(CH_3COCHCOCH_3)_2$			MDN Approx. planar mol.

Table 9.2 (continued)

Report from the Transfer-Laser Working Group

W. E. Meador
Space Technology Branch
NASA Langley Research Center

Light-absorbing molecules and lasing molecules were discussed with regard to satisfying the following criteria for blackbody transfer lasers:

(1) Good absorbers of blackbody radiation at 1500-2000°K, with the excited states sufficiently long-lived to permit transport to a laser cavity where the lasing gas is injected at room temperature and subsequently mixed with the absorbing gas.

(2) Near resonant energy transfer from the absorbing gas to the lasant, provided not too many quantum number changes are required.

(3) Dipole-dipole interactions for most efficient energy transfer.

(4) Exothermic forward transfer reaction (not critical).

(5) Polyatomic lasant molecules with at least two (preferably three) fundamental vibrational modes to ensure one or more states between the upper laser level and the ground state. The ground state cannot be used as the lower laser level because it cannot be depopulated to maintain inversion.

(6) Polyatomic lasant molecules should not be so large or so complex that fast V-V relaxation occurs, through a multitude of channels, to the first excited state. Linear or planar triatomics (eg, CO_2) or effective triatomics (eg, CO-Hg-Cl) may be the best choice.

(7) "Metastable" upper laser level for maintaining inversion, at least with respect to radiative and V-V decay.

(8) Fast V-V into the upper laser level and out of the lower laser level.

(9) Lasing wavelength less than 10.6 μm.

Possible combinations of absorbers and lasants satisfying these criteria were discussed, starting with molecules compiled by Chen and DeYoung (fig. 4.19(a)-(e)) and compared according to possible near-resonant energy transfers. About half of the proposed absorbers were eliminated on the basis of instability and chemical reactivity. The more promising of those remaining include CO, N_2, HF, DF, HCl, and SH.

Potential lasants are more difficult to evaluate, although a number of candidates were mentioned (most of them rejected). Survivors include CO_2, OCS, CS_2, HCN, N_2O, H_2O, and more complex molecules like CO-Hg-Cl, which behaves vibrationally much like CO_2. Dyes were discussed but rejected because of short excited-state lifetimes. Halogen lasants were originally rejected, but subsequently reinstated as candidates because of the possibility of rapid V-V relaxation into the upper laser level from nearby levels and rapid V-V relaxation out of the lower laser level. This illustrates the point that not all of the above criteria are hard and fast, but should be used rather as guides in selection of molecules.

It was further concluded that since theory does have limitations in lasant selection, especially the types of theory currently available, an experimental laser pumped program should be initiated as a tool in lasant

evaluation. A broad range of absorber-lasant combinations can be quickly studied in this manner.

Perhaps the most valuable aspect of the Transfer-Laser Working Group, and the workshop as a whole, is the fact that a number of scientists with a broad range of relevant expertise were brought together to discuss the problems of transfer lasers and to suggest solutions. Indeed, valuable recommendations were made throughout the two-day event. Even more importantly, contacts were made with other groups at Langley and with university professors that hold great promise of future cooperation and fruitful ideas. Key people are now aware of the significance and scope of our blackbody laser program.

Workshop Participants

L. Arriola
C. Blount
P. Brockman
K. Chang
K. Y. Chen
W. Christiansen
E. Conway
R. De Young
W. Harries
J. Heinbockel
D. Humes
N. Jalufka
J. Jones
J. Lee
M. Lee
W. Meador
G. Miner
D. Phillips
J. Quagliano
R. Rogowski
G. Schuster
L. Stock
L. Vallarino
W. Weaver
D. Williams
J. Wilson
L. Zapata

1. Report No.	2. Government Accession No.	3. Recipient's Catalog No.
NASA TM-87616		

4. Title and Subtitle	5. Report Date
Lasant Materials for Blackbody-Pumped Lasers	September 1985
	6. Performing Organization Code: 506-55-73-01
7. Author(s): Edited by R. J. De Young and K. Y. Chen	8. Performing Organization Report No.
	10. Work Unit No.
9. Performing Organization Name and Address: NASA Langley Research Center, Hampton, Virginia 23665	11. Contract or Grant No.
	13. Type of Report and Period Covered: Technical Memorandum
12. Sponsoring Agency Name and Address: National Aeronautics and Space Administration, Washington, DC 20546	14. Sponsoring Agency Code

15. Supplementary Notes

16. Abstract

Blackbody-pumped solar lasers have been proposed to convert sunlight into laser power to provide future space power and propulsion needs. There are two classes of blackbody-pumped lasers. The direct cavity-pumped system in which the lasant molecule is vibrationally excited by the absorption of blackbody radiation and laser, all within the blackbody cavity. The other system is the transfer blackbody-pumped laser in which an absorbing molecule is first excited within the blackbody cavity, then transferred into a laser cavity when an appropriate lasant molecule is mixed. Collisional transfer of vibrational excitation from the absorbing to the lasing molecule results in laser emission. A workshop was held at NASA Langley Research Center on August 1 and 2, 1985, to investigate new lasant materials for both of these blackbody systems. Emphasis was placed on the physics of molecular systems which would be appropriate for blackbody-pumped lasers.

17. Key Words (Suggested by Author(s))	18. Distribution Statement
Solar-pumped lasers Blackbody-pumped lasers Laser conversion	Unclassified - Unlimited Subject Category: 36

19. Security Classif. (of this report)	20. Security Classif. (of this page)	21. No. of Pages	22. Price
Unclassified	Unclassified	179	A09

For sale by the National Technical Information Service, Springfield, Virginia 22161